Doctoral Thesis

Thesis Title

The Role of Plasma-simulated Nanosecond Pulsed Currents in Cellular Responses

Department of Mechanical Systems Engineering
Graduate School of Engineering,
TOHOKU UNIVERSITY

CHIA-HSING CHANG

(ID No. B7TD1005)

Advising Professor at Tohoku Univ.	Professor Sato, Takehiko
Research Advisor at Tohoku Univ.	
Dissertation Committee Members Name marked with "○" is the Chief Examiner	○ Professor Sato, Takehiko 1 Professor Ishikawa, Takuji 2 Professor Kaneko, Toshiro 3 Professor Nakabayashi, Takakazu (Graduate School of Pharmaceutical Sciences)

TOHOKU UNIVERSITY
Graduate School of Engineering

The Role of Plasma-simulated Nanosecond Pulsed Currents in Cellular Responses

（プラズマ模擬ナノ秒パルス電流の細胞応答における役割）

A dissertation submitted for the degree of Doctor of Philosophy (Engineering)

Department of Mechanical Systems Engineering

by

Chia-Hsing CHANG

July 10, 2020

The Role of Plasma-simulated Nanosecond Pulsed Currents in Cellular Responses

CHANG, Chia-Hsing

Abstract

In recent decades, cold atmospheric pressure plasma (CAP) has been widely applied in various fields, such as waste destruction, surface modification, and biomedical applications, among others. Plasma medicine, using CAP for medical research and healthcare, has been found to have a high potential as a powerful device for wound healing, bacteria sterilization, cancer inactivation, to name a few. CAP contains a variety of physical and chemical components, including UV ray, photons, charged particles, electrically excited atoms, and chemically reactive species. CAP is recently regarded as a novel means for cancer therapy, because of its prominent cytotoxicity. Mainly plasma between gaseous and liquid interactions have been reported, as well as the reactive oxygen and nitrogen species (RONS) in plasma-activated medium (PAM), more specifically H_2O_2 and NO_2^-, regarded as most important species for anti-cancer therapy. Exposure of human cells to CAP has been reported to elicit various cellular responses in an intensity-dependent manner. Strong CAP efficiently induces cell death, and relatively weak treatment with CAP can stimulate cell proliferation and tissue regeneration. The combined effects of electrical and chemical factors of CAP have been considered to achieve the cytotoxicity. Whereas reactive species are well known to be important for the CAP cytotoxicity, the biological significance of electrical factors of CAP remains largely unclear.

On the other hand, cancer cell invasion, migration and metastasis require cell motility, which is driven by actin polymerization, cell adhesion, acto-myosin contraction, and so on. For human fibrosarcoma cell line, HT-1080, under certain conditions could perform two distinct cell motilities in migration: mesenchymal and amoeboid mode. In mesenchymal mode, cells become elongated morphology, fibroblast-like and form membrane protrusions at the leading edge, are dependent on integrin-mediated adhesion; on the contrary, in amoeboid mode, these cells move as rounded morphology by squeezing, are weak to the adhesion substrate. Rho GTPases play critical roles in reorganization of the actin cytoskeleton, and the processes are related to various regulatory proteins which could be activated by extracellular stimulus. Actin-rich protrusion of cell pseudopodia is a critical element of mesenchymal cell migration and invasion, primarily by Rac and Cdc42. Additionally, intracellular molecular signals, Ca^{2+} and intracellular ROS, exert proper actin remodeling and efficient cell migration, suggested that the biochemical links with small Rho GTPases. Ca^{2+} modulate proper actin remodeling and efficient cell migration, and further, mitochondrial calcium dynamics in cytoskeletal remodeling through the modulation of ROS production. What is more, the change of intracellular ROS level in cells is an important indicator of functional state. ROS signals could promote cell proliferation, participate in the regulation of certain Rho GTPase mediating cytoskeletal reorganization. Thus, the reorganization of cytoskeleton plays a critical role in the migration of cancer cells, elucidating the mechanisms of actin dynamics are important for cancer therapeutics.

This dissertation provides a novel insight into the electrical aspect of CAP, using agarose bridges to avoid effects of ionized particles or RONS around treated cells. The overall results have demonstrated that nanosecond pulsed current (nsPC) under CAP-producing conditions significantly promoted the motility of human fibrosarcoma HT-1080 cells. In this study, we explored the effects of nsPC on cell morphology associated with cell motility. Our study observed that nsPC stimulation caused extended cell shape, membrane protrusion formation, and increased cell surface area, but not cell death induction. nsPC stimulation also caused elevated intracellular ROS and Ca^{2+}. HT-1080 cells can undergo two modes of cell motility, namely mesenchymal and ameboid motility, and we found that morphological features of mesenchymal motility were partly shared with nsPC-stimulated cells. Furthermore, nsPC-stimulated cells had extended stress fibers composed of filamentous actin. Taken together, this study provides a novel insight into the electrical aspect of CAP action, and we speculate that nsPC activates a certain mechanism involving intracellular signaling for stress fiber formation, leading to altered cell morphology and increased cell motility. Our investigation proposes that nanosecond pulsed currents (nsPCs) have the ability to reflect the positive effect on Rac and Cdc42-related processes to induce human fibrosarcoma cells for mesenchymal transition, and electrical signals could also induce cancer cells to sensitive states to interact with extracellular components surrounding, such as RONS. Moreover, this study analyzed cytotoxic effects of a combination of electrical and chemical factors of CAP on cancer cells. When cells were incubated in CAP-exposed solution that contained substantial levels of H_2O_2 and NO_2^-, their viability was markedly decreased. In the absence of effects of reactive species, electrical factors of CAP did not show any adverse

influences on cells. Interestingly, CAP-exposed solution exhibited more cytotoxicity on the electrically stimulated cells than unstimulated ones. This observation suggests that the electrical stimulation altered the nature of cells and increased cell susceptibility to CAP-exposed solution.

In a word, cancer cells highly dependent on the external environment, which also provides directional cues that drive the establishment of intracellular polarity. Although the biological action of CAP is considered to be brought about by synergistic effects of reactive species and electrical factors of CAP, limited information is currently available on the contribution of electrical factors to CAP-induced cell responses. HT-1080 cells stimulated by electrical properties (e.g. nsPCs) could play a crucial role for strengthening anti-cancer capacity from RONS due to intracellular machinery activated. Perhaps that stimulated cells obtained electric signals from the small GTPases, mitochondria, or other intracellular organelles to the highly sensitive state increased susceptibility to extracellular environment, causing cell death programming and chain reactions. Our findings cast light on the biological significance of electrical factors of CAP and serve as a new clue for further investigation toward a more comprehensive understanding of biological actions of CAP.

Contents

List of Figures & Tables

Chapter 1

Introduction

1.1. General background

1.1.1. Plasma

Physics plasma is a special excited gas state, sometimes named as “the fourth state of matter”. When the continuous supply of energy increases, the matter will turn from solid, liquid, gas and finally to plasma. Plasma can be classified by temperature and pressure. Low pressure plasma requires a vacuum system, while atmospheric pressure plasma is generated in ambient air, same as living surrounding. From the view of temperature, there are two kinds of plasma: thermal and non-thermal plasma. Thermal plasma is highly ionized plasma, such as the sun. The temperature of electrons (T_e) approximately equals to the temperature of ions (T_i), and the bulk temperature can be as high as 10^7 k. However, for the non-thermal plasma, the temperature of electrons (T_e) is approximately 10^5 k, while the temperature of ions (T_i) is lower than 10^3 k due to the weak ionization percentage and mass weight differences between electrons and ions [1]. Obviously, only non-thermal atmospheric pressure plasma, also known as “cold atmospheric pressure plasma”, can be applied on living body.

1.1.2. Cold atmospheric pressure plasma

Cold atmospheric pressure plasma (CAP) is generated partially ionized gas under atmospheric pressure without causing thermal damage, which include charged particles, chemically reactive species, electronically excited atoms, UV, photons, etc. [2,3]. A wide variety of CAP devices have been developed for specific applications, like surface modification, environmental application, agriculture, and biomedical use [4]. Many investigations aim to reveal the complexity of the physics and chemistry interactions inside CAP. Among all, plasma medicine becomes the fastest growing of the current set of CAP applications, which is the main subject of this study.

1.1.3. Plasma medicine

Plasma medicine is promising health cure using CAP with a near room temperature to medical research and to the health care field, and this application offers a valid and advantageous replacement of traditional chemical-based medications, providing a fast and efficient new path to health care, for example, wound healing, blood coagulation, bacteria sterilization, tooth bleaching, inactivation of microorganisms, and cancer treatment, to name a few [5–9]. CAP could provide electrons, photons, reactive oxygen and nitrogen species (RONS), such as superoxide anions ($O_2^{\cdot -}$), hydroperoxyl radicals ($HO_2^{\cdot}$), hydrogen peroxide (H_2O_2), hydroxyl radicals ($^{\cdot}OH$), singlet oxygen ($^1O_2$), ozone (O_3), peroxynitrite ($ONOO^-$), nitrite (NO_2^-), nitrate (NO_3^-), etc., between gas and liquid phase [10]. The delivery of medically active particles or ionic species at the molecular level is current topics in this research field. Furthermore, the mechanisms by which CAP alter living cells, tissue and organisms are not well established.

Direct treatment with CAP is the common method on medical applications in many studies [11–13]. Weaker CAP treatment intensity could stimulate cell proliferation and tissue regeneration,

and stronger CAP treatment intensity could cause the inactivation of cells through apoptosis or necrosis, depending on the exposure time. Although, plasma could be changed characteristics with target, showing selectivity with cell-line, causing side-effect with long-term treatment. Also, the delivery of plasma dose would be decreased into the inner living tissue [14,15]. On the other hand, indirect treatment, using medium treated by CAP, currently becomes the novel application for cancer therapy, because liquid phase processes with long-lived species have been identified to be the main role in the anti-cancer therapy, shown in figure 1.1.

These anti-bacterial and anti-cancer properties from CAP which dissolved inside the liquid, known as plasma activated medium (PAM), can preserve the similar outcome as direct treatment, shown in figure 1.2 [16–21]. However, only few long-lived species remain in PAM for serval hours, such as H_2O_2 and NO_2^- regarded as the key role in anti-cancer effects for their cytotoxicity [22–25]. Some studies pointed out that the direct treatment causes much stronger cytotoxicity over the cancer cells compared with indirect treatment, because cancer cells were activated to the sensitive state or different factors supported the cellular responses [26–28]. There might be some unknown mechanisms between ion channels and organelles to affect the cytotoxicity of the RONS on cancer cells between the direct and indirect CAP treatment, shown in figure 1.3 [29]. In short, the academic studies of plasma in biomedicine fields are still primal, which means there are still huge potential for research.

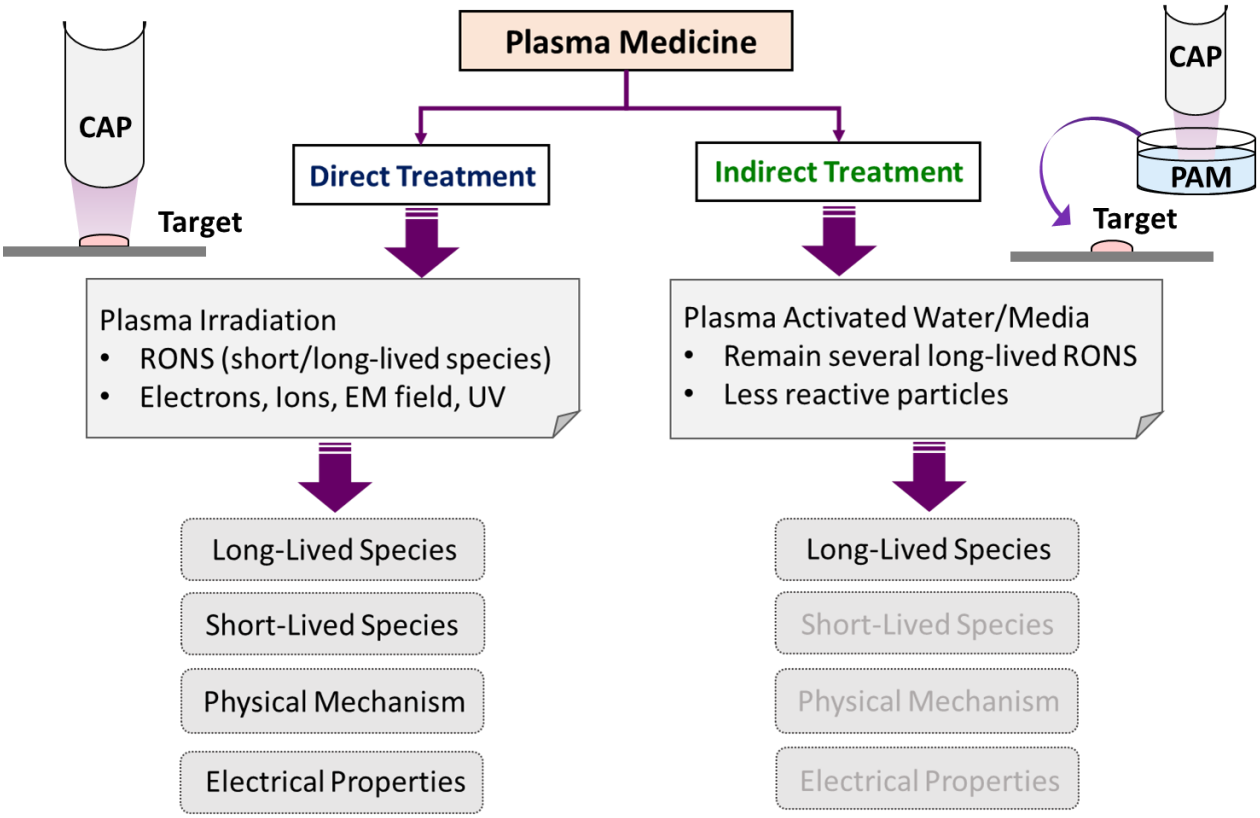

Figure 1.1 Simple classification of plasma medicine: direct treatment versus indirect treatment.

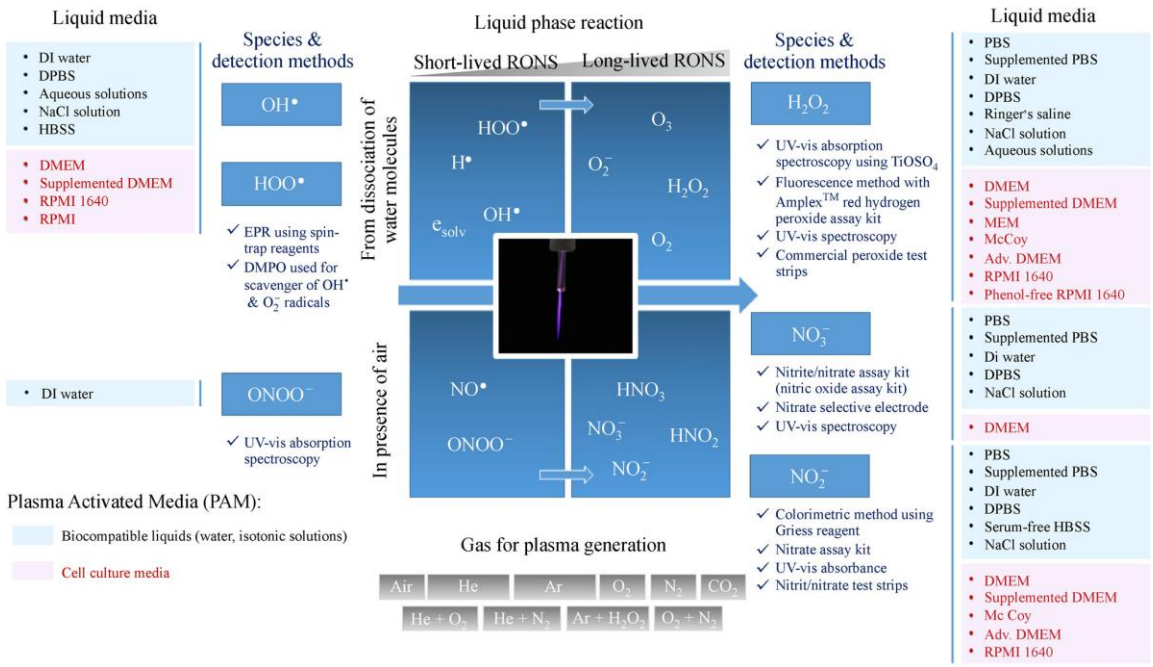

Figure 1.2 Overview of the short- and long-lived RONS generated in liquid media by CAP [23].

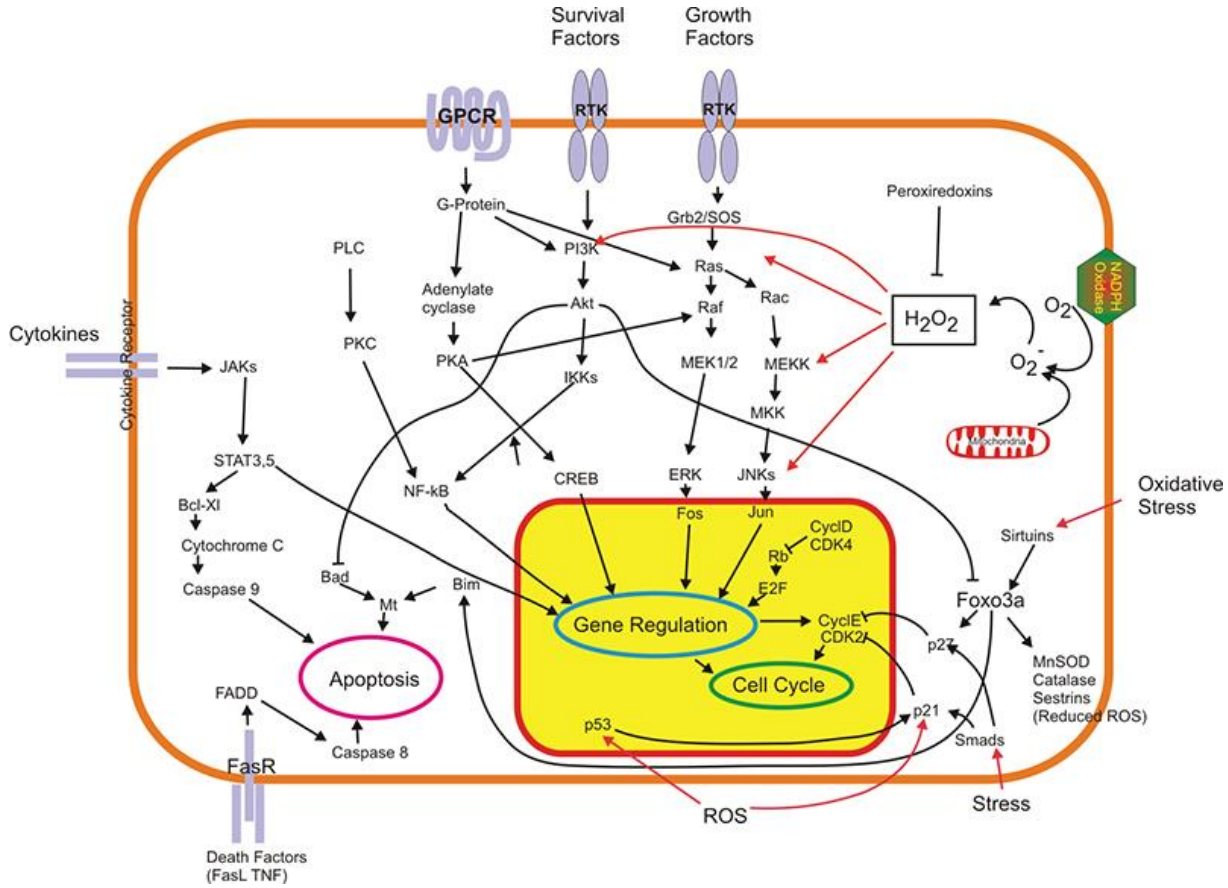

Figure 1.3 Schematic illustration of reported interactions of ROS and mitogenic cascades [29].

1.2. Biology of cancer cell

Cancer cells are created when uncontrolled cell division by gene mutations, and able to adapt environmental changes. These abnormal cells start to grow and spread rapidly in human body, overproducing grow factor proteins to migrate, major differences of cancer and normal cells given in Table 1.1. Tumor migration, invasion and metastasis require cell motility, which are driven by actin polymerization, cell adhesion, acto-myosin contraction, and so on [30–33]. Rho family of small GTPases such as Rho, Rac, and Cdc42 are essential to contribute to most steps of cancer initiation and progression including cytoskeletal organization, gene transcription, and proliferation, shown in figure 1.4 [34–39]. Many studies indicate that the regulation of Rho family proteins is important in determining cell morphology and invasion mechanism, switching on and off proteins signaling interacts actin assembly and controls the formation of filopodia, lamellipodia, and stress fibers, shown in figure 1.5 [40–42].

Single cell migration includes mesenchymal and amoeboid migration strategies. In mesenchymal mode, cells become elongated morphology, fibroblast-like and form membrane protrusions at the leading edge, are dependent on integrin-mediated adhesion. On the contrary, in amoeboid mode, these cells move as rounded morphology by squeezing, are weak to the adhesion substrate. The translocation of the mesenchymal-migrating cells begins with the formation of actin-rich filopodia and lamellipodia at the leading edge [43,44]. For human fibrosarcoma cell line, HT-1080, under certain conditions could perform two distinct cell motilities in migration, shown in figure 1.6., thereby this cancer cell line will be suitable for electrical stimulation [33, 45, 46]. Both modes of cell motility are driven by actin polymerization, cell adhesion, and act-myosin contraction, which are controlled by intracellular signaling, particularly by Rho family small GTPase members, such as Rho, Rac, and Cdc42. Rho GTPases are key players to regulate the actin cytoskeleton and

gene transcription to promote coordinated changes in cell behavior. To brief, the actin reorganization acts as an upstream regulator in metastatic cancer cells.

Table 1.1 Major differences between cancer and normal cells.

	Normal Cell	Cancer Cell
Cell shape	Uniform	Irregular
Nucleus	Spheroid shape, single nucleus	Irregular shape, multi-nucleation common
Nucleolus	Single, inconspicuous nucleolus	Multiple, enlarged nucleoli
Cytoplasm	Large cytoplasmic volume	Small cytoplasmic volume
Growth	Controlled	Uncontrolled
Maturation	Mature into specialized cells	Remain immature and undifferentiated
Energy efficiency	Very low (5%)	Very high (95%)
Location	Remain in their intended location	Can spread to different locations in the body (metastasis)

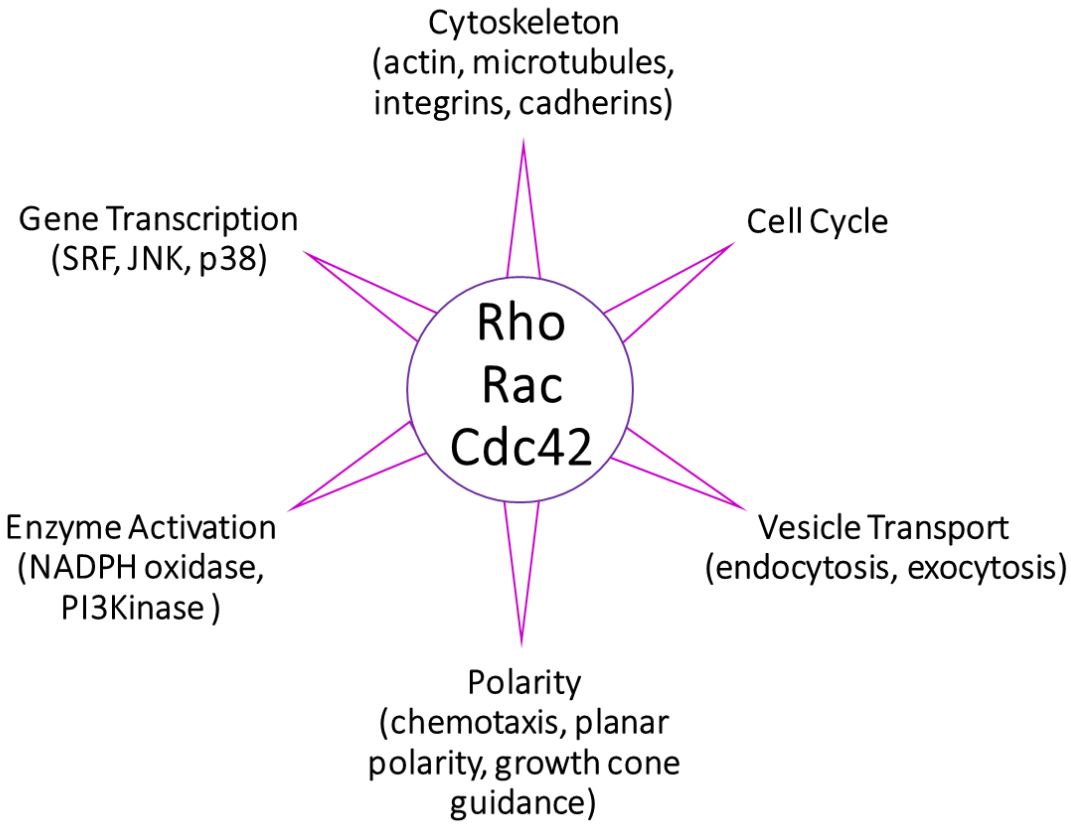

Figure 1.4 Cellular effects of Rho GTPases. Adapted from [35].

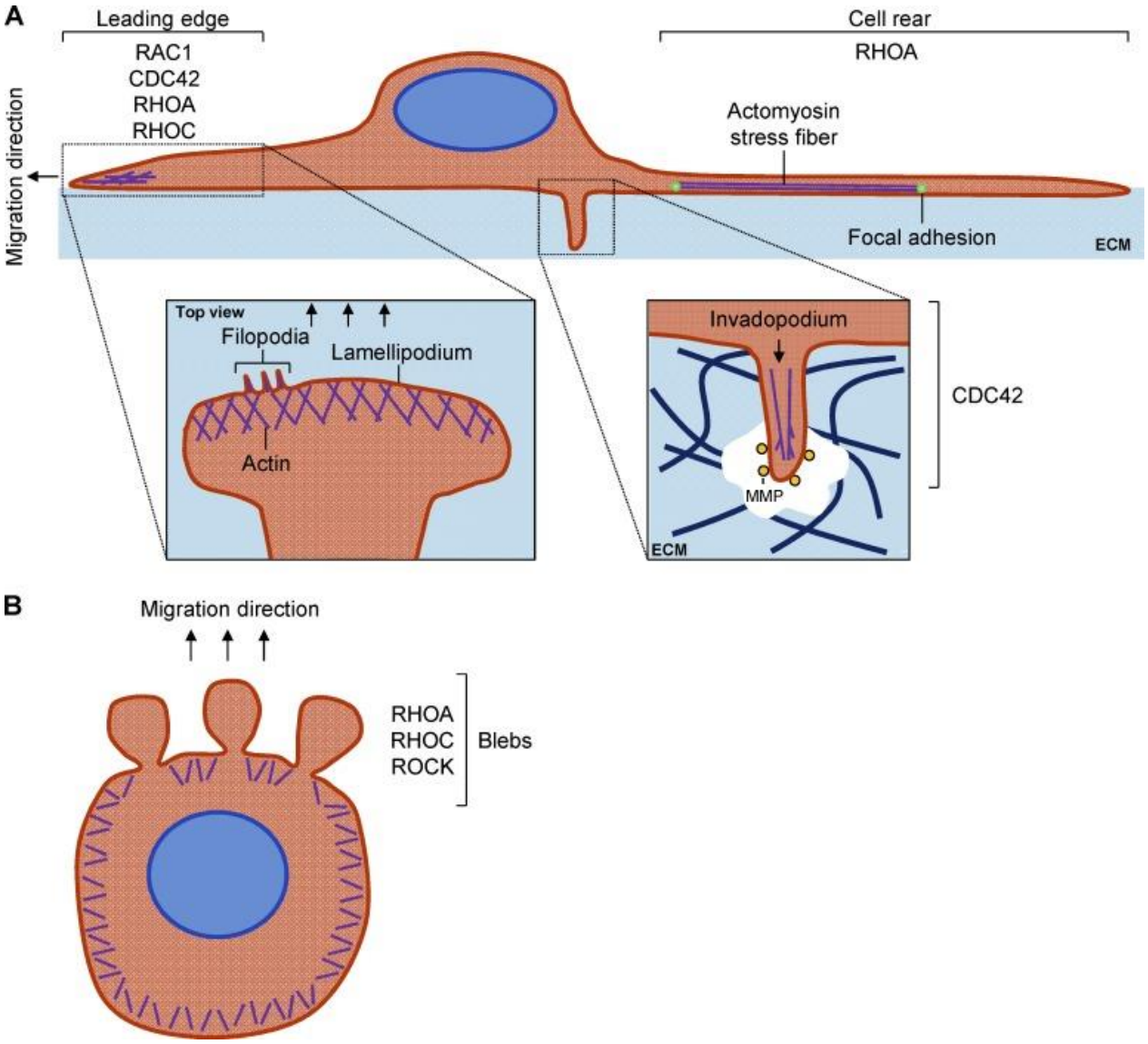

Figure 1.5 Rho GTPase-driven single cell migration modes [42].

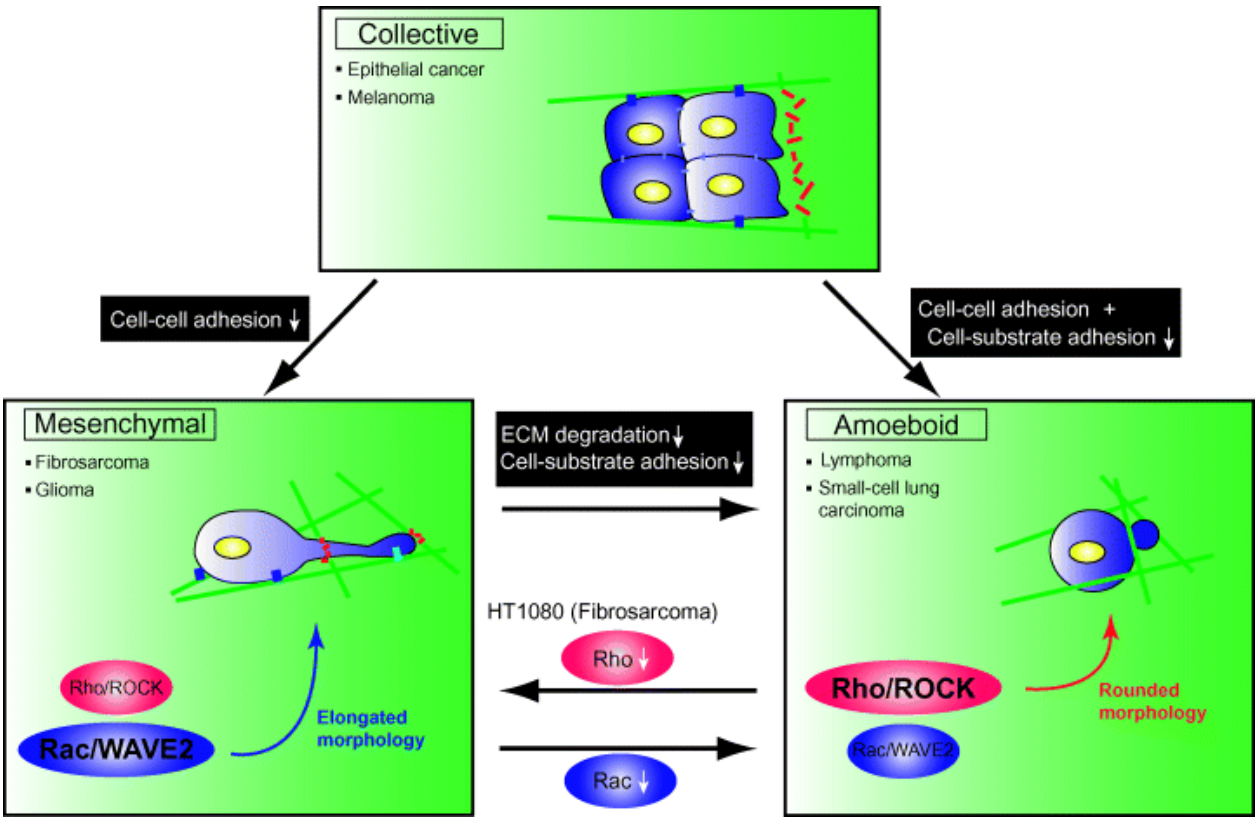

Figure 1.6 Transition of migration in HT-1080 cells [45].

1.3. Purpose of this dissertation

We aim to find the novel understanding from CAP treatments through electrical properties. For biomedical application, the weaker intensity of plasma irradiation could stimulate cell proliferation and tissue regeneration, and stronger could cause the inactivation of cells through apoptosis or necrosis. Thus, we suggested that there might be an important key trigger to elevate the efficacy from CAP, which could be “Electrical Factors”. Thus, our main goal is to investigate on bioelectrical mechanisms induced by CAP, which are important in the physiology and development of the majority of intracellular responses, shown in figure 1.7 [47, 48].

In this dissertation, we carried out the power source from nanosecond pulsed currents (nsPCs) to provide electrical properties without essential membrane damage and also have the ability to ignite the streamer discharge to manufacture plasma-activated media. According to previous studies, the power source for electrical stimulation were focused on direct current (DC), alterative current (AC), and pulsed current [49]. Different power sources may influence different mechanisms for altering cell fate. DC stimulation typically directs cell orientation, alters cell morphology, and directs cell migration; AC stimulation enhances cell differentiation and increases tissue function; for pulsed currents, the cellular responses will depend on pulse duration, number of pulses, voltage strength, to name a few. In the microsecond to millisecond pulses range result in smaller sized pores distributed plasma membrane and sometimes nucleus. In nanosecond pulses, applied high voltage may rupture subcellular structures and selectively target intracellular organelles while leaving the damage or trauma on plasma membrane, shown in figure 1.8 [50]. Moreover, as energy is transferred to the culture chamber from the power supply, increased in chamber temperature from joule heating, and this could be a critical problem for cell viability. Thus, nsPCs (low frequency range and ultra-short pulse duration) would be an ideal stimulation for nonthermal electrical destruction of proteins, cells, and tissue to clarify the electrical influence

from CAP. On the other hand, highly metastatic cancer cells have shown a stronger response to electrical signals than healthy or weakly metastatic cancer cells. HT-1080 cells are known to show two distinct modes of cell motility with highly metastatic, also been widely used in bioelectrical experiments. Thus, for the first cell line to decipher our hypothesis, it will be very suitable. All of the emphasis are as the followings:

1. To observe cell activities (cell viability and migration) stimulated by nsPCs
2. To elicit various cellular morphological changes by multiple extra-stimuli
3. To analyze the mechanisms of cancer motilities through the dynamic of cytoskeleton
4. To compare the effects of plasma-induced chemical and electrical stimuli on inactivation of cancer cells

Our study provides a novel insight into the electrical aspect of CAP action. We would like to take advantages of electrical properties of using CAP on cancer cells to trigger at the cell surface or affect membrane protein functions. These findings will help to reveal the complex interactions from CAP in cancer therapy to develop complete clinical treatments.

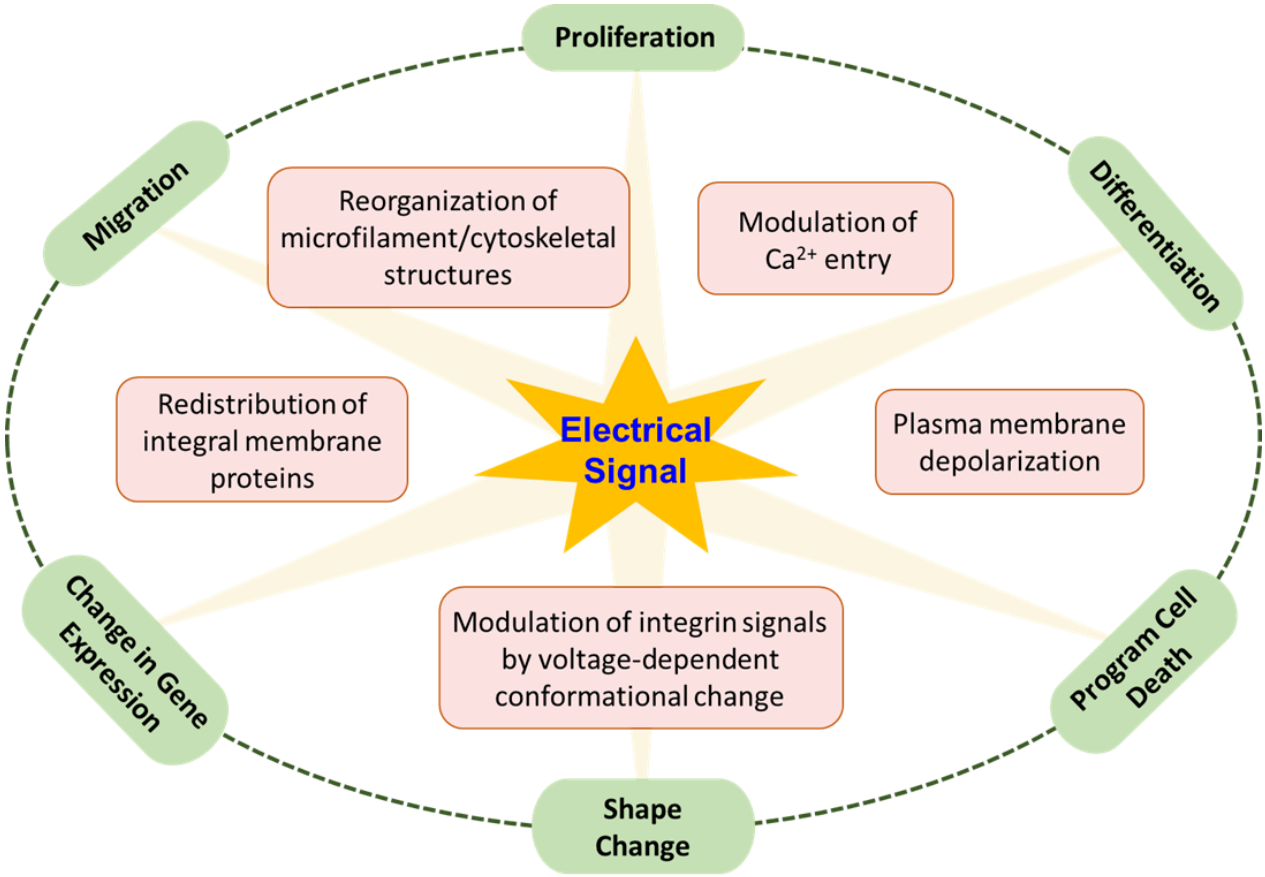

Figure 1.7 Electrical signals control mechanisms at cellular level, thus directing cell behavior. Adapted from [47] and [48].

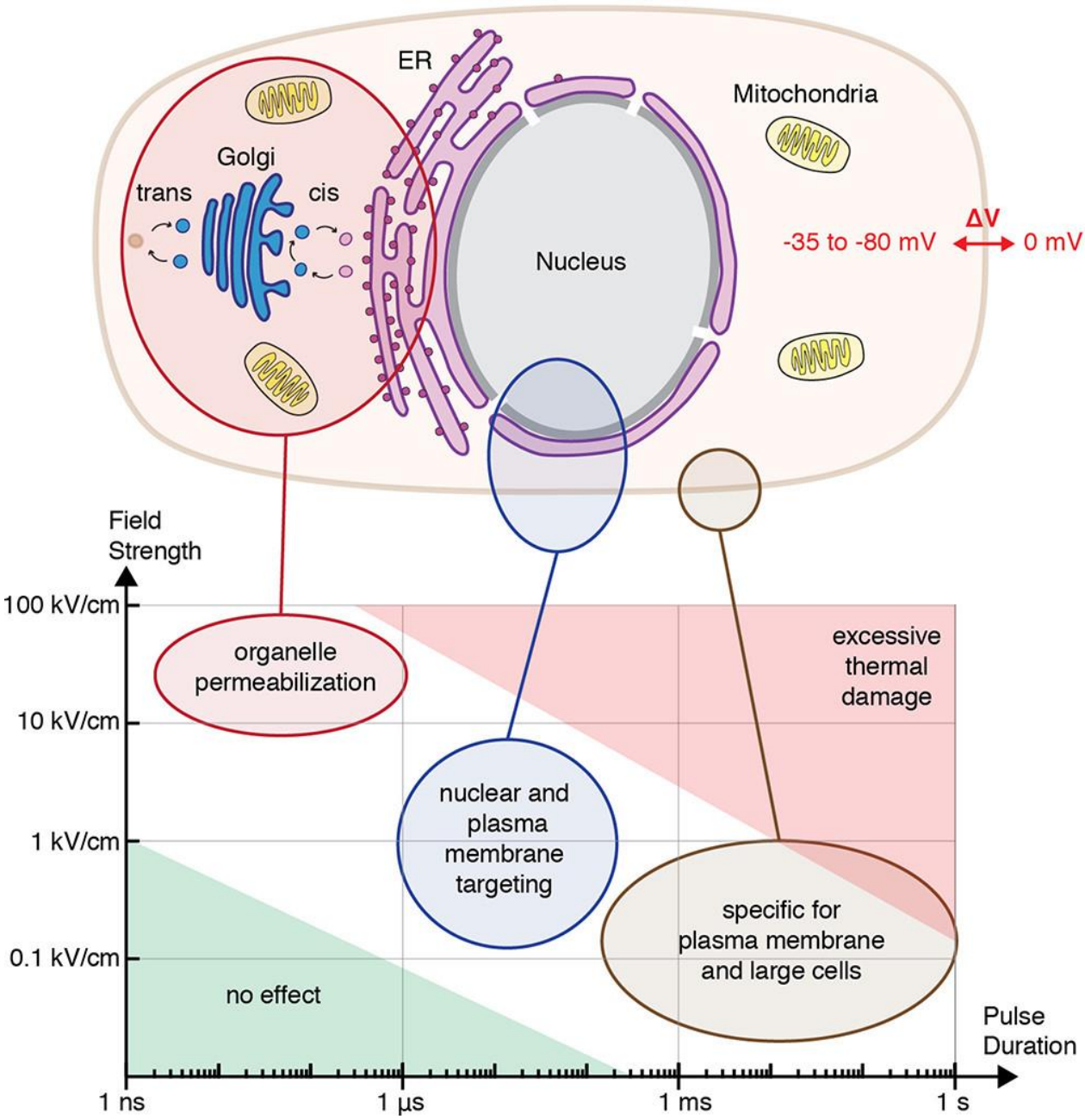

Figure 1.8 The relationship between the pulse duration and cellular targeting [50].

References

[1] M.A. Lieberman, A.J. Lichtenberg, J. Wiley, N. York, Principles of Plasma Discharges and Materials Processing, 2010.

[2] S. Samukawa, M. Hori, S. Rauf, K. Tachibana, P. Bruggeman, G. Kroesen, J.C. Whitehead, A.B. Murphy, A.F. Gutsol, S. Starikovskaia, U. Kortshagen, J.P. Boeuf, T.J. Sommerer, M.J. Kushner, U. Czarnetzki, N. Mason, The 2012 plasma roadmap, J. Phys. D. Appl. Phys. 45 (2012). doi:10.1088/0022-3727/45/25/253001.

[3] I. Adamovich, S.D. Baalrud, A. Bogaerts, P.J. Bruggeman, M. Cappelli, V. Colombo, U. Czarnetzki, U. Ebert, J.G. Eden, P. Favia, D.B. Graves, S. Hamaguchi, G. Hieftje, M. Hori, I.D. Kaganovich, U. Kortshagen, M.J. Kushner, N.J. Mason, S. Mazouffre, S.M. Thagard, H.R. Metelmann, A. Mizuno, E. Moreau, A.B. Murphy, B.A. Niemira, G.S. Oehrlein, Z.L. Petrovic, L.C. Pitchford, Y.K. Pu, S. Rauf, O. Sakai, S. Samukawa, S. Starikovskaia, J. Tennyson, K. Terashima, M.M. Turner, M.C.M. Van De Sanden, A. Vardelle, The 2017 Plasma Roadmap: Low temperature plasma science and technology, J. Phys. D. Appl. Phys. 50 (2017). doi:10.1088/1361-6463/aa76f5.

[4] K.D. Weltmann, J.F. Kolb, M. Holub, D. Uhrlandt, M. Šimek, K. (Ken) Ostrikov, S. Hamaguchi, U. Cvelbar, M. Černák, B. Locke, A. Fridman, P. Favia, K. Becker, The future for plasma science and technology, Plasma Process. Polym. 16 (2019) 1–29. doi:10.1002/ppap.201800118.

[5] M.G. Kong, G. Kroesen, G. Morfill, T. Nosenko, T. Shimizu, J. Van Dijk, J.L. Zimmermann, Plasma medicine: An introductory review, New J. Phys. 11 (2009). doi:10.1088/1367-2630/11/11/115012.

[6] G.Y. Park, S.J. Park, M.Y. Choi, I.G. Koo, J.H. Byun, J.W. Hong, J.Y. Sim, G.J. Collins, J.K. Lee, Atmospheric-pressure plasma sources for biomedical applications, Plasma Sources Sci. Technol. 21 (2012). doi:10.1088/0963-0252/21/4/043001.

[7] K.D. Weltmann, T. Von Woedtke, Plasma medicine - Current state of research and medical application, Plasma Phys. Control. Fusion. 59 (2017). doi:10.1088/0741-3335/59/1/014031.

[8] D. Yan, J.H. Sherman, M. Keidar, Cold atmospheric plasma, a novel promising anti-cancer treatment modality, Oncotarget. 8 (2017) 15977–15995. doi:10.18632/oncotarget.13304.

[9] K.Y. Cheng, C.H. Chang, Y.W. Yang, G.C. Liao, C.T. Liu, J.S. Wu, Enhancement of cell

growth on honeycomb-structured polylactide surface using atmospheric-pressure plasma jet modification, Appl. Surf. Sci. 394 (2017) 534–542. doi:10.1016/j.apsusc.2016.10.093.

[10] T. Von Woedtke, A. Schmidt, S. Bekeschus, K. Wende, K.D. Weltmann, Plasma medicine: A field of applied redox biology, In Vivo (Brooklyn). 33 (2019) 1011–1026. doi:10.21873/invivo.11570.

[11] S. Kalghatgi, G. Friedman, A. Fridman, A.M. Clyne, Endothelial cell proliferation is enhanced by low dose non-thermal plasma through fibroblast growth factor-2 release, Ann. Biomed. Eng. 38 (2010) 748–757. doi:10.1007/s10439-009-9868-x.

[12] D.B. Graves, The emerging role of reactive oxygen and nitrogen species in redox biology and some implications for plasma applications to medicine and biology, J. Phys. D. Appl. Phys. 45 (2012). doi:10.1088/0022-3727/45/26/263001.

[13] H. Tanaka, M. Mizuno, K. Ishikawa, S. Toyokuni, H. Kajiyama, F. Kikkawa, M. Hori, New Hopes for Plasma-Based Cancer Treatment, Plasma. 1 (2018) 150–155. doi:10.3390/plasma1010014.

[14] X. Lu, G. V. Naidis, M. Laroussi, S. Reuter, D.B. Graves, K. Ostrikov, Reactive species in non-equilibrium atmospheric-pressure plasmas: Generation, transport, and biological effects, Phys. Rep. 630 (2016) 1–84. doi:10.1016/j.physrep.2016.03.003.

[15] X. Lu, M. Keidar, M. Laroussi, E. Choi, E.J. Szili, K. Ostrikov, Transcutaneous plasma stress: From soft-matter models to living tissues, Mater. Sci. Eng. R Reports. 138 (2019) 36–59. doi:10.1016/j.mser.2019.04.002.

[16] T. Sato, M. Yokoyama, K. Johkura, A key inactivation factor of HeLa cell viability by a plasma flow, J. Phys. D. Appl. Phys. 44 (2011). doi:10.1088/0022-3727/44/37/372001.

[17] M. Yokoyama, K. Johkura, T. Sato, Gene expression responses of HeLa cells to chemical species generated by an atmospheric plasma flow, Biochem. Biophys. Res. Commun. 450 (2014) 1266–1271. doi:10.1016/j.bbrc.2014.06.116.

[18] D.B. Graves, Reactive species from cold atmospheric plasma: Implications for cancer therapy, Plasma Process. Polym. 11 (2014) 1120–1127. doi:10.1002/ppap.201400068.

[19] H. Jablonowski, T. von Woedtke, Research on plasma medicine-relevant plasma-liquid interaction: What happened in the past five years?, Clin. Plasma Med. 3 (2015) 42–52. doi:10.1016/j.cpme.2015.11.003.

[20] R. Furuta, N. Kurake, K. Ishikawa, K. Takeda, H. Hashizume, H. Tanaka, H. Kondo, M. Sekine, M. Hori, Intracellular responses to reactive oxygen and nitrogen species, and lipid

peroxidation in apoptotic cells cultivated in plasma-activated medium, Plasma Process. Polym. 14 (2017) 1–6. doi:10.1002/ppap.201700123.

[21] W. Van Boxem, J. Van Der Paal, Y. Gorbanev, S. Vanuytsel, E. Smits, S. Dewilde, A. Bogaerts, Anti-cancer capacity of plasma-treated PBS: Effect of chemical composition on cancer cell cytotoxicity, Sci. Rep. 7 (2017) 1–15. doi:10.1038/s41598-017-16758-8.

[22] Z. Machala, B. Tarabová, D. Sersenová, M. Janda, K. Hensel, Chemical and antibacterial effects of plasma activated water: Correlation with gaseous and aqueous reactive oxygen and nitrogen species, plasma sources and air flow conditions, J. Phys. D. Appl. Phys. 52 (2019). doi:10.1088/1361-6463/aae807.

[23] A. Khlyustova, C. Labay, Z. Machala, M.P. Ginebra, C. Canal, Important parameters in plasma jets for the production of RONS in liquids for plasma medicine: A brief review, Front. Chem. Sci. Eng. 13 (2019) 238–252. doi:10.1007/s11705-019-1801-8.

[24] G. Bauer, D. Sersenová, D.B. Graves, Z. Machala, Cold Atmospheric Plasma and Plasma-Activated Medium Trigger RONS-Based Tumor Cell Apoptosis, Sci. Rep. 9 (2019) 1–28. doi:10.1038/s41598-019-50291-0.

[25] G. Bauer, D. Sersenová, D.B. Graves, Z. Machala, Dynamics of Singlet Oxygen-Triggered, RONS-Based Apoptosis Induction after Treatment of Tumor Cells with Cold Atmospheric Plasma or Plasma-Activated Medium, Sci. Rep. 9 (2019) 1–34. doi:10.1038/s41598-019-50329-3.

[26] D. Yan, W. Xu, X. Yao, L. Lin, J.H. Sherman, M. Keidar, The Cell Activation Phenomena in the Cold Atmospheric Plasma Cancer Treatment, Sci. Rep. 8 (2018) 1–10. doi:10.1038/s41598-018-33914-w.

[27] F. Saadati, H. Mahdikia, H.A. Abbaszadeh, M.A. Abdollahifar, M.S. Khoramgah, B. Shokri, Comparison of Direct and Indirect cold atmospheric-pressure plasma methods in the B16F10 melanoma cancer cells treatment, Sci. Rep. 8 (2018) 1–15. doi:10.1038/s41598-018-25990-9.

[28] A. Kondratskyi, K. Kondratska, R. Skryma, N. Prevarskaya, Ion channels in the regulation of apoptosis, Biochim. Biophys. Acta - Biomembr. 1848 (2015) 2532–2546. doi:10.1016/j.bbamem.2014.10.030.

[29] P. Held, I. BioTek Instruments, An introduction to reactive oxygen species measurement of ROS in yeast cells, TechNote. (2015) 1–21. doi:10.1017/CBO9781107415324.004.

[30] M.F. Olson, E. Sahai, The actin cytoskeleton in cancer cell motility, Clin. Exp. Metastasis.

26 (2009) 273–287. doi:10.1007/s10585-008-9174-2.

[31] D. Yamazaki, S. Kurisu, T. Takenawa, Involvement of Rac and Rho signaling in cancer cell motility in 3D substrates, Oncogene. 28 (2009) 1570–1583. doi:10.1038/onc.2009.2.

[32] S. Tojkander, G. Gateva, P. Lappalainen, Actin stress fibers - Assembly, dynamics and biological roles, J. Cell Sci. 125 (2012) 1855–1864. doi:10.1242/jcs.098087.

[33] D. Yamazaki, T. Itoh, H. Miki, T. Takenawa, SrGAP1 regulates lamellipodial dynamics and cell migratory behavior by modulating Rac1 activity, Mol. Biol. Cell. 24 (2013) 3393–3405. doi:10.1091/mbc.E13-04-0178.

[34] A. Hall, Rho GTpases and the actin cytoskeleton, Science (80-.). 279 (1998) 509–514. doi:10.1126/science.279.5350.509.

[35] A. Hall, Rho GTPases and the control of cell behaviour, Biochem. Soc. Trans. 33 (2005) 891–895. doi:10.1042/BST20050891.

[36] M. Raftopoulou, A. Hall, Cell migration: Rho GTPases lead the way, Dev. Biol. 265 (2004) 23–32. doi:10.1016/j.ydbio.2003.06.003.

[37] A.B. Jaffe, A. Hall, RHO GTPASES: Biochemistry and Biology, Annu. Rev. Cell Dev. Biol. 21 (2005) 247–269. doi:10.1146/annurev.cellbio.21.020604.150721.

[38] M. Parri, P. Chiarugi, Rac and Rho GTPases in cancer cell motility control, Cell Commun. Signal. 8 (2010) 1–14. doi:10.1186/1478-811X-8-23.

[39] G. Jacquemet, H. Hamidi, J. Ivaska, Filopodia in cell adhesion, 3D migration and cancer cell invasion, Curr. Opin. Cell Biol. 36 (2015) 23–31. doi:10.1016/j.ceb.2015.06.007.

[40] H. Yamaguchi, J. Condeelis, Regulation of the actin cytoskeleton in cancer cell migration and invasion, Biochim. Biophys. Acta - Mol. Cell Res. 1773 (2007) 642–652. doi:10.1016/j.bbamcr.2006.07.001.

[41] C.D. Lawson, K. Burridge, The on-off relationship of Rho and Rac during integrin-mediated adhesion and cell migration, Small GTPases. 5 (2014). doi:10.4161/sgtp.27958.

[42] C.D. Lawson, A.J. Ridley, Rho GTPase signaling complexes in cell migration and invasion, J. Cell Biol. 217 (2018) 447–457. doi:10.1083/jcb.201612069.

[43] T. Vallenius, Actin stress fibre subtypes in mesenchymal-migrating cells, Open Biol. 3 (2013). doi:10.1098/rsob.130001.

[44] J. Shankar, I.R. Nabi, Actin cytoskeleton regulation of epithelial mesenchymal transition in metastatic cancer cells, PLoS One. 10 (2015) 1–12. doi:10.1371/journal.pone.0119954.

[45] D. Yamazaki, S. Kurisu, T. Takenawa, Regulation of cancer cell motility through actin

reorganization, Cancer Sci. 96 (2005) 379–386. doi:10.1111/j.1349-7006.2005.00062.x.

[46] M.P. Schwartz, R.E. Rogers, S.P. Singh, J.Y. Lee, S.G. Loveland, J.T. Koepsel, E.S. Witze, S.I. Montanez-Sauri, K.E. Sung, E.Y. Tokuda, Y. Sharma, L.M. Everhart, E.H. Nguyen, M.H. Zaman, D.J. Beebe, N.G. Ahn, W.L. Murphy, K.S. Anseth, A quantitative comparison of human HT-1080 fibrosarcoma cells and primary human dermal fibroblasts identifies a 3D migration mechanism with properties unique to the transformed phenotype, PLoS One. 8 (2013) 1–24. doi:10.1371/journal.pone.0081689.

[47] K.A. McLaughlin, M. Levin, Bioelectric signaling in regeneration: Mechanisms of ionic controls of growth and form, Dev. Biol. 433 (2018) 177–189. doi:10.1016/j.ydbio.2017.08.032.

[48] G. Thrivikraman, S.K. Boda, B. Basu, Unraveling the mechanistic effects of electric field stimulation towards directing stem cell fate and function: A tissue engineering perspective, Biomaterials. 150 (2018) 60–86. doi:10.1016/j.biomaterials.2017.10.003.

[49] B. Cortese, I.E. Palamà, S. D'Amone, G. Gigli, Influence of electrotaxis on cell behaviour, Integr. Biol. (United Kingdom). 6 (2014) 817–830. doi:10.1039/c4ib00142g.

[50] K.A. McLaughlin, M. Levin, Bioelectric signaling in regeneration: Mechanisms of ionic controls of growth and form, Dev. Biol. 433 (2018) 177–189. doi:10.1016/j.ydbio.2017.08.032.

Chapter 2

Effect of nanosecond pulsed current supplied by plasma generator on cell morphology and activity

2.1. Introduction

The amount of active species and ionic particles play the critical role in medical applications. To clarify of the mechanisms is important for precisely therapeutic use. Although, most studies have focused on reactive oxygen species (ROS) or reactive nitrogen species (RNS) in aqueous phase, and ions transmission processes have not been completely investigated [1]. To understand the biological effect of the electric particles and accumulated charges of CAP, it is essential to eliminate the influence of reactive oxygen and nitrogen species (RONS). Thus, the cell culture stimulation system with agar salt bridges were designed for the purpose of preventing reactive faradaic products of electrolysis, not only physically isolated cells from pH variations and metal elution from the electrodes but transported currents from the power supply to identify electrical factors that induce cellular responses. Without this system, the gradual accumulation of RONS and other cytotoxic species were occurred at the electrodes to cause multiple influences on cells [2,3].

CAP can be generated by multiple power sources, such as direct current (DC), alternating current (AC), or pulsed current in micro- or nanosecond. In this chapter, we focused on the electrical stimulation, which has been widely stimulated in living cells [4–6]. According to previous studies, electrical fields (EFs) are used for cell growth, cell migration, cell differentiation, neurite elongation, and a large number of cell behaviors [7–12]. Nanosecond electric fields (nsPEFs) generated by ultra-short voltages and currents led the permeabilization of plasma membranes and caused intracellular delivery, then affected cell functions and induced cell death [13–15]. The pores created by nsPEFs, which is known as "electroporation", are widely applied to cancer treatments or drugs delivery, existing as either irreversible or reversible pores due to power intensity [16–18]. Additionally, one report discovered nano-pores in the cell membrane after CAP treatment, where cell charging and lipid peroxidation were two proposed mechanisms [19]. Furthermore, calcium ions (Ca^{2+}) and sodium ions (Na^{2+}) were found to cross plasma membranes via nsPEFs to active cellular events and induce intracellular or extracellular responses [20,21]. Understanding mechanisms of cell interaction with DC, AC, or pulsed current are critical to clarify the impacts on the function and biology of cells. Nevertheless, electrical factors (charged particles, ionic currents, etc.) supplied by CAP has not been studied thoroughly.

The interactions of RONS with cells have been demonstrated by great numbers of studies. However, CAP produces not only chemical components but also electrical properties. As such, defining the electrical interactions could help us understand the mechanism complementary to CAP treatment. This chapter focused on one of the plasma sources to investigate the influence of electrical factors, using the power source without plasma irradiation to model only the influence from a nanosecond pulsed current supplied by the plasma generator on cell morphology and activity, suggesting the accumulation of ionic currents might be the trigger to cause the downstream responses.

2.2. Materials and methods

2.2.1. Cell lines and culture conditions

In this dissertation, the electrical stimulation focused on HT-1080 cells, and this cancer cells have been widely used in biomedical studies (provided by Japanese Collection of Research Bioresources Cell Bank, human sarcoma cell line). Cells were cultured in minimum essential medium eagle (Sigma-Aldrich, cat. no. M4655-500) containing 10% fetal bovine serum (Gibo, Invitrogen, cat. no. 10437077) and 1% penicillin/streptomycin (Nacalai Tesque, INC., 26253-84). More, 0.25 w/v % trypsin 1 mmol/l EDTA·4Na solution with phenol red (Wako, 201-16945) was used for dispersing the cells for passage (see Appendix A). All experiments were carried out in a humidified incubator at 5% CO_2 and 37°C.

2.2.2. Experimental design

Previous studies have used electrotactic systems with DC and AC stimulation to elucidated the galvanotaxis of EFs on cells. However, in this study, we focused on nanosecond pulsed current (nsPC) to discover more possible and novel interactions between currents and cells. First, we constructed the stimulation system with a salt bridge design and a cell culture chamber, the schematic of which is shown in Figure 2.1. The device was set up for the nsPC transfer via Ag/AgCl electrodes and agarose bridges; internal agarose bridges consisting of 8 mm glass tubes filled with 2% agarose (Sigma-Aldrich, cat. no. A7002) connected the chambers and reservoirs filled with phosphate buffered saline (PBS), and main ion concentrations inside bridges were around: Na^+ (160.57 mM), Cl^- (155.17 mM), K^+ (1.54 mM), PO_4^{3-} (4.24 mM) without calcium and magnesium

ion. Moreover, a silver electrode was used to fabricate the Ag/AgCl electrode due to its stability and reversibility (Nilaco Corp., AG-401325) [22]. The cell culture chamber was composed of cover glass slides, with four small chambers on one slide (IWAKI, cat. no. 5222-004), suitable for cell attachment and convenient and high resolution for the observation of cell morphology. The small chamber size was 10 × 20 × 10 mm (width × length × height) filled with 1.2 ml of the culture medium. Each small chamber was used for one treatment, where one small chamber was selected for the stimulated group, one for the control group, another two were not used.

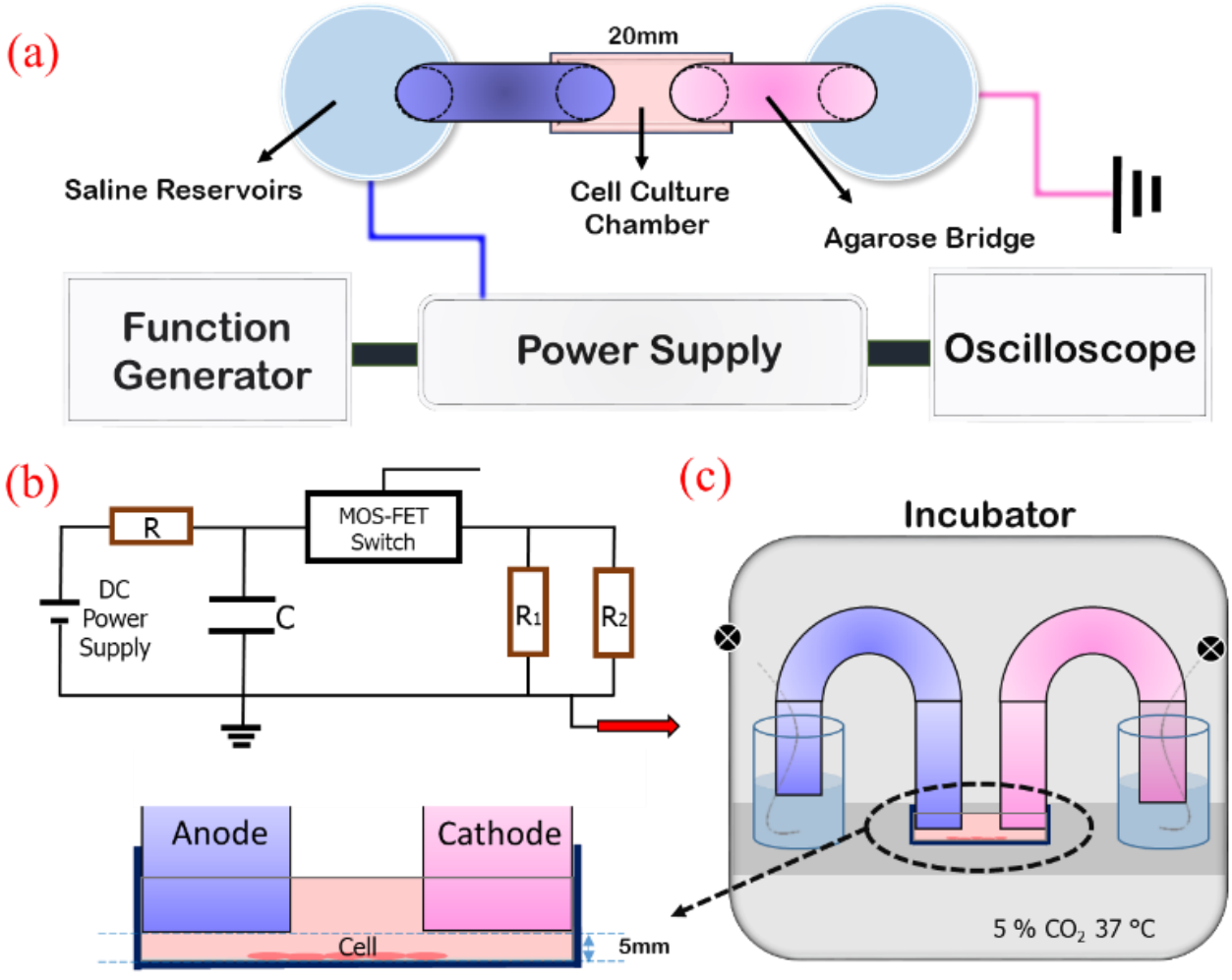

Figure 2.1 (a) The schematic illustration of cell culture stimulation system. (b) Power supply circuit (supplied the nsPC). (c) Side view of the system inside the incubator.

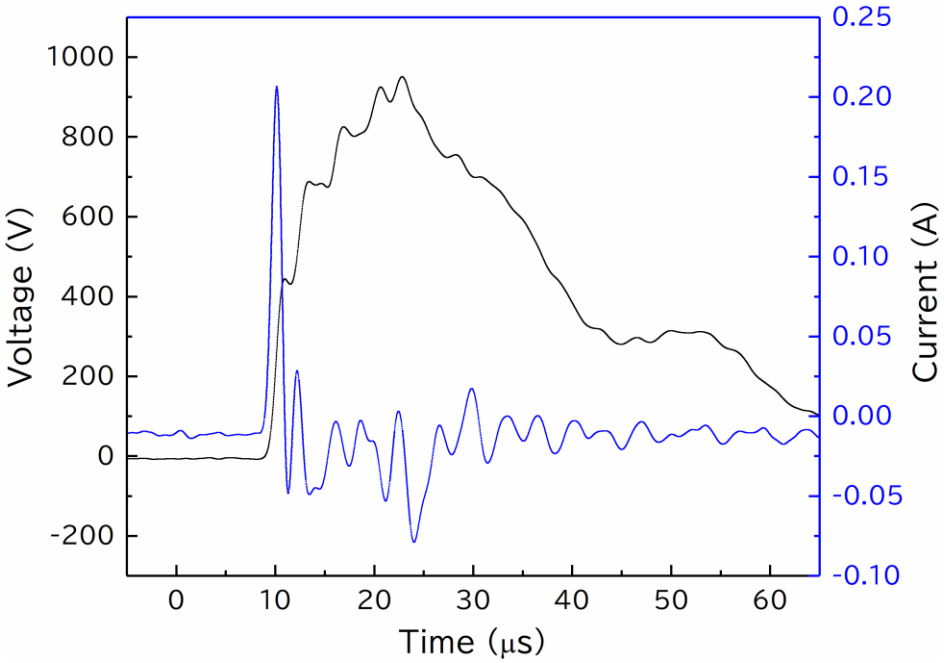

Figure 2.2 The waveform of voltage and current.

(The rising time for the nsPC to increase from 10% to 90% was less than 10 ns)

Great numbers of research on cell stimulation have been carried out via DC and AC using electrotactic systems. We selected the nsPC as our research point since this could not only stimulate cells for ultra-short duration time but also discharge streamer. The power supply was designed and constructed by our laboratory, and the electrical circuit is given in Figure 2.1 (b). The function generator (NF, WF1974) was providing the signal for nsPC generation, set the burst mode at a frequency of 100 Hz, 33.333% duty. Figure 2.2 is the waveform of the voltage and current measured by the oscilloscope (Teledyne LeCroy, WaveSurfer 104MXs), presented that the maximum voltage was 990–1000 V (the duration time was around 800 ns) and the maximum current was 200–220 mA (the duration time was around 200 ns). To be mentioned, the rising time for the nsPC to increase from 10% to 90% was less than 10 ns.

Keeping a stable temperature and suitable pH value during electrical stimulation in the culture medium is essential for cell cultivation. As such, these parameters were monitored in various experimental conditions for several hours while applying the nsPC. During treatments, pH value and temperature were maintained in acceptable range, according to three tests carried out for all conditions, including the control sample without stimulation, as shown in the Figure 2.3 (a) and (b). Temperature plays a critical role in cell culture, also suggests that temperature was controlled due to the negligible joule heating effect in each test, where slightly increased were caused by the incubator (37°C). The pH was also maintained. Moreover, as time increases, pH levels decline as a result of CO_2 dissolution inside the culture medium to around pH 7, which is suitable for cell growth. It is worth mentioning that the pH value was lower in the stimulated groups. The reason for this might be agarose gel (pH 7.2) decomposition for long-term treatments. Hence, for every experiment, treatment times were kept under 24 hours.

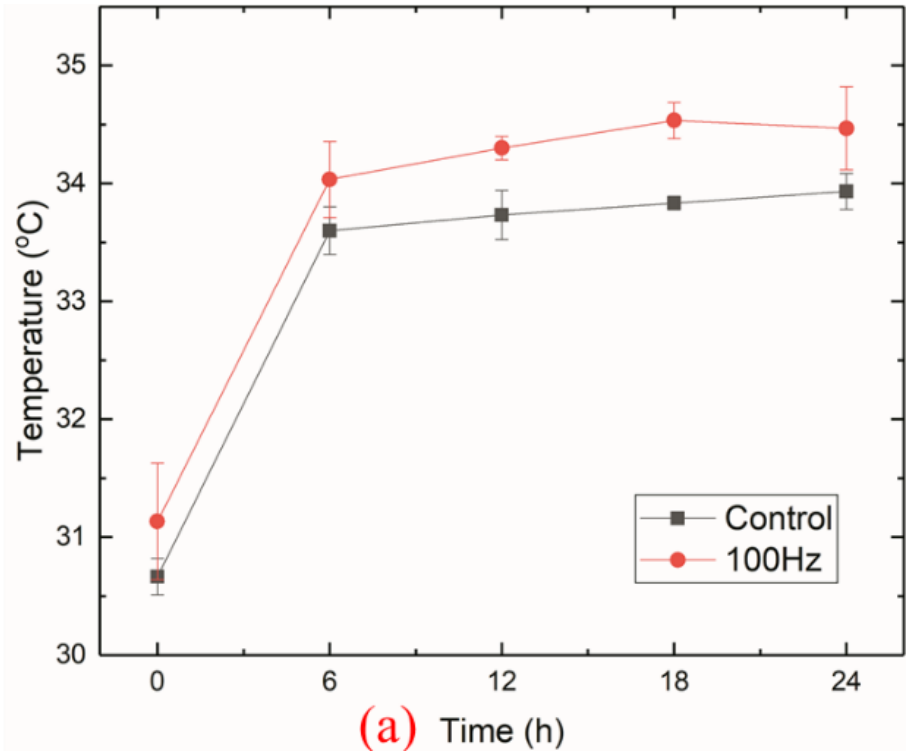

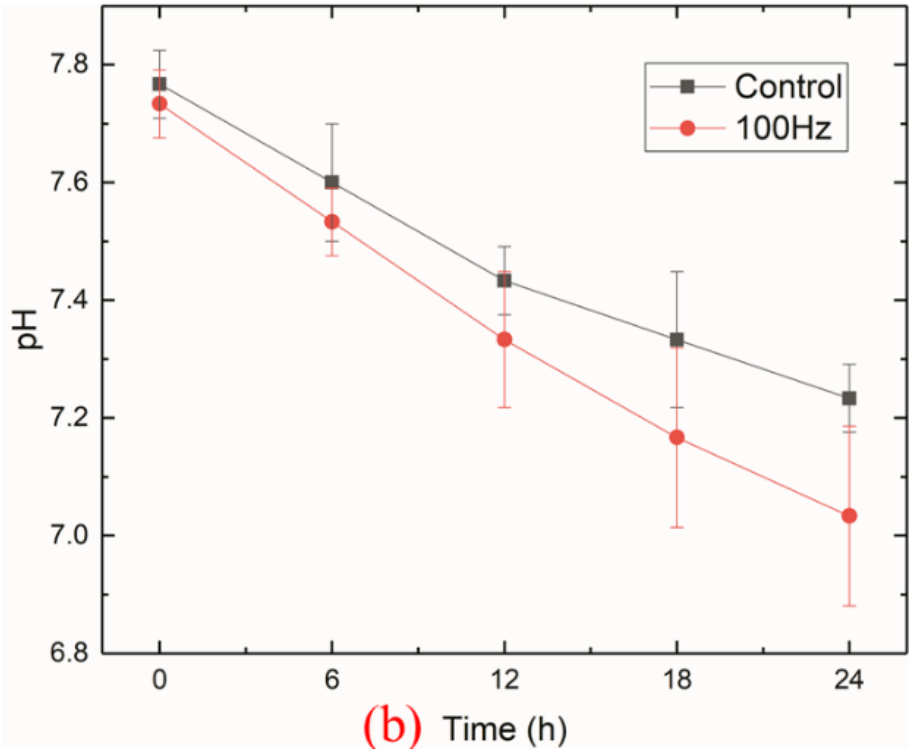

Figure 2.3 (a) Temperatures changed in the chambers. (b) pH values changed in the chambers.

Temperatures at time 0 were slightly lower than during the rest of the time course because the incubator door was kept open for setting up the chambers.

2.2.3. Measurement for cell activity

To observe the cell activity under various conditions, we investigated cell morphology, migration, and viability. Cells were counted by an automated cell counter (Thermo Scientific, AMQAX1000) for cultivating specific numbers and checking the viability before specimen preparation. After all treatments, cell count reagent SF (Nacalai Tesque, cat. no. 07553-15), allowed sensitive colorimetric assays by utilizing highly water-soluble tetrazolium salt (see Appendix C), were used to obtain the double validated data by the microplate reader (Thermo Fisher, Multiskan FC) to match with the automated cell counter data.

An Axio Observer D1 inverted microscope equipped with Axio Observer D1 software (Carl Zeiss) was used for fluorescence and differential interference contrast (DIC) microscopy. Captured images were

analyzed by use of Zeiss Blue and ImageJ software. Furthermore, cell stains, Hoechst 33342 (Wako, cat. no. 346-07951), MitoRed (Wako, cat. no. 344-08851), and SytoX green nucleic acid stain (Thermo Scientific, cat. no. S7020), were used to and calculate viability and observe intracellular organelles via fluorescence.

2.2.4. Cell treatment

For cell stimulation, we prepared two types of treatments to investigate cell activity, as shown in Figure 2.4. In type A: cell migration, the culture-insert (ibid, cat. no. ib80209) was placed inside the chamber. One insert owned two wells, and each well was seeded with 1×10^6 cells/mL for 12 hr incubation to create a 500 ± 50 μm gap between two wells. Nevertheless, type A is the simplest method to observe cell migration, it was difficult to observe individual and clear whole cell shape. As such, in type B: cell morphology, random cells were seeded in the central chamber

with less concentration (1×10^5 cells/mL). The cells were stood for 4 hr while they fell to the bottom before treating with various conditions. DIC microscopy was used to observe cell morphology in different resolutions. Finally, two types of cells were dyed with stains. A fluorescence microscope was used to observe the living/dead cell nuclei (blue fluorescence after staining with Hoechst 33342), the death cell nuclei (green fluorescence after staining with SytoX green), and the mitochondria (red fluorescence after staining with MitoRed). This allowed us to quantify the numbers of living or dead cells and calculate the graph of cell survival rate, as well as approximately estimate cell size and the area occupied in type A using Image J analysis (National Institutes of Health, Bethesda, MD).

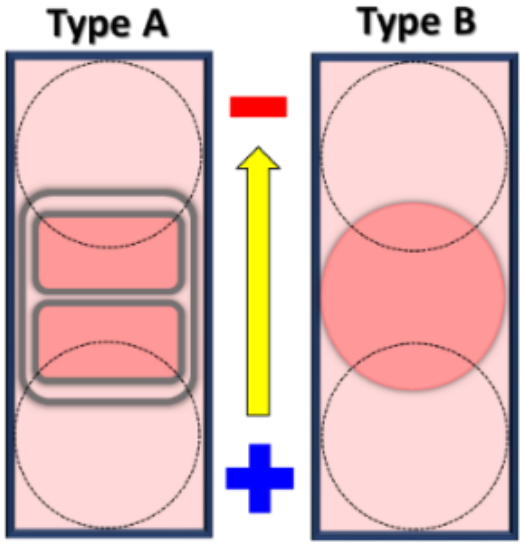

Figure 2.4 (Left) Type A for cell migration with the culture-insert inside the small chamber. (Right) Type B for cell morphology inside the small chamber with random cells seeding.

2.2.5. Immunofluorescence

The immunofluorescence protocol has several steps, including fixation, permeabilization, blocking, and immunostaining (see Appendix D). The reagents such as paraformaldehyde

phosphate buffer solution (Nacalai Tesque, 09154-14), triton X-100 (Sigma-Aldrich, T8787-50ML), and bovine serum albumin (Wako Pure Chemical, 013-15101) were used for fixation, permeabilization, and blocking, respectively. Rhodamine phalloidin (Amanita phalloides, Cat. PHDR1), with a high affinity to the polymerized form of actin filaments, was used to perform filopodia and lamellipodia preservation for immunostaining.

2.2.6. Statistical analysis

All of the experiments were repeated three times. The data are expressed as the mean ± standard deviation (SD). The differences between groups were analyzed by Student's t-test, where $p < 0.05$ was considered significant.

2.3. Results

Two methods were set up to investigate cellular responses, type A and type B. Each test included a control and stimulated group, and treatments were applied for several hours to elucidate the impact of nsPC on cells.

2.3.1. Cell treatment by Type A (cell migration)

Cell migration were observed to determine whether they effected differently to after serval hours treatments. Cells were seeded in culture-insert overnight to create a gap between the two wells as previously described (Figure 2.5(a)) using the nsPC to stimulate cells for 6, 12, and 24 hr, respectively. This is presented in Figure 2.5, where the blue line denotes the anode side and the red line as the cathode side. After 6 hr, the stimulated group expressed the high rate of movement to

the central chamber, yet we also find that there was no consistent orientation for cell activation compared with other studies using DC. On the contrary, the control group did not show any obvious movement, as shown in Figure 2. 5 (b). After 12 hrs, the cells were found to cover the entire gap area in the stimulated group. In comparison, a gap was still visible in the cells of the control group after 12 hr, and other areas also showed residual voids (Figure 2.5 (c)). After 24 hr, both groups were filled with cells and were not distinguishable by the DIC images (data not shown). To confirm the numbers of cell migration between the gap, we counted the residual amount of cells inside the gap according to the blue and green fluorescence (Figure 2.6). This quantification showed that cells migrated more to central under nsPC stimulation. Moreover, in this result, we were unable to observe the consistency of cell movement in same direction, so ruled out the possibility of electrophoresis from the nsPC.

According to cell migration, there are two possible reasons for the phenotypic changes of the stimulated group, one is increased cell proliferation, and another is individual cell shape expansion. Figure 2.7 indicates that OD density did not change significantly over the course of each treatment, suggesting that cell proliferation was not the cause of the changes od cell migration. The high survival rates of cell viability were the same in both groups, and no significant changed throughout both treatments. Cell viability was determined by the number of nuclei observed in SytoX Green and Hoechst 33342 staining, and the survival rate was determined as follows: [100% – ((SytoX intensity/Hoechst 33342 intensity) × 100%)]. The data were calculated at the same magnification (×5), shown in Table 1. Overall, the nsPC did not cause dissimilar values of cell inactivation or accelerate cell division and proliferation. Thus, to identify another possible explanation, we designed another set of tests.

2.3.2. Cell treatment by Type B (cell morphology)

In the type B, the cells were cultured 4 hr for attachment before each treatment as shown in Figure 2.8. After 6 hr, a small number of stimulated cells were elongated, and an increased number of connections was observed (Figure 2.8 (a)). Whereas, no difference was performed in the control cells in terms of appearance. After 12 hr, cells treated with the nsPC had a larger expanded membrane, were closely aligned to the bottom of the chamber surface, contained an increased number of cell junctions (Figure 2.8 (b)). After 24 hr, a significant increase in area was observed in the stimulated group, where the cells had an elongated morphology and appeared hypertrophy (Figure 2.8 (c)). This suggests that the electrical stimulation enhanced cell body expansion by intracellular functions. Unlike, the control group had a steady growth which was slightly slower than the stimulated group. After treatments, the cells were dyed with multiple stains for 20 min for observation fluorescent images. The intracellular organelles were observed according to blue, red, and green fluorescence (Figure 2.9). Despite there being no large difference in terms of cell size after 6 hr (Figure 2.9 (a)), large numbers of cell connections were observed in the stimulated group which started to expand attachment territory after 12 hr. After 24 hr, cell size was gradually enhanced by nsPC, also the fluorescent intensity of mitochondria enhanced.

Additionally, MitoRed was used to indicate the status of the mitochondria involved in the energy conversion (like, ATP) and storage of calcium ions (Ca^{2+}) in the cells (Figure 2.10). To analyze the proportion of intracellular mitochondria expansion, MitoRed increase area ratio in type B treatment for 6, 12, and 24 hr was calculated by the formula: [stimulated MitoRed area/control MitoRed area], using Image J to select the occupied areas without the Hoechst 33342 stained (blue) area. The data shows a slowly increasing value of the MitoRed increase area ratio after 6 and 12 hrs. Instead, after 24 hr, the value of MitoRed increase area ratio became 1.8, performed dramatically variation. Thus, increasing the numbers or activating mitochondria after electrical stimulation could lead the cells to perform different morphologies.

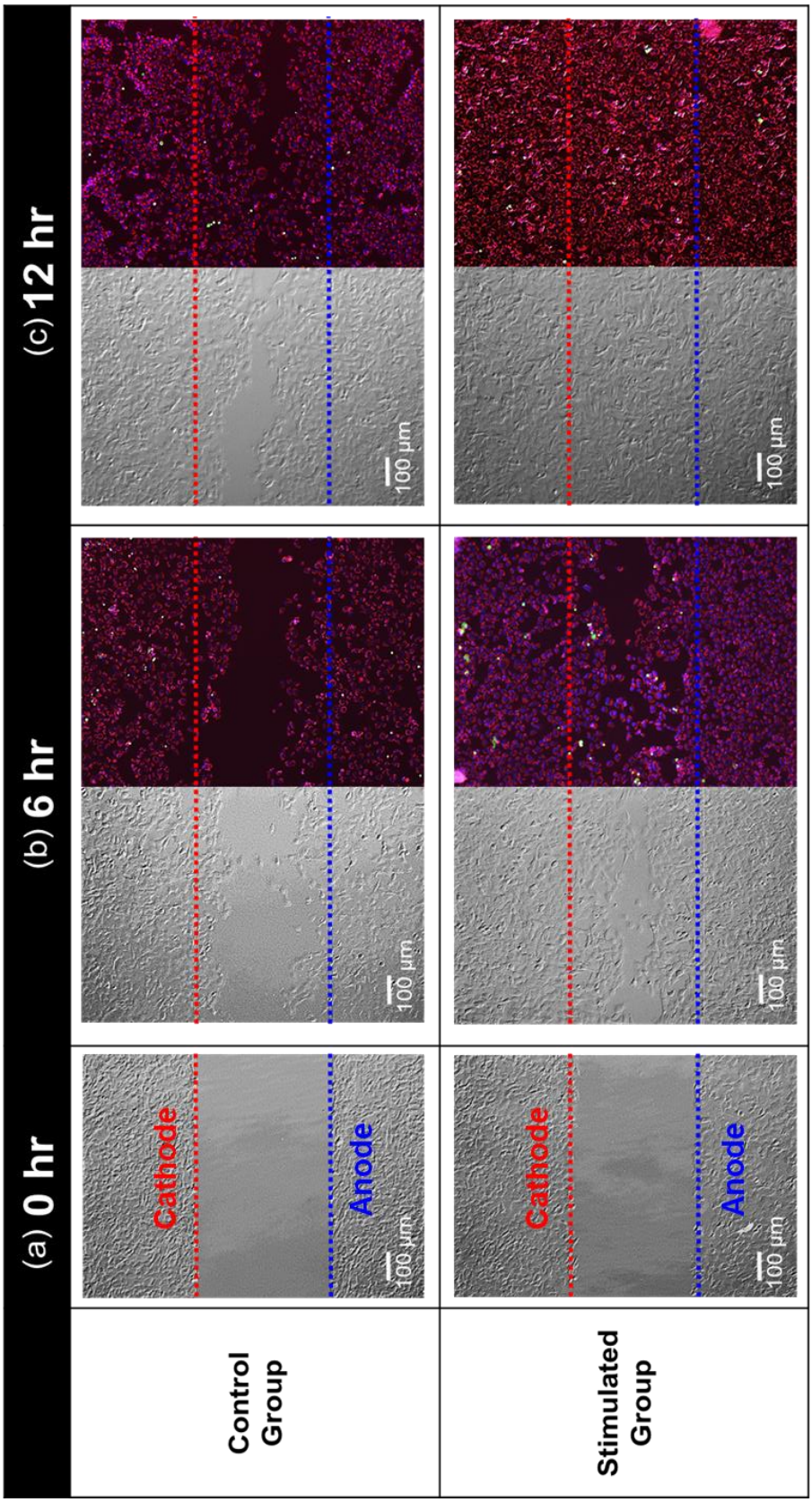

Figure 2.5 Representative time sequence of differential interference contrast images with type A treatment for (a) 6, (b) 12, and (c) 24 hr at ×5 magnification.

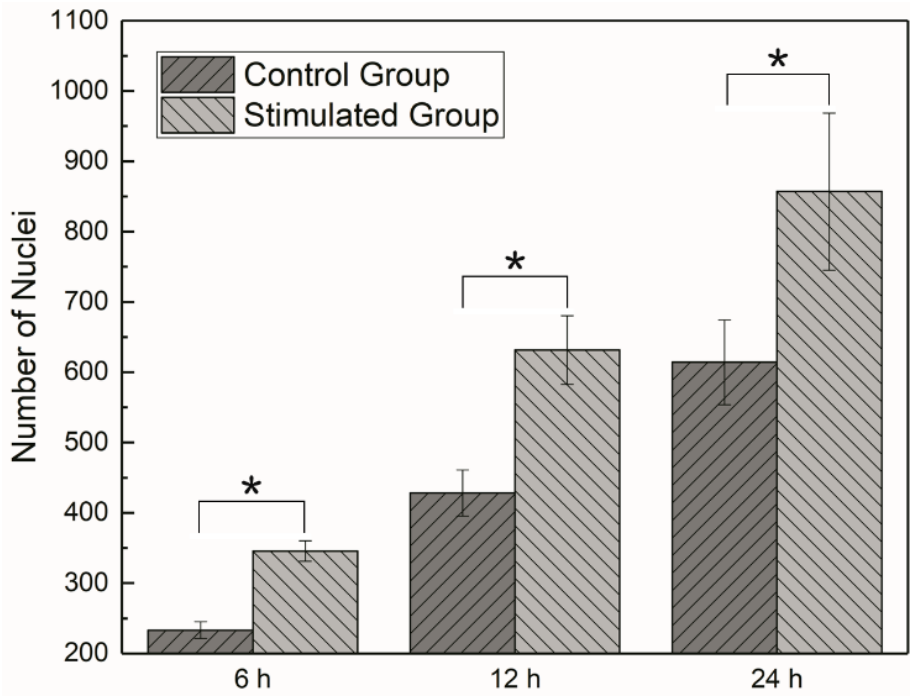

Figure 2. 6 Number of Nuclei inside the gap of type A.

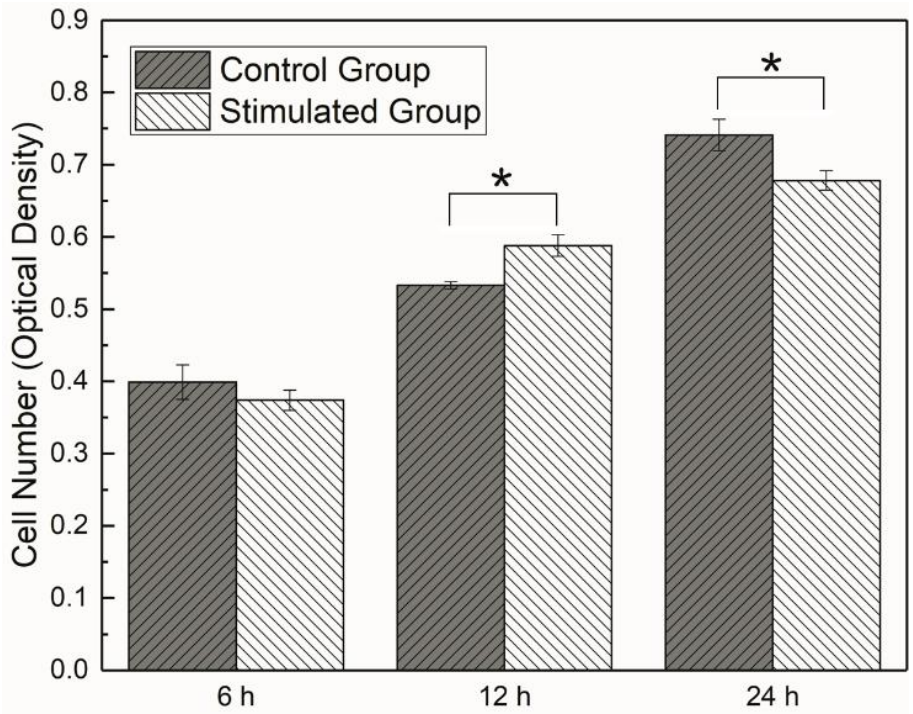

Figure 2.7 Cell number from OD with type A treatment for 6, 12, and 24 hr.

(*$p<0.05$ compared to the control group)

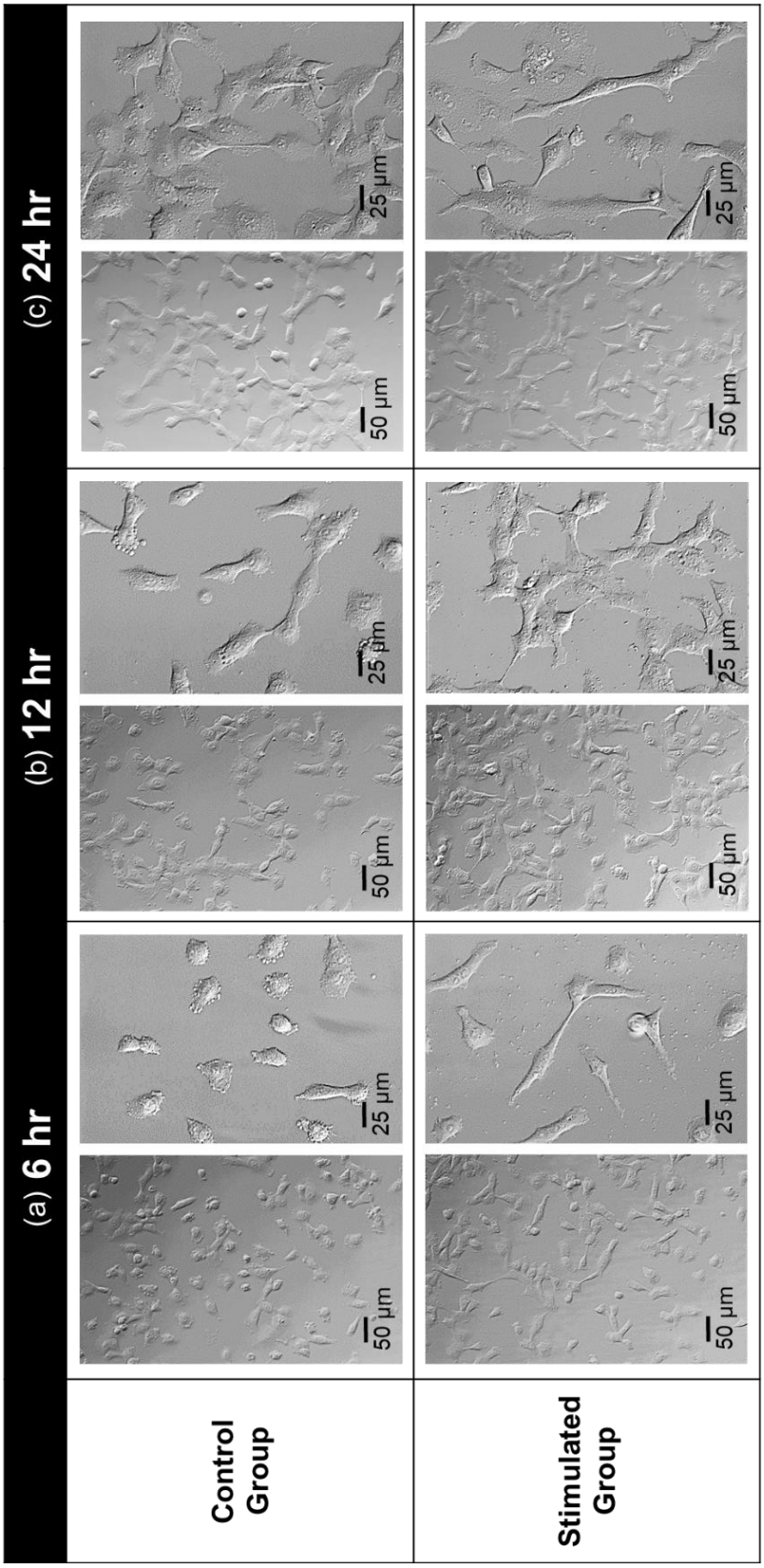

Figure 2.8 Representative time sequence of DIC and fluorescence images with type B treatment for (a) 6, (a) 12, and (c) 24 hr at ×20 magnification.

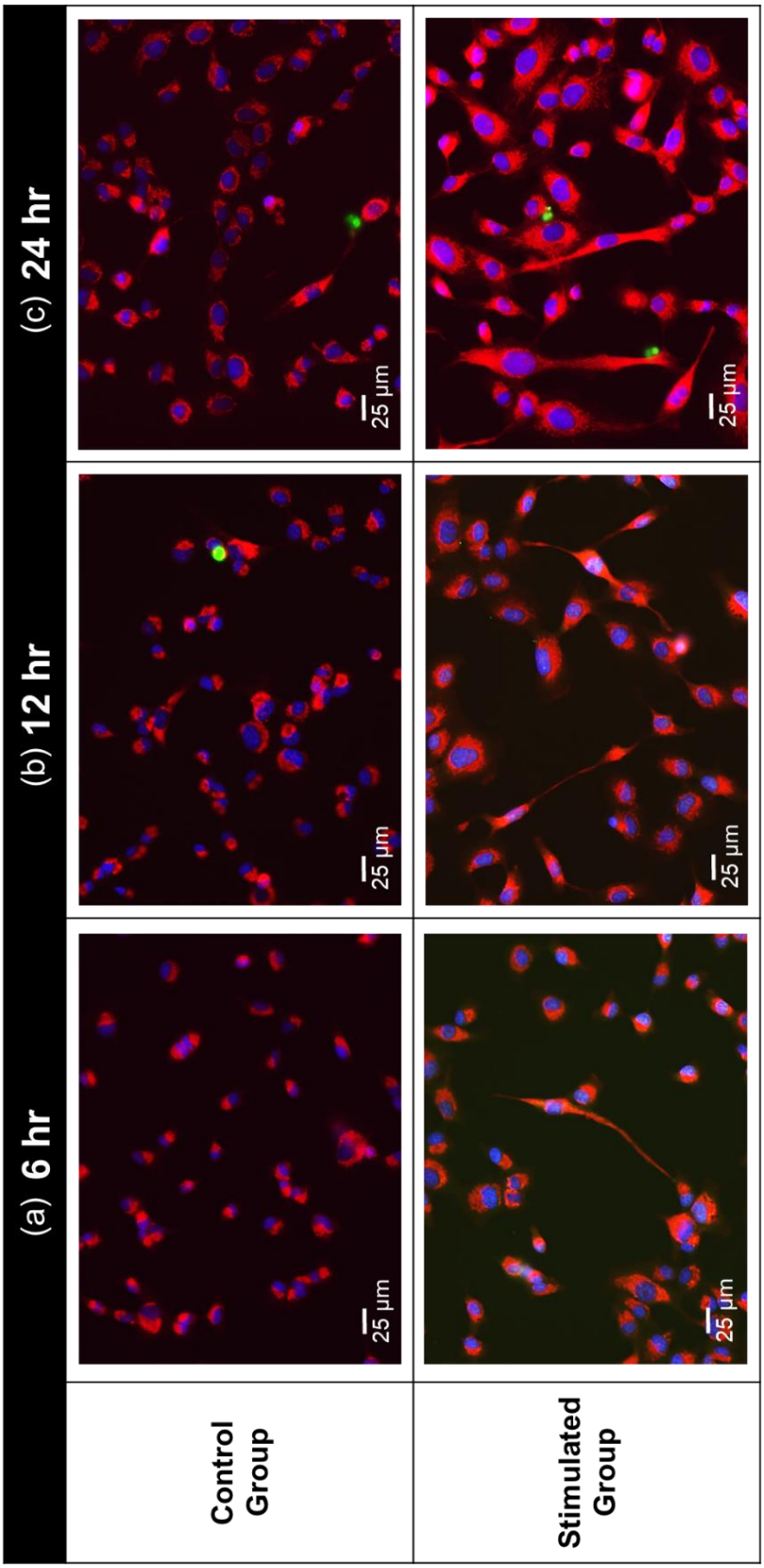

Figure 2.9 Representative time sequence of fluorescence images with type A treatment for after (a) 6, (b) 12, and (c) 24 hr, at ×20 the same magnification.

2.4. Discussions

The nsPC stimulation combined with agarose bridges was created to prevent non-reversible cytotoxic reactions taking place near cells undergoing electrical treatment. In this chapter, the nsPC provides an ultra-short stimulus of less than 1 μs at 100 Hz, so certain mechanisms occurred in DC and AC stimulation would not be applicable, such as the galvanotactic control of cell migration. Unlike the uninterrupted currents of DC and AC, the nsPC could have a beneficial impact on cancer cells, might be control some parts of intracellular functions. In other words, for long period of treatments, the variation of electrical properties in the extracellular environment becomes the crucial factor to further affect cell responses. Our results propose that electrical properties gradually accumulated on cell surface or directly activated intracellular functions over long period.

For cell responses, we set two types of experimental methods to investigate cell migration, viability, proliferation, and morphology. In type A treatment, after 6 hr, the cells inside the stimulated group promoted the process of migration. This was also followed by further expansion after 12 to 24 hrs. In type B treatment, cell attachment started to slightly increase without inactivation after 6 hr stimulation. After 12 to 24 hr, the size of cells increased than those in the control group, providing the explanation why the gap in the stimulated group almost disappeared during type A treatment after 12 hrs. Furthermore, cell proliferation and viability were similar in both treatments. All treatments presented a survival rate of over 90 %, and there was no significant variation in cell numbers after 24 hrs.

Changing in cell shapes led to increase spatial occupation and induce subsequent cell motility from our observation. To be mentioned, no electroporation was found on cell surface or membrane, which is one of the reasons why no cell inactivation was occurred due to the low energy consumption and the ultra-short duration time. In addition, different forms of actin filaments were

observed between the control and stimulated groups after 24 hr (Figure 2.11). It is worth noting that the actin filaments in the stimulated group were reorganized in a similar direction to the outspread cell membrane. Our results also supported that the increasing number of mitochondria could influence actin generation and organization (Figures 2. 10 and 2. 11), which has been previously reported to be involved in cytoskeletal remodeling with [23]. Besides, actin filament growth needs the participation of adenosine triphosphate (ATP), which could be related to mitochondria [24]. Hence, this demonstrates the relationship between mitochondria and actin dynamics. On the other hand, Ca^{2+} flux has been mentioned in several reports, suggesting that the accumulation of intracellular Ca^{2+} could be another mechanism for cell response. Ca^{2+} is presented in the intracellular organelles, endoplasmic reticulum (ER), sarcoplasmic reticulum (SR), or mitochondria, involving in cytoskeletal reorganization. So, we propose that the nsPC might induce the depolarization of cell membrane and the subsequent release of Ca^{2+}. Furthermore, the mitochondria could accumulate Ca^{2+} provided by ER, resulting in gain of ATP and the polymerization of actin filaments. Together, our results provide the potential highlight of nsPC [25,26].

To conclude, our study first focuses on the impact of plasma-supplied nsPC which could cause intracellular reactions to accelerate cell attachment and expansion. As previously stated, the nsPC stimulation did not have any noticeable difference on cell viability and proliferation. Moreover, cell migration and morphological changes were observed in the type A and type B, respectively. Further observing a significant increase in cell migration along with altered cell morphology from reorganizing the actin filaments, providing the novel understanding of nsPC and CAP.

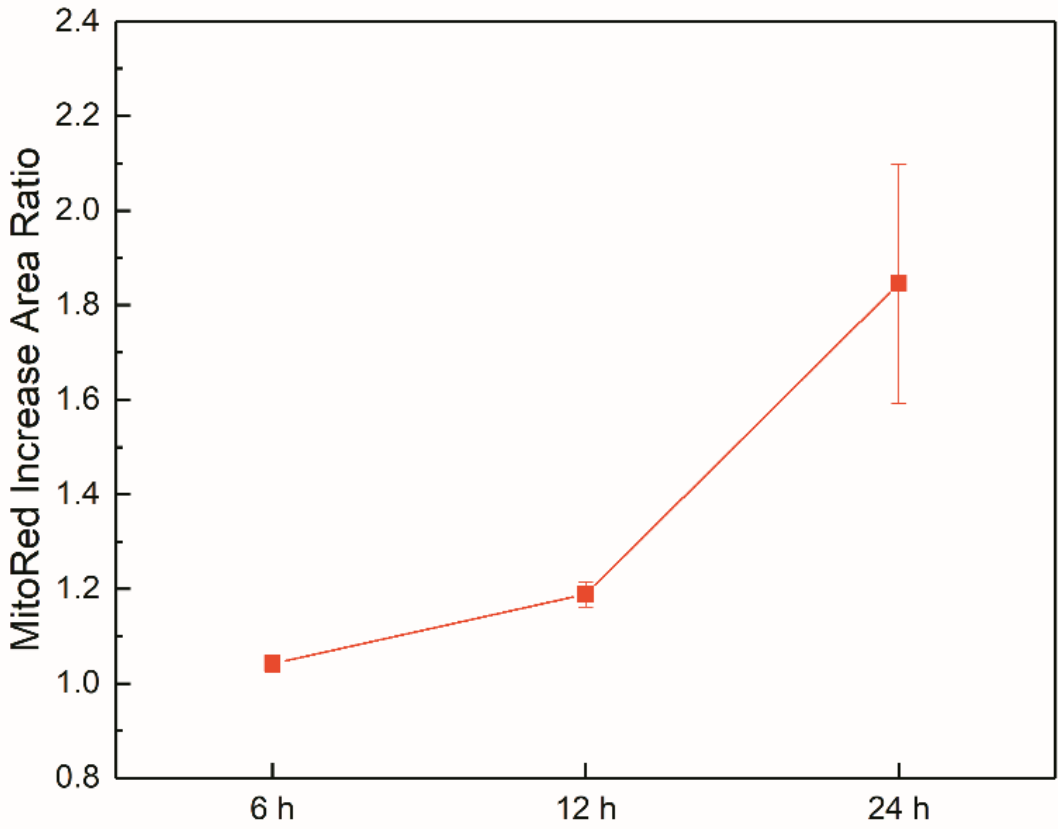

Figure 2.10 MitoRed increase area ratio in type B treatment for 6, 12, and 24 hr.

Table 2.1 Cell viability with type A for 6, 12 and 24 hr treatment.

Percentage (%)	6 h	12 h	24 h
Control Group	94.4 ± 1.5	97.2 ± 0.9	98.3 ± 0.2
Stimulated Group	93.7 ± 0.9	96.7 ± 1.2	98.5 ± 0.8

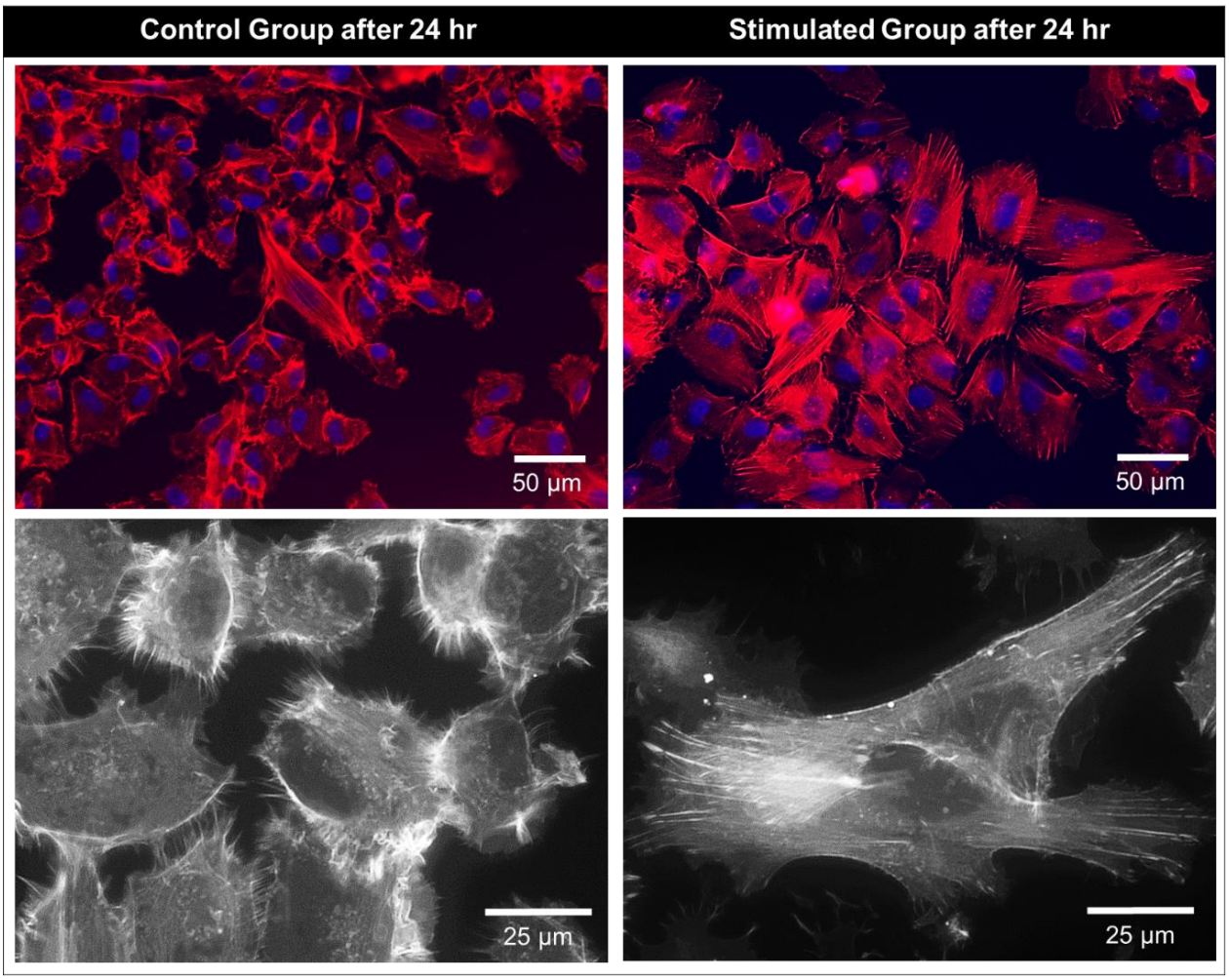

Figure 2.11. Different forms of actin filaments between the control and stimulated group after 24 hr at ×20 (color-type images; blue: DAPI, red: phalloidin) and ×63 magnification (white: phalloidin).

References

[1] M. Jinno, Y. Ikeda, H. Motomura, Y. Kido, S. Satoh, Investigation of plasma induced electrical and chemical factors and their contribution processes to plasma gene transfection, Arch. Biochem. Biophys. 605 (2016) 59–66. doi:10.1016/j.abb.2016.04.013.

[2] B. Song, Y. Gu, J. Pu, B. Reid, Z. Zhao, M. Zhao, Application of direct current electric fields to cells and tissues in vitro and modulation of wound electric field in vivo, Nat. Protoc. 2 (2007) 1479–1489. doi:10.1038/nprot.2007.205.

[3] N. Tandon, B. Goh, A. Marsano, P.H.G. Chao, C. Montouri-Sorrentino, J. Gimble, G. Vunjak-Novakovic, Alignment and elongation of human adipose-derived stem cells in response to direct-current electrical stimulation, Proc. 31st Annu. Int. Conf. IEEE Eng. Med. Biol. Soc. Eng. Futur. Biomed. EMBC 2009. (2009) 6517–6521. doi:10.1109/IEMBS.2009.5333142.

[4] A.K. Dubey, S.D. Gupta, B. Basu, Optimization of electrical stimulation parameters for enhanced cell proliferation on biomaterial surfaces, J. Biomed. Mater. Res. - Part B Appl. Biomater. 98 B (2011) 18–29. doi:10.1002/jbm.b.31827.

[5] N. Tandon, C. Cannizzaro, P.P.-H.G. Chao, R. Maidhof, A. Marsano, H.T.H. Au, M. Radisic, G. Vunjak-Novakovic, 19180087, Nat. Protoc. 4 (2009) 155–173. doi:10.1038/nprot.2008.183.Electrical.

[6] X. Yuan, D.E. Arkonac, P.H.G. Chao, G. Vunjak-Novakovic, Electrical stimulation enhances cell migration and integrative repair in the meniscus, Sci. Rep. 4 (2015) 1–12. doi:10.1038/srep03674.

[7] M. Hronik-Tupaj, D.L. Kaplan, A review of the responses of two-and three-dimensional engineered tissues to electric fields, Tissue Eng. - Part B Rev. 18 (2012) 167–180. doi:10.1089/ten.teb.2011.0244.

[8] K.E. Hammerick, M.T. Longaker, F.B. Prinz, In vitro effects of direct current electric fields on adipose-derived stromal cells, Biochem. Biophys. Res. Commun. 397 (2010) 12–17. doi:10.1016/j.bbrc.2010.05.003.

[9] C.W. Huang, H.Y. Chen, M.H. Yen, J.J.W. Chen, T.H. Young, J.Y. Cheng, Gene expression of human lung cancer cell line cl1-5 in response to a direct current electric field, PLoS One. 6 (2011). doi:10.1371/journal.pone.0025928.

[10] R. Babona-Pilipos, I.A. Droujinine, M.R. Popovic, C.M. Morshead, Adult subependymal

neural precursors, but not differentiated cells, undergo rapid cathodal migration in the presence of direct current electric fields, PLoS One. 6 (2011). doi:10.1371/journal.pone.0023808.

[11] D. Wu, X. Ma, F. Lin, DC Electric Fields Direct Breast Cancer Cell Migration, Induce EGFR Polarization, and Increase the Intracellular Level of Calcium Ions, Cell Biochem. Biophys. 67 (2013) 1115–1125. doi:10.1007/s12013-013-9615-7.

[12] S.J. Pelletier, M. Lagace, I. St-Amour, D. Arsenault, G. Cisbani, A. Chabrat, S. Fecteau, M. Levsque, F. Cicchetti, The morphological and molecular changes of brain cells exposed to direct current electric field stimulation, Int. J. Neuropsychopharmacol. 18 (2015) 1–16. doi:10.1093/ijnp/pyu090.

[13] L. Chopinet, M.P. Rols, Nanosecond electric pulses: A mini-review of the present state of the art, Bioelectrochemistry. 103 (2015) 2–6. doi:10.1016/j.bioelechem.2014.07.008.

[14] T. Batista Napotnik, M. Reberšek, P.T. Vernier, B. Mali, D. Miklavčič, Effects of high voltage nanosecond electric pulses on eucaryotic cells (in vitro): A systematic review, Bioelectrochemistry. 110 (2016) 1–12. doi:10.1016/j.bioelechem.2016.02.011.

[15] J.C. Weaver, K.C. Smith, A.T. Esser, R.S. Son, T.R. Gowrishankar, A brief overview of electroporation pulse strength-duration space: A region where additional intracellular effects are expected, Bioelectrochemistry. 87 (2012) 236–243. doi:10.1016/j.bioelechem.2012.02.007.

[16] D. Xiao, C. Yao, H. Liu, C. Li, J. Cheng, F. Guo, L. Tang, Irreversible electroporation and apoptosis in human liver cancer cells induced by nanosecond electric pulses, Bioelectromagnetics. 34 (2013) 512–520. doi:10.1002/bem.21796.

[17] C. Jiang, R. V. Davalos, J.C. Bischof, A review of basic to clinical studies of irreversible electroporation therapy, IEEE Trans. Biomed. Eng. 62 (2015) 4–20. doi:10.1109/TBME.2014.2367543.

[18] M. Leduc, D. Guay, R.L. Leask, S. Coulombe, Cell permeabilization using a non-thermal plasma, New J. Phys. 11 (2009). doi:10.1088/1367-2630/11/11/115021.

[19] A.G. Pakhomov, S. Xiao, O.N. Pakhomova, I. Semenov, M.A. Kuipers, B.L. Ibey, Disassembly of actin structures by nanosecond pulsed electric field is a downstream effect of cell swelling, Bioelectrochemistry. 100 (2014) 88–95. doi:10.1016/j.bioelechem.2014.01.004.

[20] L. Guo, C. Xu, D. Li, X. Zheng, J. Tang, J. Bu, H. Sun, Z. Yang, W. Sun, X. Yu, Calcium

ion flow permeates cells through SOCs to promote cathode-directed galvanotaxis, PLoS One. 10 (2015) 1–17. doi:10.1371/journal.pone.0139865.

[21] C.C. Wang, Y.C. Kao, P.Y. Chi, C.W. Huang, J.Y. Lin, C.F. Chou, J.Y. Cheng, C.H. Lee, Asymmetric cancer-cell filopodium growth induced by electric-fields in a microfluidic culture chip, Lab Chip. 11 (2011) 695–699. doi:10.1039/c0lc00155d.

[22] M. Grys, Z. Madeja, W. Korohoda, Avoiding the side effects of electric current pulse application to electroporated cells in disposable small volume cuvettes assures good cell survival, Cell. Mol. Biol. Lett. 22 (2017) 1–13. doi:10.1186/s11658-016-0030-0.

[23] B. Cortese, I.E. Palamà, S. D'Amone, G. Gigli, Influence of electrotaxis on cell behaviour, Integr. Biol. (United Kingdom). 6 (2014) 817–830. doi:10.1039/c4ib00142g.

[24] E. Bartolák-Suki, J. Imsirovic, Y. Nishibori, R. Krishnan, B. Suki, Regulation of mitochondrial structure and dynamics by the cytoskeleton and mechanical factors, Int. J. Mol. Sci. 18 (2017) 7–11. doi:10.3390/ijms18081812.

[25] M.J. Berridge, P. Lipp, M.D. Bootman, The versatility and universality of calcium signalling Berridge 2000, 1 (2000).

[26] E. Carafoli, The fateful encounter of mitochondria with calcium: How did it happen?, Biochim. Biophys. Acta - Bioenerg. 1797 (2010) 595–606. doi:10.1016/j.bbabio.2010.03.024.

Chapter 3

Nanosecond pulsed current under plasma-producing conditions induces morphological alterations and cytoskeleton reorganizations in human fibrosarcoma HT-1080 cells

3.1. Introduction

In last chapter [1], we attempted to analyze the significance of electrical properties from nsPC for a better understanding of CAP actions on cancer cells. We developed a novel device, in which cells were indirectly stimulated with nsPC through agarose bridges. The use of this device markedly reduced the contact of RONS with cells and allowed us to analyze biological effects of the electrical factors under CAP-producing conditions. Interestingly, the direction of increased cell movement was random and was not associated with the direction of electric current. This observation suggested that nsPC under the CAP-producing conditions stimulated a certain mechanism for cell motility and led to the activation of cell movement in random directions, instead of one-directional movement guided by electric current [2,3].

HT-1080 cells are known to show two distinct modes of cell motility [4,5]. Cell motility is generally modulated by extracellular stimuli, such as growth factors and mechanical contact to extracellular matrices (EMS). Rho activity is increased by contact with extracellular matrices mediated by integrin [6] and N-cadherin [7], leading to stress fiber formation. Rac is stimulated by growth factors, including PDGF and EGF, and facilitates membrane protrusion formation [8–10]. Cells in mesenchymal motility exhibit fibroblast-like extended cell shape with membrane protrusions that undergo integrin-mediated adhesion [11–13]. Actin-rich protrusions play a critical role in mesenchymal motility and called pseudopodia. The process in which a cell gains the ability for mesenchymal motility is called an epithelial-to-mesenchymal transition and is a critical step for the malignant transformation [14]. Another form of cell motility is amoeboid motility that is accompanied with round cell shape and relatively weak adhesion [15]. In the human body, cancer cells undergo invasion and metastasis by switching these modes of cell motility [16,17]. Both modes of cell motility are driven by actin polymerization, cell adhesion, and act-myosin contraction, which are controlled by intracellular signaling, particularly by Rho family small GTPase members, such as Rho, Rac, and Cdc42. Rho GTPases are key players to regulate the actin cytoskeleton and gene transcription to promote coordinated changes in cell behavior: Rac controls cell protrusion, and Cdc42 modulates cell polarity [18–21]. The Rho family members play critical roles in cell morphology and motility: they regulate the formation of filopodia and lamellipodia through the control of actin polymerization by switching on/off their activities [22,23]. Of note, two modes of cell motility can be induced in HT-1080 cells by use of inhibitors for ROCK, a downstream factor of Rho which suppresses Rho-mediated signal transduction, and Rac1. Intracellular signaling for cell motility can be modulated by other factors, such as reactive oxygen species or calcium ions. For example, superoxide anion derived from the mitochondrial respiratory chain can affect cytoskeleton formation through modulating ERK activity [24,25]. In some reports, variation of

Ca^{2+} is present in organelles, also involved in cytoskeletal reorganization and might be accelerates adenosine triphosphate (ATP) production to occur polymerization of actin [26,27].

Based on these observations in our previous results, we undertook further exploration of the biological action of nsPC under CAP producing conditions in this study. Here, we analyzed morphological features of nsPC-stimulated HT-1080 cells, because it is well established that the status of cell motility frequently manifests as characteristic morphological features. In this chapter, we stimulated HT-1080 cells with nsPC under the CAP-producing conditions and analyzed their morphological alterations. Furthermore, we compared the morphological features of nsPC-stimulated cells with those of two modes of cell motility. We observed that nsPC induced morphological alterations in HT-1080 cells. Common morphological features between nsPC-stimulated cells and those in mesenchymal motility were observed, suggesting the presence of a shared mechanism. Our observations provide further insights into the biological actions of CAP and are important for better medical applications for CAP.

3.2. Materials and methods

3.2.1. Cell culture

Same as previous introduction, the human sarcoma cell line HT-1080 was selected for its suitable characteristics (see Appendix A). Cell suspension was prepared in culture medium at 2×10^5 cells/mL, and a 100 μL aliquot of cell suspension was placed in each chamber. Cells were allowed to attach to the bottom of the slide for 5 hr, and subsequently, 1 mL of fresh culture medium was added to fill a whole chamber, yielding total 1.1 ml medium/chamber.

3.2.2. Stimulation of cells with nsPC

A cell stimulation system was essentially same as described previously, and nsPC at 100 Hz was delivered to chambers on a glass bottom slide through a pair of agarose-bridged electrodes, and cells were prepared on a 4-chamber slide as described above and placed in a humidified atmosphere with 5% CO_2 at 37°C, shown in figure 3.1. A stimulation process was driven by voltage, and the maximum voltage was measured to fall in a range between 980–1050 V with duration time of approximately 800 ns. Duration of pulsed current was estimated to be approximately 200 ns, and our experimental setup achieved rapid rising time of pulsed current (less than 15 ns from 10% to 90% maximum). The maximum pulsed current was estimated to fall in a range between 850–1000 mA, which was five-times larger than that in our previous study (200 mA), shown in figure 3.2. Furthermore, we confirmed that not only the nsPC but also the voltage inside the chamber slide were nearly constant. Hence, we focused on the influence of nsPC, but not electrical field, in this study. During treatments, we also confirmed the pH value and temperature to be suitable cultivated circumstance. After 24 hours, the control group kept in pH 7.5 and 35.4°C, the stimulated group kept in pH 7.1 and 36.8°C, also the conductivities were measured as 9.57 mS and 13.56 mS, respectively. Despite of pH and conductivity in this two groups are slightly different, we could not detect chemical concentrations varied including H_2O_2, NO_2^-, and NO_3^-.

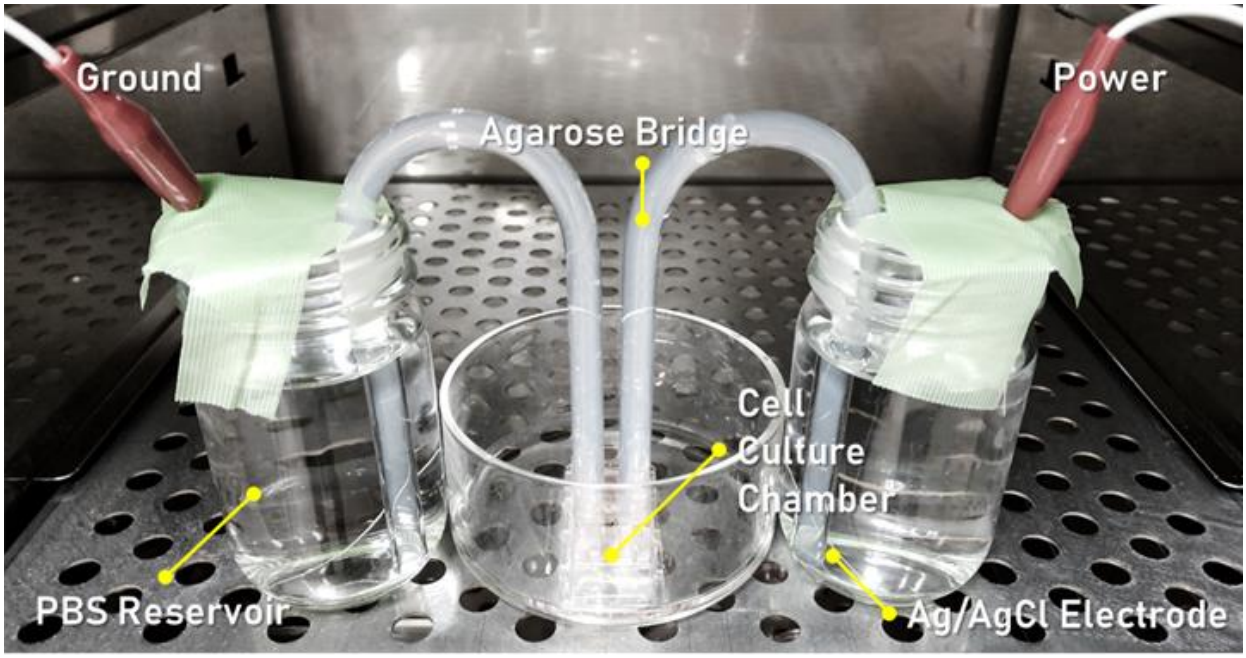

Figure 3.1 The photograph of cell stimulation system.

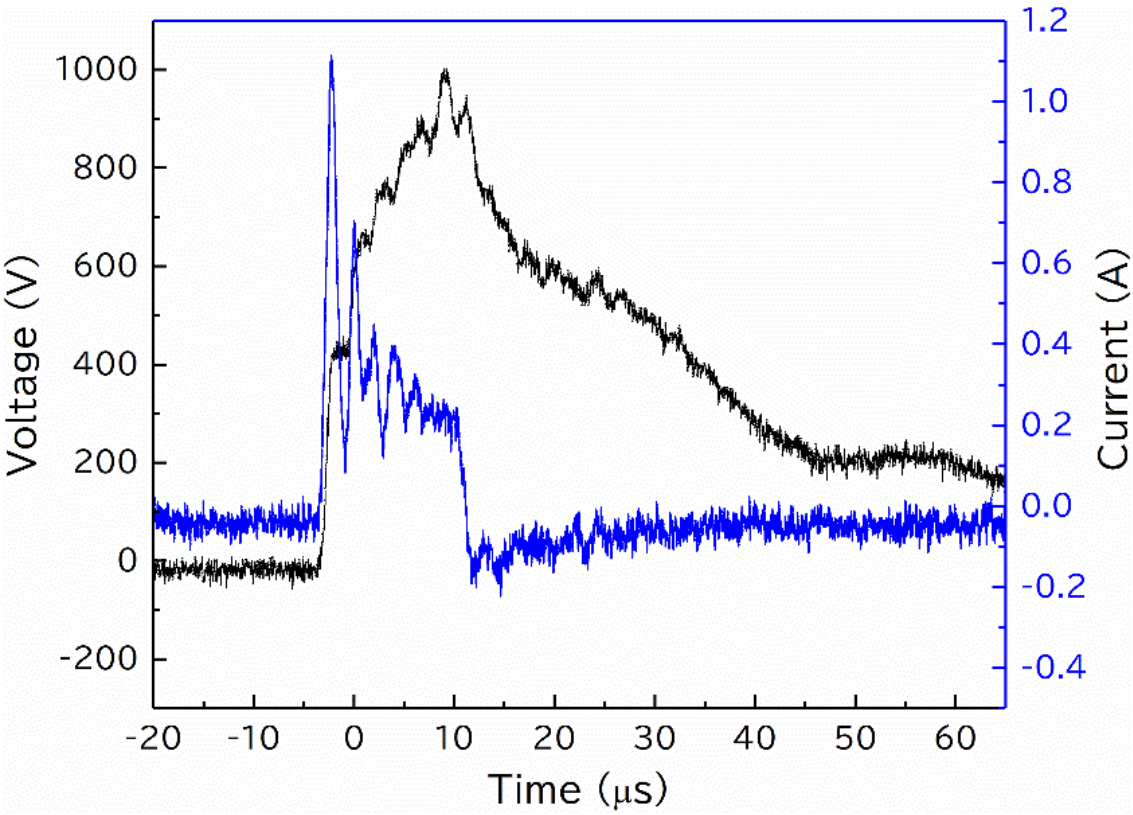

Figure 3.2 The waveform of voltage and current.

(The rising time for the nsPC to increase from 10% to 90% was less than 10 ns.)

3.2.3. Cell staining

As previous description, cells were stained with 1 μg/ml Hoechst 33342 and 1 μg/ml propidium iodide for analysis of cell viability. FluoVolt loading solution (10 μM, Invitrogen, cat. no. F10488) was used for analyzing cell morphology and size from fluorescent membrane. Fluo-4, AM (10 μM, Thermo Fisher Scientific) is for intracellular calcium indicator (green fluorescence). Generation of intracellular ROS is detected by 2',7'-Dichlorofluorescin diacetate (DCFH-DA, 10 μM, Sigma-Aldrich), which is primary for H_2O_2 (green fluorescence). Dihydroethidium (DHE, 10 μM, Sigma-Aldrich) is a $O_2^{\bullet -}$ detector (red fluorescence). (see Appendix G)

3.2.3. Immunostaining

For immunofluorescence of α-Tubulin, cells were fixed in 4% paraformaldehyde dissolved in phosphate-buffered saline (PBS) for 20 min at 4°C. After brief treatment with 0.2% Triton X-100 for membrane permeabilization, cells were blocked with 2% bovine serum albumin solution and subsequently reacted with an antibody against α-Tubulin (Sigma-Aldrich). After washing with PBS, cells were incubated with goat anti-mouse IgG-Alexa Fluor488 (Thermo Fisher Scientific) and mounted in a Vectashield mounting medium with DAPI (Vector Laboratories, CA, USA). For analysis of stress fiber formation, rhodamine-labeled phalloidin (Cosmo Bio, Tokyo, Japan) with a high affinity to the polymerized form of actin filaments was used. (see Appendix D)

3.2.3. GTPases inhibitors

Rho inhibitor, Y-27632 (5 μg/ml, ENZO Life Sciences, cat. no. ALX-270-333-M001), is a cell-permeable to inhibit the Rho-associated, coiled-coil containing protein kinase (ROCK); Rac

inhibitor, NSC-23766 (5 µg/ml, ENZO Life Sciences, cat. no. ENZ-CHM116-0005), is a cell-permeable and selective Rac1 inhibitor.

3.2.4. Microscopy and image analysis

Using an Axio Observer D1 inverted microscope equipped with Zeiss Blue software (Carl Zeiss) to capture fluorescence and differential interference contrast (DIC) microscopy, then analyzed by use of ImageJ software. To analyze effects of nsPC on cell morphology, length and width of a single cell were measured using ImageJ. Cell shape was categorized into 3 groups based on a ratio of length to width, which was termed "elongation index" in this study. Cells with 3 or larger elongation indices were considered to exhibit "elongated" cell shape. Cells with 2 or less indices were regarded as "round" cells. Cells with indices between "elongated" and "round" were classified into "intermediate". For quantitative comparison of fluorescent signals between nsPC-stimulated and untreated cells, images were captured under the same exposure conditions. Fluorescence signals in 8-bit color were converted into a gray scale and quantified by use of ImageJ (see Appendix E).

3.2.5. Statistical analysis

All experiments were repeated at least three times. Data were expressed as mean ± SD. Statistical differences were evaluated by Student's t-test, where $p < 0.05$ was considered to be significant.

3.3. Results

3.3.1. nsPC stimulation caused elongated cell shape and increased size in HT-1080

Cancer cell invasion or metastatic needs self-transformation involving morphological alterations such as pseudopodial protrusion and the formation of invadopodia. Therefore, to understand the cancer motility transition is tracking cell shape with various conditions. In the previous chapter, we found that nsPC promoted the migration of HT-1080 cells. Therefore, to obtain insights into nsPC actions on human fibrosarcoma cells, we analyzed morphological characteristics of nsPC-stimulated cells at higher intensity in comparison with unstimulated control cells.

First, we assessed the effects of nsPC on cell viability. Cells were stimulated with 1000 mA nsPC at 100 Hz for 24 hr and stained with Hoechst 33342 and propidium iodide. As judged by propidium incorporation into the nucleus, 93% of both nsPC-stimulated and control cells were viable and no significant variation in cell numbers and any visible electropore on cell membrane from DIC images during 24 hours observation, indicating that nsPC stimulation under the current experimental conditions did not significantly affect cell viability (Figure 3.3 a, b). Next, we stained cells with FluoVolt, a membrane potential indicator [28]. As shown in Fig. 3.3 c, intensities of green fluorescence were indistinguishable between nsPC-stimulated and control cells, demonstrating that nsPC stimulation did not affect the membrane potential. Interestingly, FluoVolt staining clearly illuminated the cell edge and thus highlighted the morphological differences between nsPC-stimulated and control cells (Figure 3.3 c). We observed that nsPC-stimulated cells had many cell protrusions, such as spider-like elongation and filopodia-like structure (marked with yellow arrowhead), yet unstimulated cells appeared round-like and nearly no connection.

Next, we analyzed the effects of nsPC on cell shape. HT-1080 cells displayed a mixed morphology (both elongated and round cells), to investigate two groups variation, we distinguished three morphology type as elongated, intermediate and round (see method: microscopy and image analysis). From figure 3. 4, after 24 hours, without nsPC stimulation still remained about 74 % round morphology, and only 10 % cells transformed to elongated type, with 16 % intermediate type remained. In contrast, 61% cells with nsPC stimulation changed to elongation, and around 19 % in round shape, and intermediate type still had 20%. Furthermore, we calculated cell area after 6, 12 and 24 hours. The results shown in Figure 3.5 indicate that was no significant different between two groups in first 12 hours, but the cell area with nsPC stimulation increased to 1.35 times larger than without after 24 hours. Thus, during 12 to 24 hours stimulation could be speeded up cell size and transformed their appearance to invasion mode. nsPC-stimulated cells for 6 and 12 hours were insufficient to bring about obvious effects on the cell surface area. Taken together, the above observations demonstrated that nsPC stimulation of HT-1080 cells exerted profound effects on cell morphology, including protrusion formation, elongated cell shape, and extended cell surface area.

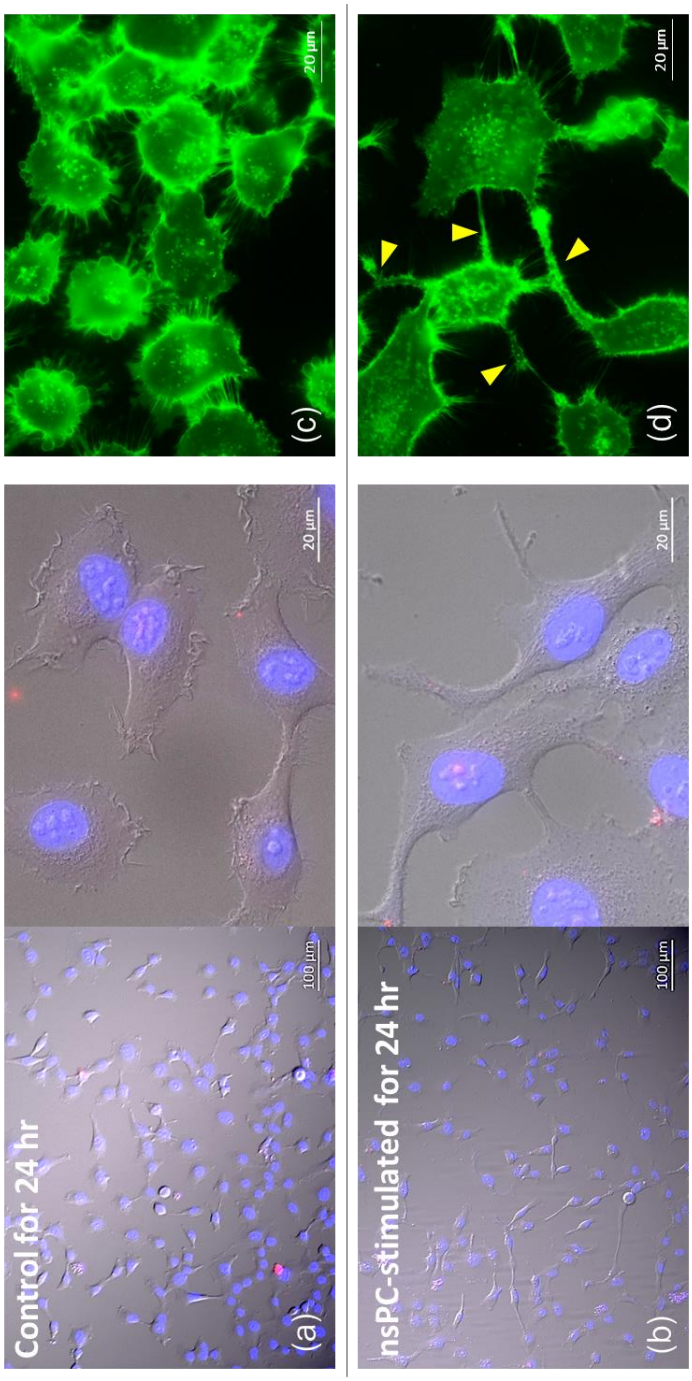

Figure 3.3 Microscopic observations of nsPC-stimulated and control cells.

HT-1080 cells were stimulated with nsPC for 24 hr. In parallel, unstimulated cells were cultured for 24 hr as a control. (a), (b): Cells were costained with Hoechst33342 (blue) and propidium iodide (PI, red). Nuclear staining with PI was judged to be dead cells. Over 93% cells were evaluated to be viable after 24 hr culture in both stimulated and control groups. (c), (d): After 24 hr culture, stimulated and control cells were stained with the membrane potential indicator FluoVolt. nsPC stimulation caused morphological alterations such as spider-like elongation and filopodia formation as shown with yellow arrowheads.

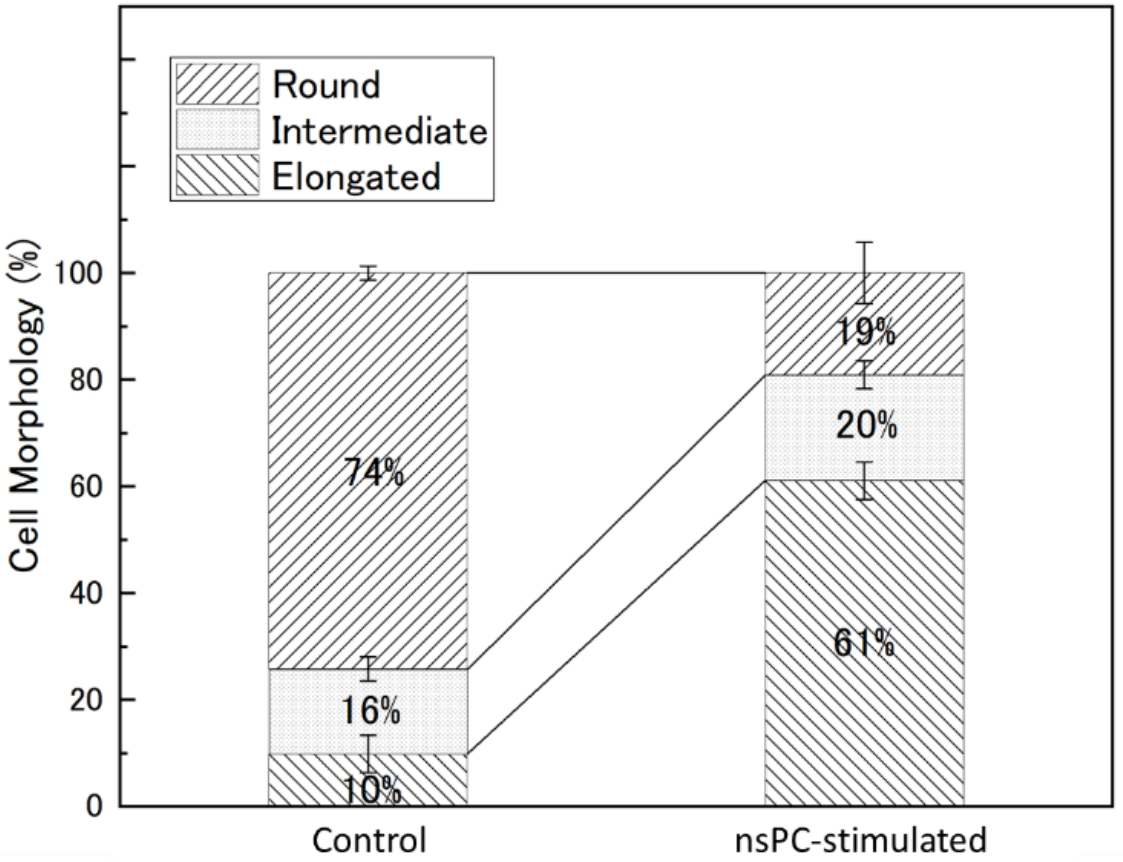

Figure 3.4 Proportion of three cell morphologies in nsPC-stimulated and control cells.

Microscope images of cells were captured after 24 hr culture, and the length and width of individual cells were measured using ImageJ software. According to the ratio of length to width, cell morphology was categorized into 3 groups (Round, Elongated, and Intermediate). 250 cells in a stimulated group or an untreated control group were analyzed. Experiments were repeated three times, and average values with SD are shown.

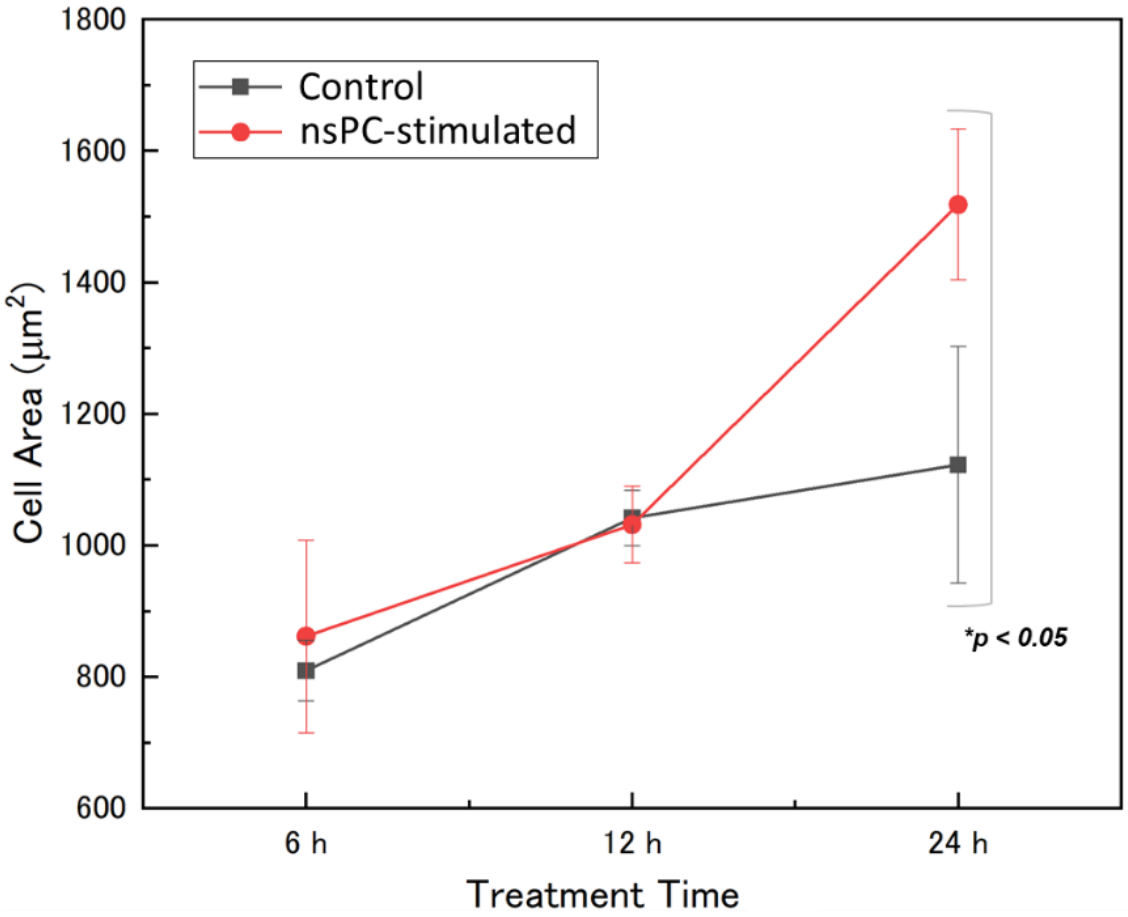

Figure 3.5 Cell surface areas of nsPC-stimulated and control cells.

Microscope images of cells were captured at the indicated time points, and the surface area of individual cells was analyzed by use of ImageJ software. 50 cells in both stimulated and control groups at each time point were analyzed, and experiments were repeated 5 times. The average surface area of stimulated cells at 24 hr was estimated to be 1.35 times larger than that of control cells with statistical significance (*$p < 0.05$).

3.3.2. Effects of nsPC stimulation on intracellular ROS and Ca^{2+} levels

Previous studies have shown that a substantial portion of biological effects of CAP can be attributed to the action of ROS [29,30]. In addition, it is well known that increased levels of cytoplasmic Ca^{2+} affect various cellular activities [31]. To investigate whether ROS or Ca^{2+} is generated by previous treatments, HT-1080 cells were stained with the redox sensitive dye DCFH-DA which is a intracellular ROS detector and cell-permeable compound that is metabolically converted to DCFH in a living cell. When bound to ROS, DCFH emits green fluorescence. DHE emits red fluorescence when oxidized with $O_2{\cdot}^-$. Fluo-4 AM is also cell-permeable and converted to the Ca^{2+}-sensitive green fluorescent dye Fluo-4 in a cell.

First, cells were incubated with these dyes separately, and fluorescence microscopy was performed. We observed strong fluorescence signals for ROS in nsPC-stimulated cells when compared to control cells (Figure 3.6 a, b). Similarly, fluorescence signals for Ca^{2+} in nsPC-stimulated cells were stronger than in control cells (Figure 3.6 c, d). Red fluorescence for $O_2{\cdot}^-$ was no significant difference between nsPC-stimulated and control cells (Figure 3.6 e, f). We next tried to confirm the results of fluorescence microscopy by quantifying the fluorescence intensities of individual cells in the captured images (see method: microscopy and image analysis). Fluorescence intensities for intracellular ROS were estimated to be 0.131 ± 0.005 in nsPC-stimulated cells and 0.102 ± 0.007 in control cells. Superoxide-derived fluorescence was determined to be 0.090 ± 0.007 and 0.092 ± 0.003 in control and nsPC-stimulated cells, respectively. Fluorescence signals for intracellular Ca^{2+} were 0.103 ± 0.019 in nsPC-stimulated cells and 0.077 ± 0.008 in control cells. These quantitative data are summarized in Figure 3.7, which is in good agreement with microscopic observations in Figure 3.6, that is, nsPC stimulation increased the intracellular ROS and Ca^{2+}, but not $O_2{\cdot}^-$.

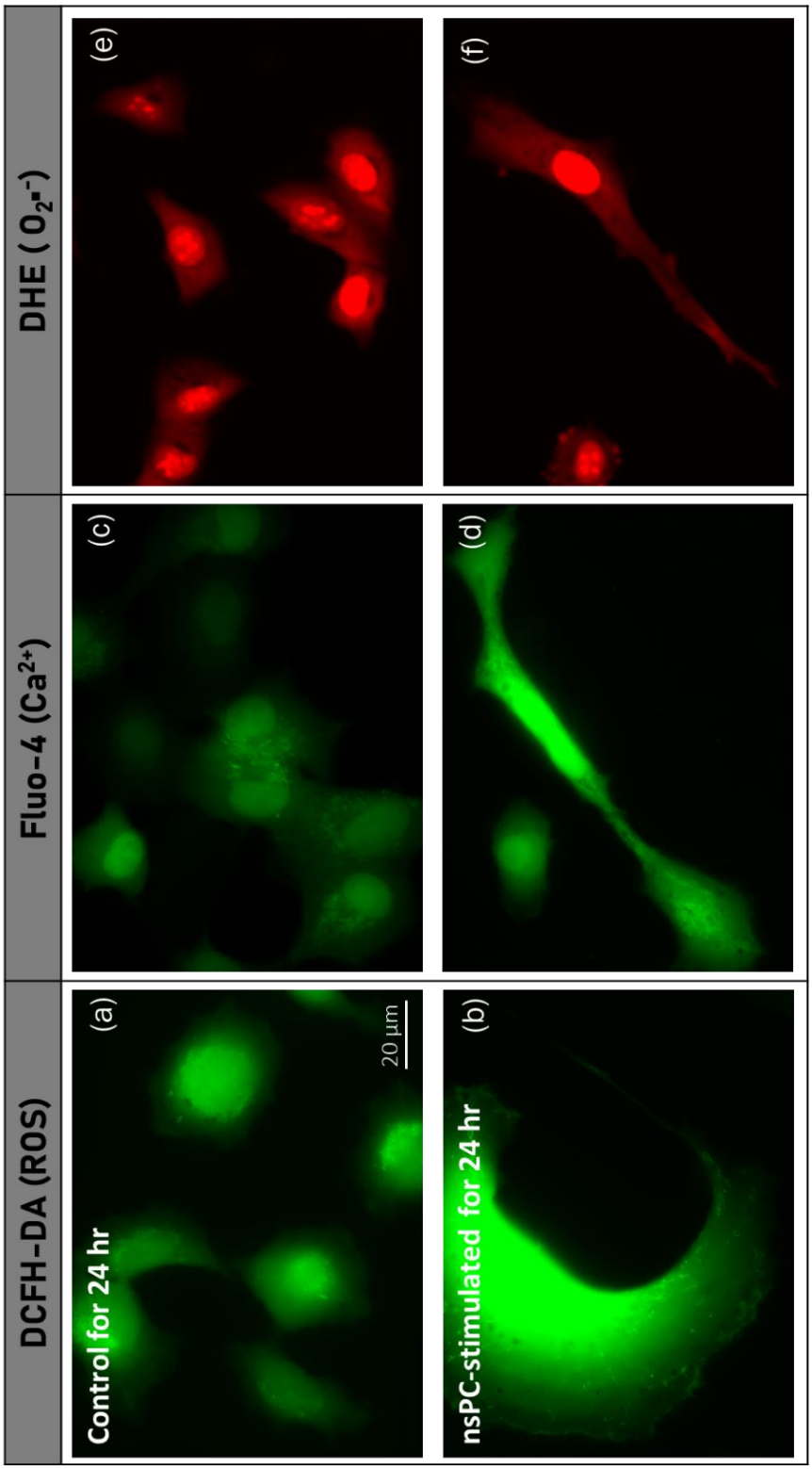

Figure 3.6 Analysis of ROS, Ca^{2+} and $O_2^{\bullet -}$ in nsPC-stimulated and control cells.

nsPC-stimulated cells and untreated control cells were stained with either the ROS indicator DCFH-DA (a, b), the Ca^{2+} indicator Fluo-4 AM (c, d) or the $O_2^{\bullet -}$ indicator DHE (e, f). Typical fluorescence images are shown.

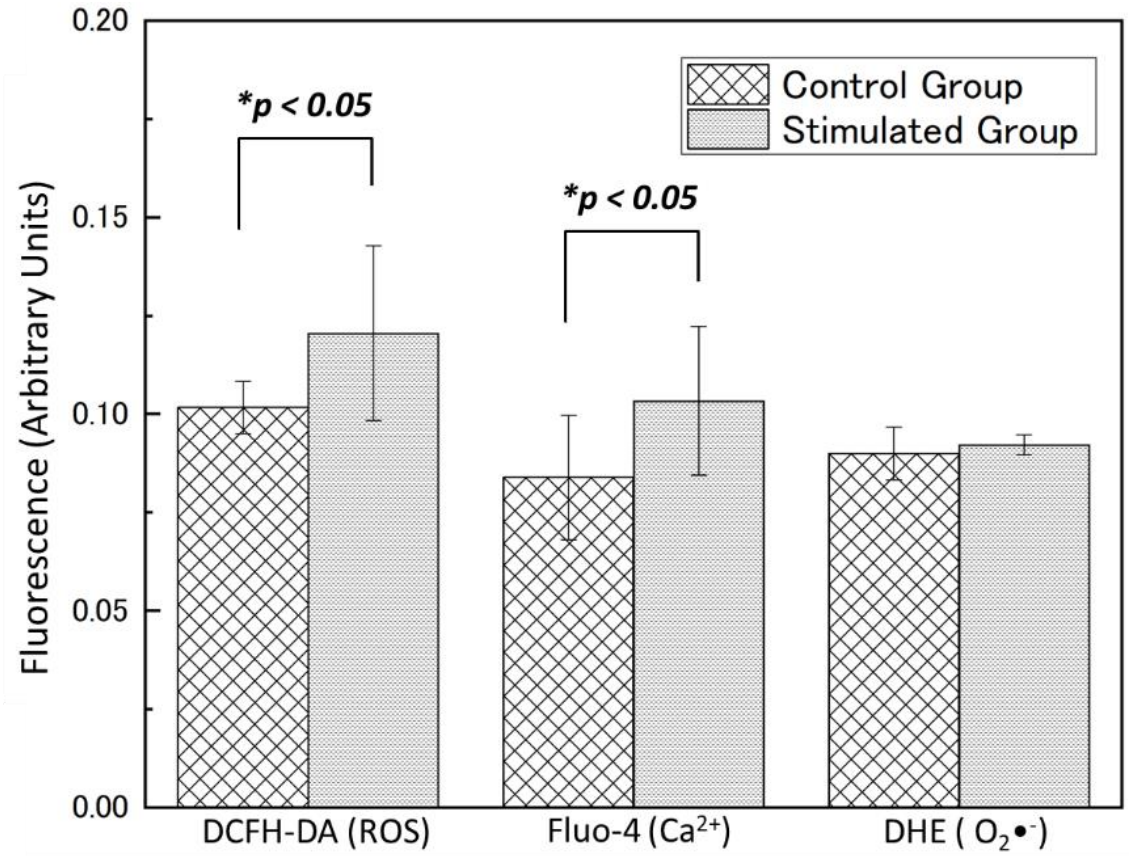

Figure 3.7 Quantitative analysis of intracellular ROS, Ca^{2+} and $O_2^{\cdot -}$ in nsPC-stimulated and control cells.

nsPC-stimulated and control cells were stained with either DCFH-DA, Fluo-4 AM, or DHE for ROS, Ca^{2+}, or $O_2^{\cdot -}$ detection, respectively. Fluorescence images were captured under the same exposure conditions among treatments. Intracellular fluorescence was quantified and expressed in arbitrary unit. 50 cells were analyzed in each treatment, and experiments were repeated 3 times (*p < 0.05).

3.3.3. Possible involvement of intracellular signaling in morphological alterations and stress fiber formation in nsPC-stimulated cells

HT-1080 cells have been widely used to investigate cellular motility, and previous studies have shown that this cell type shows two modes of cell motility, namely mesenchymal motility and ameboid motility. Each mode of motility involves distinct intracellular signaling, and inhibition of one mode of inhibition enforces another mode of motility; more specifically, treatment with a Rho inhibitor induces mesenchymal motility, and Rac inhibitor induces ameboid motility. Last chapter showed that nsPC stimulation (200 mA) increased the motility of HT-1080 cells, and in the present study, we observed that nsPC stimulation (1000 mA) caused altered cell morphology. Our previous observation on nsPC-induced motility and the present observations on nsPC-induced morphological alterations prompted us to compare morphological features of nsPC-stimulated cells to those characteristics of two modes of cell motility.

First, we confirmed the morphological alterations caused by inhibitors for ROCK and Rac1, which are known to induce mesenchymal and ameboid motility, respectively. Each mode of motility manifests as characteristic morphological features that are detectable by microscopy. In general, HT-1080 cells without any extracellular stimuli could randomly appear these two morphologies; however, when the external environment changed, it would induce cancer cells to force in the specific migration. In Figure 3. 8, when cells were treated with the ROCK inhibitor (Y-27632) for 24 hr, we observed characteristics of mesenchymal motility, such as stretched cell shape and extended pseudopodial protrusions; on the other hand, treatment with the Rac1 inhibitor (NSC-23766) led to the alteration of cell shape into ameboid morphology with extensive membrane blebbing. Also, we stimulated cells with nsPC for 24 hr and observed that cells exhibited extended cell shape with pseudopodial protrusions, which closely resembled mesenchymal morphology

induced by the Rho inhibitor, proposing that the increased motility by nsPC in our previous study may be driven by a similar mechanism for mesenchymal motility, despite of less complicated and shorter protrusions compared cells treated with Rho inhibitor.

To gain further insights into the effects of ncPC, we carried out fluorescence microscopy of filamentous actin (F-actin) and microtubles, both of which play important roles in cell morphology as well as cell motility. The nucleus and microtubles were stained with DAPI (blue) and anti-α-tubulin antibody (green), respectively. F-actin was visualized with rhodamine-labeled phalloidin (red), which binds to F-actin, but not to actin monomers. As shown in Figure 3.9, we observed obvious differences in F-actin distribution among nsPC-stimulated and drug-treated cells. Cells treated with the Rac1 inhibitor had round cell shapes with multiple blebs, and strong signals for F-actin were detected in the blebs as the ameoboid migration which present a non-oriented movement by contraction of the cell body (Figure 3.9 d). On the other hand, nsPC-stimulated and ROCK inhibitor-treated cells had extended cell shapes without blebbing. In nsPC-stimulated cells, strong signals for F-actin were detected in pseudopods (Figure 3.9 b). To be noticed, ROCK inhibitor-treated cells owned the longest and most complex protrusion, also there were small nodes in the extremely long pseudopod, but no obvious stress fibers (Figure 3.9 c).

During cell migration, the actin cytoskeleton should dynamically be remodeled, so reorganization of F-actin could be expected to occur in different stimuli. Thus, for obtained more information about cytoskeleton, we converted images into black/white type to investigate intracellular details and carried out high-resolution imaging of F-actin (Figure 3.10) and observed remarkable formation of stress fibers after nsPC stimulation for 12 hr. In addition, a large number of stress fibers were formed in the peripheral areas of nsPC-stimulated cells, but not in control cells. These observations suggest that nsPC stimulation promoted stress fiber formation, presumably leading to the increased cell motility observed in our previous study.

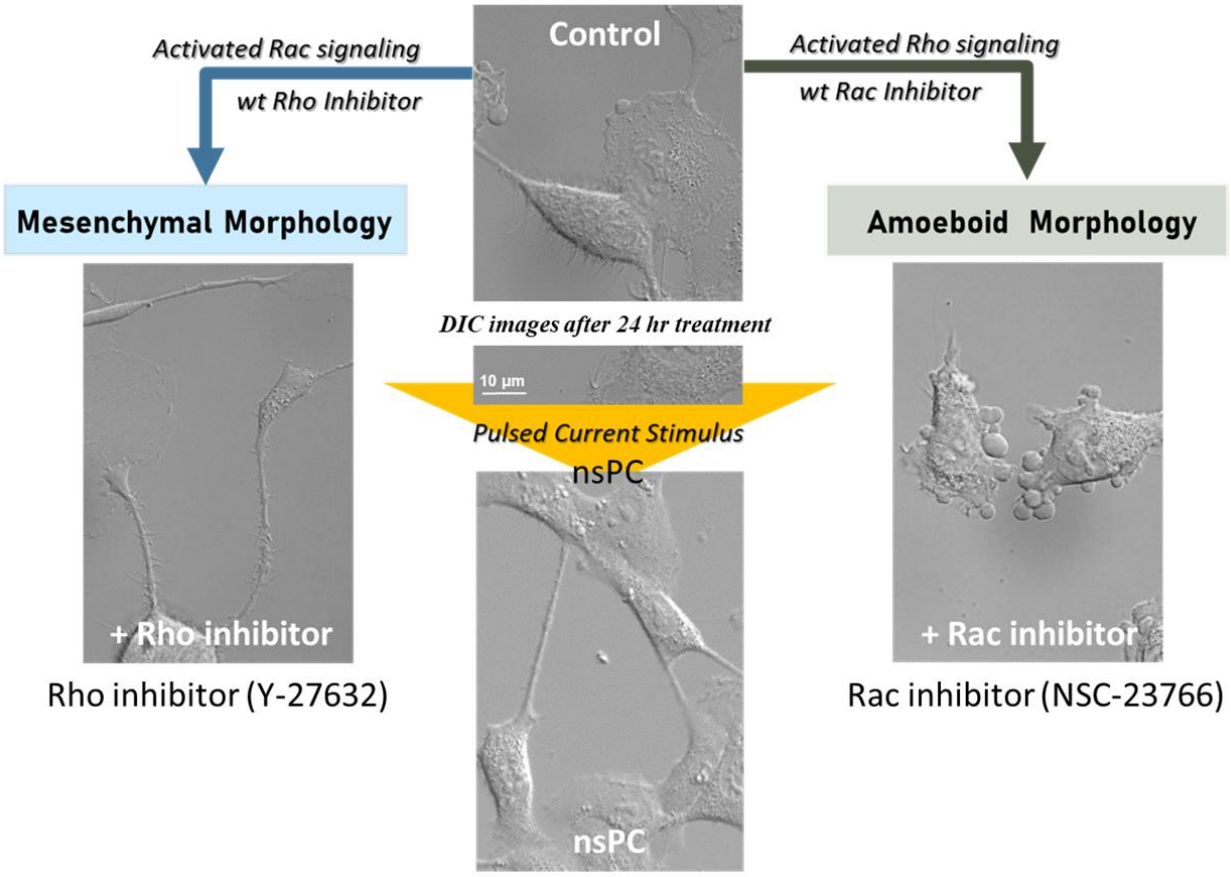

Figure 3.8 Effects of nsPC, ROCK inhibitor, and Rac inhibitor on cell morphology.

Cells were treated with either the Rac1 inhibitor NSC-23766, the ROCK inhibitor Y-27632, or nsPC for 24 hr. Cells treated with the Rac1 inhibitor exhibited ameboid morphology, whereas cells treated with the ROCK inhibitor showed mesenchymal morphology. Cell morphology after nsPC stimulation was similar to that of ROCK inhibitor treatment.

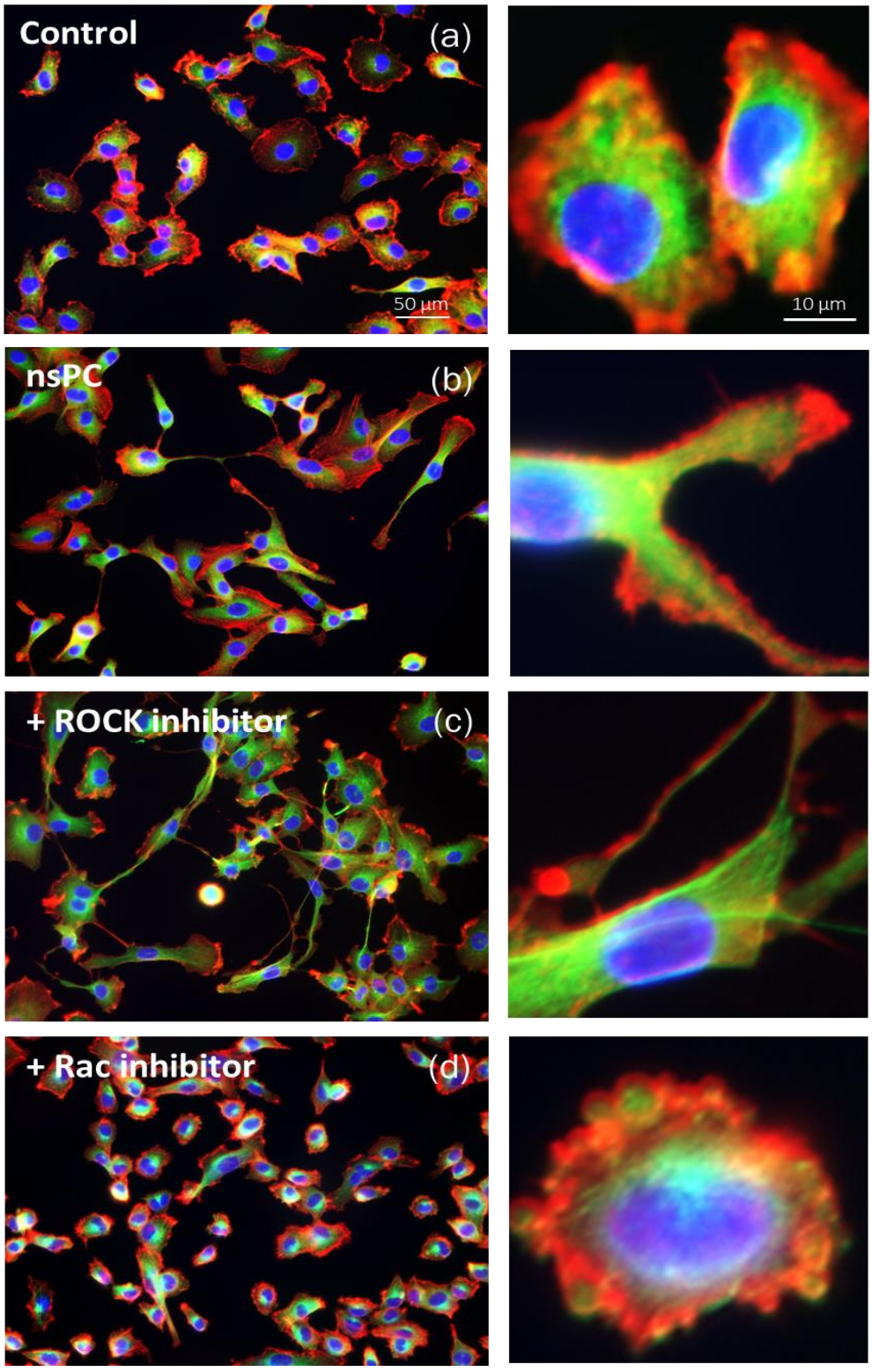

Figure 3.9 Comparison of cell morphology in immunofluorescence

Cells were treated with either nsPC, the Rac1 inhibitor NSC-23766, or the ROCK inhibitor Y-27632 as indicated for 24 hr. Immunofluorescence images of DAPI (blue), anti-α-tubulin antibody (green) and rhodamine-labeled phalloidin (red) were merged.

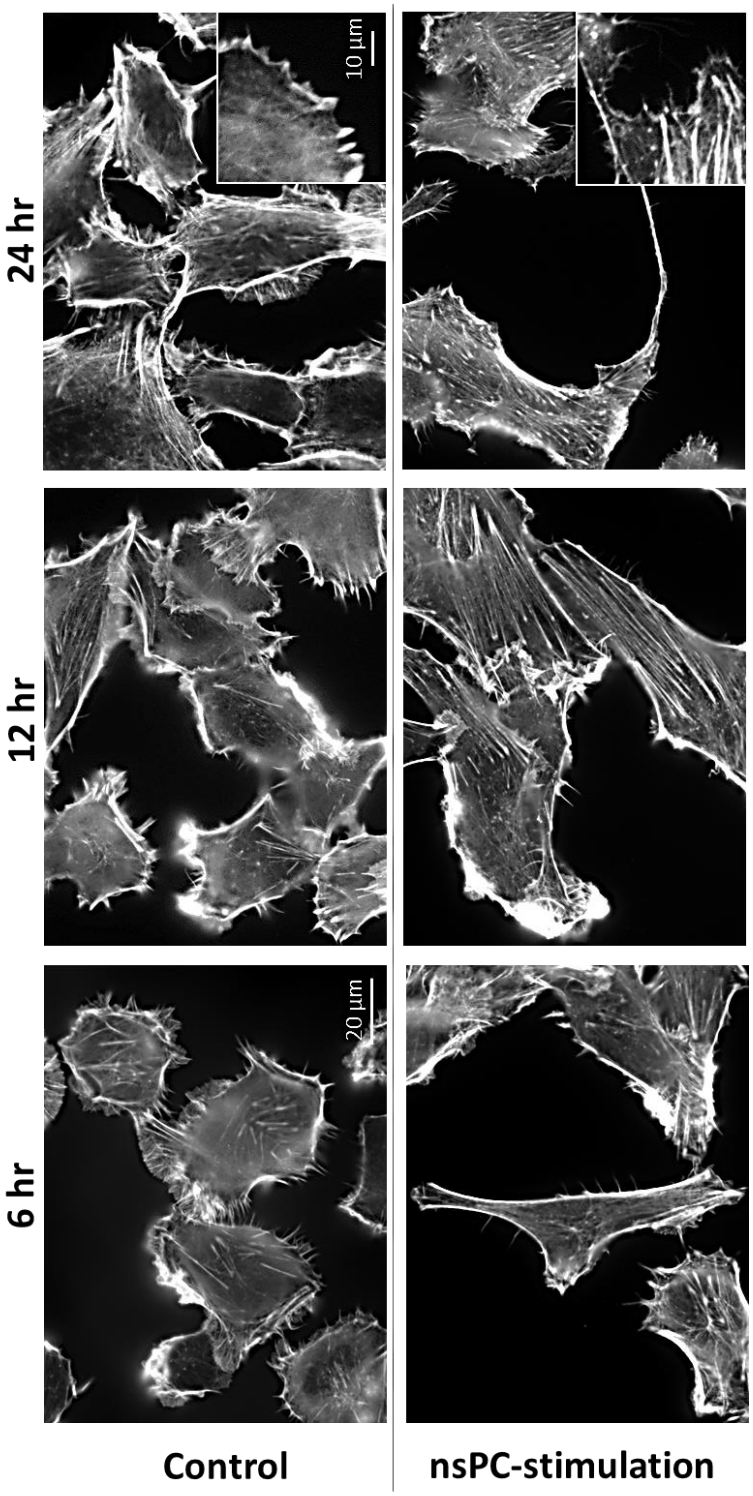

Figure 3.10 Increased stress fiber formation in nsPC-stimulated cells.

Cells were stimulated with nsPC-stimulation. Stimulated and control cells at the indicated time periods were subjected to staining with rhodamine-phalloidin that specifically reacts with F-actin. Extended stress fibers were detectable in nsPC-stimulated cells at 12 hr. At 24 hr, nsPC-stimulated cells exhibited actin-rich protrusions as evident in the enlarged images.

3.4. Discussions

The dynamic actin cytoskeleton in pseudopod protrusion is a key characteristic to inspect mesenchymal motility. In this chapter, we applied nsPC to cells under CAP-producing conditions using a device developed in our previous study and analyzed the alterations in cell morphology. We observed that nsPC stimulation caused extended cell shape and increased cell surface area without a significant decrease in cell viability. We also compared morphological features of nsPC-stimulated cells with cells in those of mesenchymal and amoeboid motility and found similarities between nsPC-stimulated cells and mesenchymal morphology. The inhibition of Rho signaling indicated a transition from amoeboid to mesenchymal migration, an elongated morphology; on the contrary, inhibition of Rac signaling transformed from mesenchymal to amoeboid migration. Cell shape is highly dependent on the external environment, which also provides directional cues that drive the establishment of intracellular polarity. Finally, we observed extended stress fibers in nsPC-stimulated cells. Collectively, these morphological alterations caused by nsPC stimulation suggest that nsPC either activated or inhibited certain functions in a cell, leading to morphological alterations.

Since there was no external ROS change in culture medium during 24 hours continuous treatment and no electroporation was detected, we excluded extracellular ROS into cells to produce effects. Nevertheless, we observed increased levels of intracellular ROS and Ca^{2+}, but not superoxide in nsPC-stimulated cells. Previous studies have demonstrated the involvement of various forms of ROS in the modulation of signaling pathways for cell invasion and migration, leading to lamellipodia formation, actin cytoskeleton remodeling, and focal adhesion turnover [32,33]. In addition to cell morphology, H_2O_2 is implicated in cell differentiation, growth and survival, as well as apoptosis induction at high levels [34]. Furthermore, ROS generated in the

mitochondrial respiratory chain is reported to cause the cytoskeleton remodeling [35]. We speculated that increased ROS levels in nsPC-stimulated cells may alter Rho family signaling, leading to edge protrusion, lamellipodia formation, and ultimately mesenchymal motility. Additionally, previous studies have demonstrated that Ca^{2+} plays critical roles in various cellular events, including cytoskeletal remodeling and cell motility [27,36]. It is intriguing to note that nsPC stimulation may open ion channels on the cell membrane or increase the membrane permeability, leading to the influx of extracellular Ca^{2+}. Our observation on the nsPC-induced intracellular Ca^{2+} increase suggests that a certain mechanism involving Ca^{2+} may influence nsPC-induced cellular alterations. Taken together, we speculate that increased ROS and Ca^{2+} levels may be a part of the mechanism for altered actin filament formation, leading to pseudopodia formation and accelerated mesenchymal motility in nsPC-stimulated cells.

In a word, we propose that nsPC stimulation affects actin dynamics and alters cytoskeleton organization. nsPC-induced increases in intracellular ROS and Ca^{2+} appear to be involved in these processes. Furthermore, nsPC may exert either the negative effect on Rho-related processes or the positive effect on Rac-related processes, both of which can lead to mesenchymal morphology. Further investigation is needed to understand more detailed mechanistic aspects of nsPC actions under CAP-producing conditions. Especially, the selectivity of treatment for cancer cells is one of the most important issues in cancer therapy, and the influence of electrical factors on normal and cancer cells deserve further study.

References

[1] C.-H. Chang, K.-I. Yano, T. Okumura, T. Sato, Effect of plasma-generator-supplied nanosecond pulsed current on cell response, J. Phys. D. Appl. Phys. 51 (2019). doi:10.1088/1361-6463/ab0733.

[2] N. Tandon, C. Cannizzaro, P.P.-H.G. Chao, R. Maidhof, A. Marsano, H.T.H. Au, M. Radisic, G. Vunjak-Novakovic, 19180087, Nat. Protoc. 4 (2009) 155–173. doi:10.1038/nprot.2008.183.Electrical.

[3] B. Cortese, I.E. Palamà, S. D'Amone, G. Gigli, Influence of electrotaxis on cell behaviour, Integr. Biol. (United Kingdom). 6 (2014) 817–830. doi:10.1039/c4ib00142g.

[4] M.F. Olson, E. Sahai, The actin cytoskeleton in cancer cell motility, Clin. Exp. Metastasis. 26 (2009) 273–287. doi:10.1007/s10585-008-9174-2.

[5] D. Yamazaki, S. Kurisu, T. Takenawa, Involvement of Rac and Rho signaling in cancer cell motility in 3D substrates, Oncogene. 28 (2009) 1570–1583. doi:10.1038/onc.2009.2.

[6] A.F. Palazzo, C.H. Eng, D.D. Schlaepfer, E.E. Marcantonio, G.G. Gundersen, Localized Stabilization of Microtubules by Integrin- and FAK-Facilitated Rho Signaling, Science (80-.). 303 (2004) 836–839. doi:10.1126/science.1091325.

[7] S. Charrasse, M. Meriane, F. Comunale, A. Blangy, C. Gauthier-Rouvière, N-cadherin-dependent cell-cell contact regulates Rho GTPases and β-catenin localization in mouse C2C12 myoblasts, J. Cell Biol. 158 (2002) 953–965. doi:10.1083/jcb.200202034.

[8] A.J. Ridley, H.F. Paterson, C.L. Johnston, D. Diekmann, A. Hall, The small GTP-binding protein rac regulates growth factor-induced membrane ruffling, Cell. 70 (1992) 401–410. doi:10.1016/0092-8674(92)90164-8.

[9] and M.M. Kazuo Kurokawa, Reina E. Itoh, Hisayoshi Yoshizaki, Yusuke Ohba Takeshi Nakamura, Coactivation of Rac1 and Cdc42 at Lamellipodia and Membrane Ruffles Induced by Epidermal Growth Factor, Mol. Biol. Cell. 15 (2004) 1003–1010. doi:10.1091/mbc.E03.

[10] M.L. Gardel, I.C. Schneider, C.M.W. Yvonne Aratyn-Schaus, Mechanical Integration of Actin and Adhesion Dynamics in Cell Migration, Annu. Rev. Cell Dev. Biol. 26 (2010) 315–333. doi:10.1016/j.physbeh.2017.03.040.

[11] M. Parri, P. Chiarugi, Rac and Rho GTPases in cancer cell motility control, Cell Commun. Signal. 8 (2010) 1–14. doi:10.1186/1478-811X-8-23.

[12] J. Shankar, A. Messenberg, J. Chan, T.M. Underhill, L.J. Foster, I.R. Nabi, Pseudopodial actin dynamics control epithelial-mesenchymal transition in metastatic cancer cells, Cancer Res. 70 (2010) 3780–3790. doi:10.1158/0008-5472.CAN-09-4439.

[13] S. Tojkander, G. Gateva, P. Lappalainen, Actin stress fibers - Assembly, dynamics and biological roles, J. Cell Sci. 125 (2012) 1855–1864. doi:10.1242/jcs.098087.

[14] T. Vallenius, Actin stress fibre subtypes in mesenchymal-migrating cells, Open Biol. 3 (2013). doi:10.1098/rsob.130001.

[15] M. Parri, P. Chiarugi, Rac and Rho GTPases in cancer cell motility control, Cell Commun. Signal. 8 (2010) 1–14. doi:10.1186/1478-811X-8-23.

[16] H. Yamaguchi, J. Condeelis, Regulation of the actin cytoskeleton in cancer cell migration and invasion, Biochim. Biophys. Acta - Mol. Cell Res. 1773 (2007) 642–652. doi:10.1016/j.bbamcr.2006.07.001.

[17] G. Jacquemet, H. Hamidi, J. Ivaska, Filopodia in cell adhesion, 3D migration and cancer cell invasion, Curr. Opin. Cell Biol. 36 (2015) 23–31. doi:10.1016/j.ceb.2015.06.007.

[18] A. Hall, Rho GTpases and the actin cytoskeleton, Science (80-.). 279 (1998) 509–514. doi:10.1126/science.279.5350.509.

[19] A.B. Jaffe, A. Hall, RHO GTPASES: Biochemistry and Biology, Annu. Rev. Cell Dev. Biol. 21 (2005) 247–269. doi:10.1146/annurev.cellbio.21.020604.150721.

[20] M. Raftopoulou, A. Hall, Cell migration: Rho GTPases lead the way, Dev. Biol. 265 (2004) 23–32. doi:10.1016/j.ydbio.2003.06.003.

[21] A. Hall, Rho GTPases and the control of cell behaviour, Biochem. Soc. Trans. 33 (2005) 891–895. doi:10.1042/BST20050891.

[22] C.D. Lawson, K. Burridge, The on-off relationship of Rho and Rac during integrin-mediated adhesion and cell migration, Small GTPases. 5 (2014). doi:10.4161/sgtp.27958.

[23] C.D. Lawson, A.J. Ridley, Rho GTPase signaling complexes in cell migration and invasion, J. Cell Biol. 217 (2018) 447–457. doi:10.1083/jcb.201612069.

[24] F. Li, H. Wang, L. Li, C. Huang, J. Lin, G. Zhu, Z. Chen, N. Wu, H. Feng, Superoxide plays critical roles in electrotaxis of fibrosarcoma cells via activation of ERK and reorganization of the cytoskeleton, Free Radic. Biol. Med. 52 (2012) 1888–1896. doi:10.1016/j.freeradbiomed.2012.02.047.

[25] F. Li, T. Chen, S. Hu, J. Lin, R. Hu, H. Feng, Superoxide Mediates Direct Current Electric Field-Induced Directional Migration of Glioma Cells through the Activation of AKT and

ERK, PLoS One. 8 (2013). doi:10.1371/journal.pone.0061195.

[26] A. Kondratskyi, K. Kondratska, R. Skryma, N. Prevarskaya, Ion channels in the regulation of apoptosis, Biochim. Biophys. Acta - Biomembr. 1848 (2015) 2532–2546. doi:10.1016/j.bbamem.2014.10.030.

[27] P.K. Hepler, The cytoskeleton and its regulation by calcium and protons, Plant Physiol. 170 (2016) 3–22. doi:10.1104/pp.15.01506.

[28] A.G. Pakhomov, I. Semenov, M. Casciola, S. Xiao, Neuronal excitation and permeabilization by 200-ns pulsed electric field: An optical membrane potential study with FluoVolt dye, Biochim. Biophys. Acta - Biomembr. 1859 (2017) 1273–1281. doi:10.1016/j.bbamem.2017.04.016.

[29] W. Van Boxem, J. Van Der Paal, Y. Gorbanev, S. Vanuytsel, E. Smits, S. Dewilde, A. Bogaerts, Anti-cancer capacity of plasma-treated PBS: Effect of chemical composition on cancer cell cytotoxicity, Sci. Rep. 7 (2017) 1–15. doi:10.1038/s41598-017-16758-8.

[30] H. Tanaka, M. Mizuno, K. Ishikawa, S. Toyokuni, H. Kajiyama, F. Kikkawa, M. Hori, New Hopes for Plasma-Based Cancer Treatment, Plasma. 1 (2018) 150–155. doi:10.3390/plasma1010014.

[31] S. Sasaki, R. Honda, Y. Hokari, K. Takashima, M. Kanzaki, T. Kaneko, Characterization of plasma-induced cell membrane permeabilization: Focus on OH radical distribution, J. Phys. D. Appl. Phys. 49 (2016). doi:10.1088/0022-3727/49/33/334002.

[32] C. Lennicke, J. Rahn, R. Lichtenfels, L.A. Wessjohann, B. Seliger, Hydrogen peroxide - Production, fate and role in redox signaling of tumor cells, Cell Commun. Signal. 13 (2015) 1–19. doi:10.1186/s12964-015-0118-6.

[33] A. Stanley, K. Thompson, A. Hynes, C. Brakebusch, F. Quondamatteo, NADPH oxidase complex-derived reactive oxygen species, the actin cytoskeleton, and rho GTPases in cell migration, Antioxidants Redox Signal. 20 (2014) 2026–2042. doi:10.1089/ars.2013.5713.

[34] L. Zang, H. He, Q. Xu, Y. Yu, N. Zheng, W. Liu, T. Hayashi, S.I. Tashiro, S. Onodera, T. Ikejima, Reactive oxygen species H2O2 and OH, but not O 2- promote oridonin-induced phagocytosis of apoptotic cells by human histocytic lymphoma U937 cells, Int. Immunopharmacol. 15 (2013) 414–423. doi:10.1016/j.intimp.2013.01.004.

[35] E. Bartolák-Suki, J. Imsirovic, Y. Nishibori, R. Krishnan, B. Suki, Regulation of mitochondrial structure and dynamics by the cytoskeleton and mechanical factors, Int. J. Mol. Sci. 18 (2017) 7–11. doi:10.3390/ijms18081812.

[36] L. Guo, C. Xu, D. Li, X. Zheng, J. Tang, J. Bu, H. Sun, Z. Yang, W. Sun, X. Yu, Calcium ion flow permeates cells through SOCs to promote cathode-directed galvanotaxis, PLoS One. 10 (2015) 1–17. doi:10.1371/journal.pone.0139865.

Chapter 4

Cdc42/Rac1 and other possible pathways activated by nsPC to regulate actin dynamics in human fibrosarcoma HT-1080 cells

4.1. Introduction

From previous chapters, we have investigated that small Rho GTPases are related to various regulatory proteins which could be activated by extracellular stimuli, also using an ultra-short pulsed current of stimulation over a long period of time cause fibrosarcoma cell changed its cellular morphology [1]. Furthermore, Ca^{2+} and intracellular ROS signals are perfect candidates to demonstrate intracellular activity. Ca^{2+} modulate proper actin remodeling and efficient cell migration, and further, mitochondrial calcium dynamics in cytoskeletal remodeling through the modulation of ROS production. What is more, the change of intracellular ROS level in cells is an important indicator of functional state. ROS signals could promote cell proliferation, participate in the regulation of certain Rho GTPase mediating cytoskeletal reorganization, yet be toxic at high level to induce apoptosis [2–5]. Additionally, mitochondrial respiratory chain generated $O_2^{\bullet -}$ could be another crucial element inside fibrosarcoma cells through the activation of extracellular signal-

regulated kinases (ERKs) and reorganization of the cytoskeleton [6,7]. In a word, we propose that the nsPC induced depolarization on the cell membrane and reorganized cytoskeleton via actin dynamics and intracellular molecules. Next, we will discuss the mutual mechanisms between nsPC and cancer cell, summarizing the intracellular pathways might be occurred during the electrical stimulation.

4.2. Material and methods

All experimental protocols, such as cell cultivation, immunostaining methods and the stimulation system were following former introductions. To be mentioned, we used the new reagent, Cdc42/Rac1 GTPase inhibitor (ML141, CAS 71203-35-5) which is a potent, selective, reversible and non-competitive inhibitor of Cdc42 GTPases. Cells were cultured in the presence of 1 μg/ml Rho/ROCK inhibitor and 1 μg/ml Cdc42/Rac1 GTPase inhibitor with nsPC stimulation for 24 hours, investigating whether the Cdc42/Rac1 GTPase play the key on actin reorganization on HT-1080 cells. Additionally, we constructed the new power supply to generate maximum 2000 mA current (rising time less than 15 ns) for cell stimulation. With different intensities of nsPC, the data would be named as nsPC-200 (max. to 200 mA), nsPC-1000 (max. to 1000 mA), and nsPC-2000 (max. to 2000 mA), at same frequency and duration time.

4.3. Results

4.3.1. nsPC-1000 stimulation co-treated with the Rho/ROCK or Cdc42/Rac1 inhibitor

To investigate which Rho family of small GTPases related with the mesenchymal mode by nsPC stimulation, cells were added the Rho/ROCK or Cdc42/Rac1 inhibitor with HT-1080 cells for various conditions, then co-treated for 24 hr. Figure 4.1 shows the results at several conditions 24 hr later, listed as follows: nsPC-1000 with Rho/ROCK inhibitor, nsPC-1000, and nsPC-1000 with Cdc42/Rac1 inhibitor. Figure 4.1. (c) shows that HT-1080 cells added Cdc42/Rac1 inhibitor combined with nsPC-1000 stimulation, performed typically normal shape and dramatically decreased the protrusion numbers. A dominant negative form of Rac and Cdc42 was stably expressed into HT-1080 cells to inhibit actin dynamics. Conversely, the cells added Rho/ROCK inhibitor cotreated with nsPC-1000 stimulation reacted more aggressive morphology and generated more invadopodium than those treated only with nsPC-1000, shown in Figure 4.1. (a). These responses explain that the Rac/Cdc42 GTPases control the main switch of mesenchymal morphology in HT-1080 fibrosarcoma cells from nsPC.

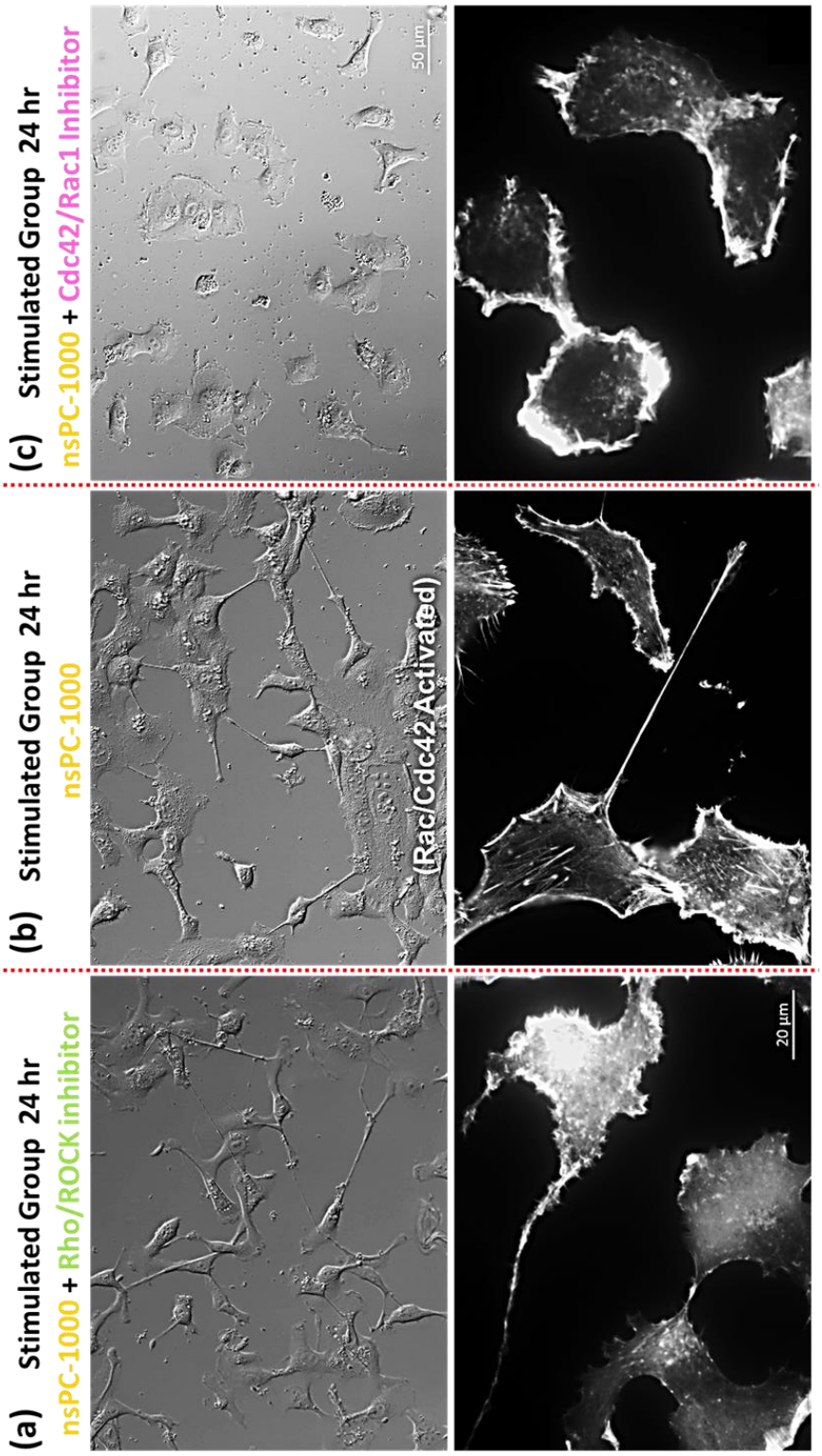

Figure 4.1 Effects of nsPC-1000 with Rho/ROCK inhibitor, nsPC-1000, and nsPC-1000 with Cdc42/Rac1 inhibitor on cell morphology and comparison of actin dynamics.

Cells were treated with multiple conditions for 24 hr, stained with Phalloidin for visualization of actin filaments (white).

4.3.2. Mesenchymal transition by nsPC stimulations in HT-1080 Cells

The dynamic actin cytoskeleton in pseudopod protrusion is a key characteristic to inspect mesenchymal motility. Cellular transformation toward a mesenchymal state has the connection with actin-rich protrusion of cell pseudopodia, which begins with the extension of lamellipodia (protrusions containing a branched network of the actin filaments) and filopodia (thin rod-like projections composed of the parallel actin fibers) at the cell edge. Figure 4.2 presents the time sequence of actin cytoskeleton organization in three conditions: control, stimulated with nsPC-200, and stimulated with nsPC-1000. Figure 4.2. (b) shows the initial cell polarization and formation of the leading protrusion by nsPC-200 after 6 hr, and parallel stress fibers (traversing the cell) and cell membrane extensions observed at 12 hr, formed bundles of stress fibers and new actin-rich membrane projections 24 hr later. Additionally, increasing the nsPC intensity to 1000 mA, cytoskeleton presented faster reorganization toward mesenchymal motility, actin bundles already spread across intracellular after 6 hr, actin meshwork and membrane ruffles after 12 hr, finally elongated spindle-like shape with lamellipodia and filopodia branching to mesenchymal morphology. The complete mesenchymal morphology was not found in nsPC-200 stimulation after 24 hr. This demonstrates that the strength of nsPC could speed up the process of mesenchymal migration.

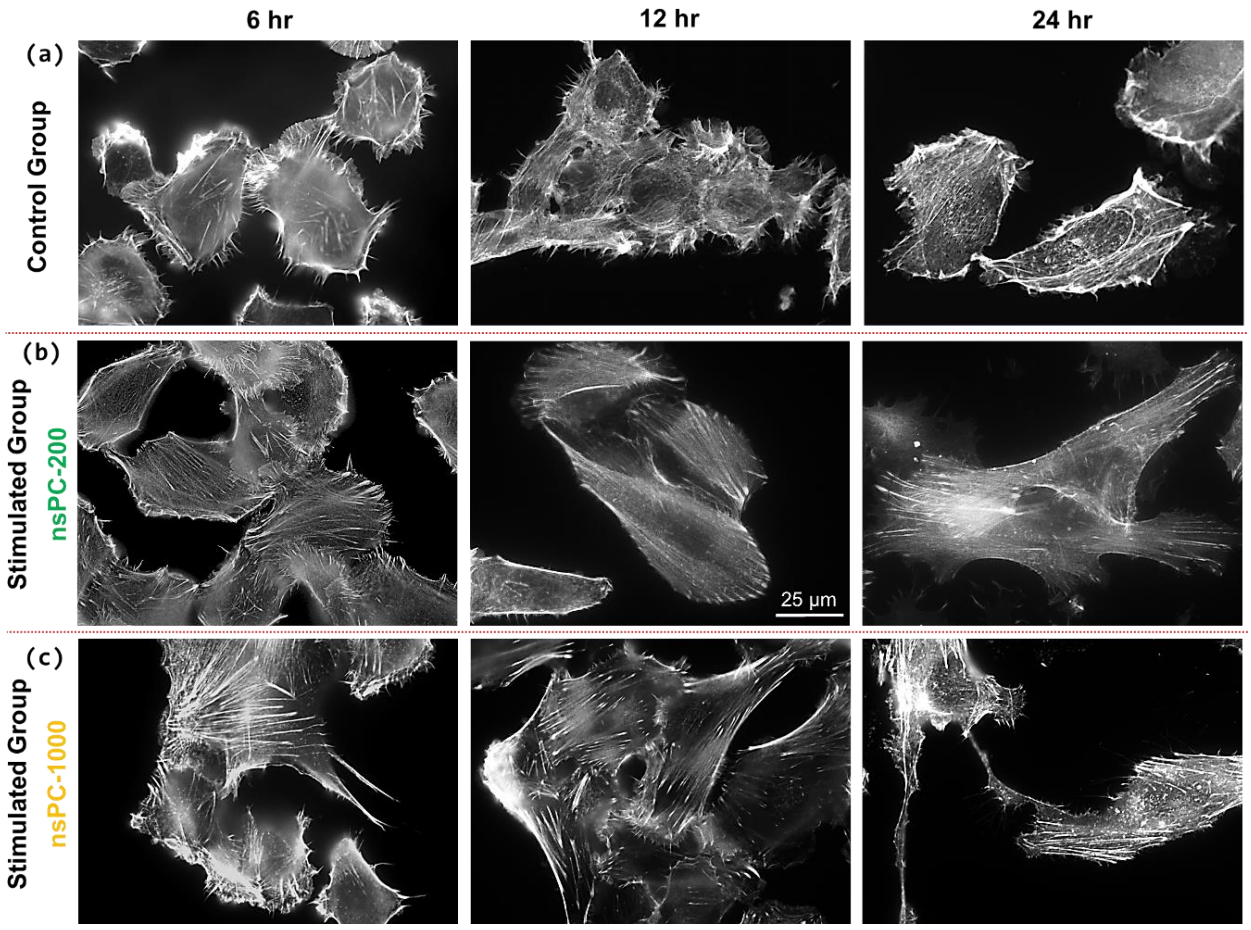

Figure 4.2 Fluorescence microscopy images of HT-1080 cells.

Cell stained with Phalloidin for visualization of actin filaments (white). F-actin components, such as the stress fibers (large bundles demarcated by the open arrow) and microvilli protruding from apical surface (arrowhead), are highlighted. Further to this, features of migrating cell can be seen: filopodium (white asterisk) and membrane ruffles (solid arrow).

4.3.3. HT-1080 cells morphological transition from nsPC-200, nsPC-1000, and nsPC-2000 stimulation

According to previous results, we assumed that increasing the intensity of nsPC might be accelerated morphology transition on HT-1080 cells. Hence, we supplied three multiple nsPCs. Figure 4.3. shows the morphology evolution by increasing the strength of nsPCs. In same period stimulation, cells stimulated with highest nsPC could appear faster mesenchymal transition which has longer invadopodia of the cell and retraction at the rear for displacement. In contrast, the lower strength of nsPC performed slower deformation with less and shorter protrusions. Thus, this demonstrates that the nsPC level has the possibility to enhance Rac and Cdc42 GTPases signals to promote morpho-dynamics to mesenchymal invasion.

4.3.4. Intracellular calcium ion and ROS increase in mesenchymal migration

Ca^{2+} and intracellular ROS signals are perfect candidates to regulate cell migration modules, so we suggest that in various invasions have different intracellular signaling. Compared the fluorescent intensity from Fluo4-AM (Ca^{2+}), DCF (ROS), and DHE ($O_2{\cdot}^-$), shown in Table 1, it is clear that mesenchymal and amoeboid mode appeared opposite molecular signals. In mesenchymal state, with nsPC-1000 stimulated or Cdc42/Rac1 inhibitor, treated cells could be measured the higher level of Ca^{2+} signals and ROS intensity. To be noticed, $O_2{\cdot}^-$ might be rapidly degraded by superoxide dismutase (SOD) to H_2O_2, so there would no difference between control and mesenchymal cells in DHE fluorescence. Interestingly, amoeboid mode, with Rho/ROCK inhibitor, presented weaker molecular signals, which had lower level of Fluo4-AM and DCF fluorescence, but DHE fluorescence increased significantly inside cytoplasm might due to different pathways.

Table 4.1 The fluorescent intensity from Fluo4-AM (Ca^{2+}), DCF (ROS), and DHE ($O_2^{\cdot -}$).

	Fluo4-AM	DCF	DHE	DHE
Control	–	–	–	–
+ nsPC-1000 Stimulated	↗	↗	–	–
+ Cdc42/Rac1 Inhibitor	–	–	–	↗↗
+ Rho/ROCK Inhibitor	↗	↗↗	–	–
* Same exposure time compared with control group	Calcium Ion Indicator	Intracellular ROS Indicator	Superoxide (Chromatin) Indicator	Superoxide (Cytoplasm) Indicator

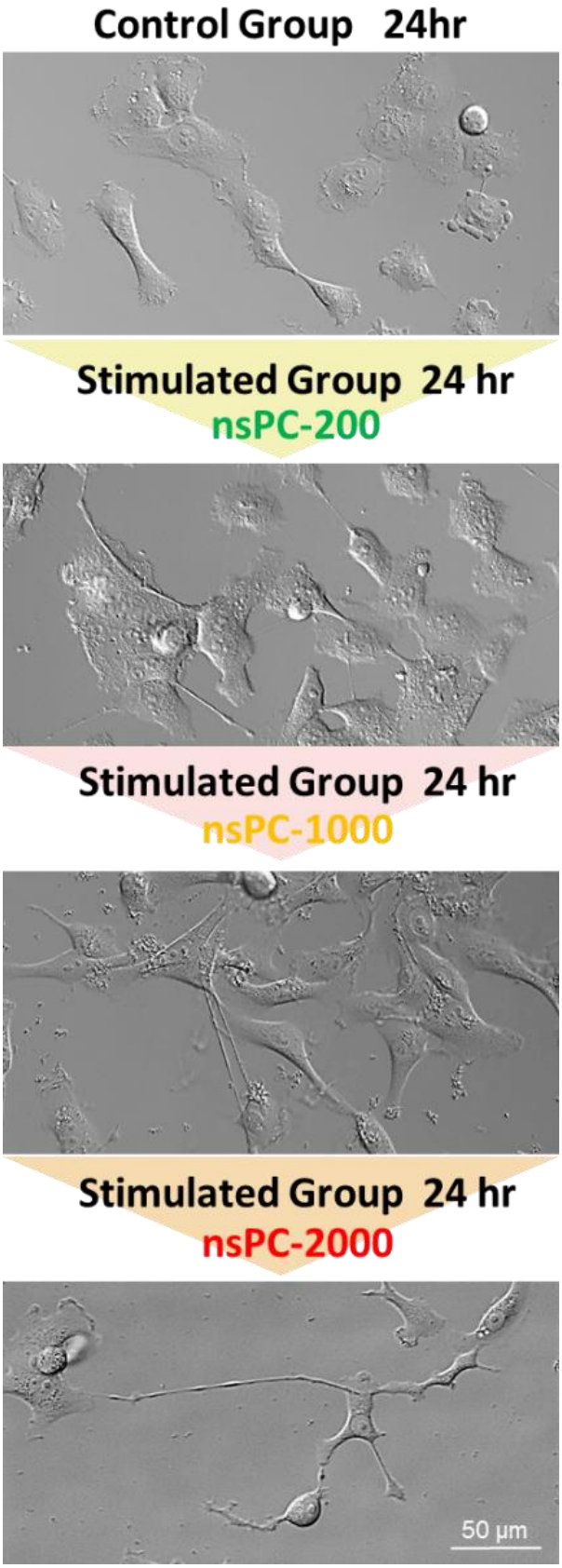

Figure 4.3 As the intensity of nsPC increasing, HT-1080 cells morphology changed sequentially.

4.4. Discussions

Cell responses are highly dependent on the external environment, so electrical surroundings could provide the conditions to trigger cancer cell migration and invasion. The procedure of migration from actin dynamics are arranged cytoskeleton to promote various types of movement. Our results show the identical phenomena from actin reorganization that nsPC successfully activated cancer cell to mesenchymal motility. As increasing the strength of nsPC and stimulated time, fibrosarcoma cells were induced gradually to mesenchymal mode, which likely linked with Rho family. Figure 4.4. presents the interactions among the components of signaling pathways documented to be involved in the mesenchymal transition of HT-1080 cells stimulated by nsPC. Therefore, we propose that nsPC stimulus could reflect the positive effect on Rac-related processes, created the new pathway to induce mesenchymal-migrating cells.

During cancer cell migration, actin polymerization, lamellipodia and filopodia formation require high energy production and Ca^{2+} buffering. Many studies elucidate that Rac and Cdc42 mediate actin polymerization by the regulation of proteins, also act as upstream to release Ca^{2+} from the endoplasmic reticulum (ER) and mitochondria [8]. Ca^{2+} is a ubiquitous intracellular messenger responsible for controlling numerous cellular processes, such as regulators of actin assembly and disassembly, the role of mitochondrial Ca^{2+} in cell migration, triggering wound healing, and so on [5,9–11]. Because HT-1080 cells are known to express various types of ion channels [12,13], we imagine that multiple types of ion channels may participate in nsPC-induced Ca^{2+} elevation. Thus, deciphering the complicated involvement of multiple ion channels in nsPC-induced Ca^{2+} influx and cell motility is very important for better understanding of nsPC, so we assume some possible mechanisms of intracellular calcium dynamic during electrical stimulation. On membrane side, the transient receptor potential vanilloid channel (TRPV) family plays the

important role that can transmit information between intra- and extracellular, related with proliferation, differentiation, apoptosis, and migration of cancer cells by regulation of Ca^{2+} and its downstream signaling pathways. Two of the subfamilies, TRPV2 and TRPV4 (member 2 & 4) could be activated by various physical and chemical stimuli to control multiple cellular functions in HT-1080 cells. TRPV4 could promote tumor metastasis transformed to mesenchymal motility with spindle-shaped fibroblast-like morphology [13]. On interior side, nuclear membranes and ER are likely to receive more signals than other organelles using the ultra-short duration of power source. Inositol trisphophate receptor (IP3R) activated physically by electrical stress is one of ion channels on the ER that release intracellular calcium into the cytoplasm, and ryanodine receptor (RyR) could be another possible channel to involve or be activated by electrical signals [14,15]. Intracellular Ca^{2+} is a strong candidate signaling mechanism, nevertheless, more careful time-lapse analysis of Ca^{2+} gradients from various sources and channels should be performed on cell response during applied electrical stimulation for further understanding.

On the other hand, cancer cells have more ROS and antioxidants than normal cells, they may be more susceptible to changes in ROS levels from extracellular surrounding [16]. Intracellular ROS play important roles in the modulation of signaling pathways in invasion and migration, which involved in protrusion formation, actin cytoskeleton remodeling, focal adhesion turnover, and so on. Moreover, hydroperoxide (H_2O_2) derived from either NADPH oxidases or the mitochondria is one of key molecular player of regulated intracellular ROS sources, implicated in cell differentiation, growth and survival, yet high levels of H_2O_2 can also induce cells to mutation or apoptosis [17]. Consequently, intracellular molecular signals, Ca^{2+} and ROS, exert proper actin remodeling and efficient cell migration, suggested that the biochemical links with small Rho GTPases [10,18–20].

Collectively, our results are consistent with those of a model with Rho/ROCK inhibitor, revealed potential cross talk between nsPC and intracellular pathways regulating cell motility by Rac and Cdc42 GTPases. The electrical stimulation possibly offers a unique opportunity for non-chemical mobilization of the internal calcium, caused by permeabilization of these membranous structures. Figure 4.5 is given the summary of the concepts on the mutual interactions between electrical stimulus and cell responses. Rho family of Rac and Cdc42 activated from nsPC control cell movement by actin cytoskeleton reorganization, inducing stress fibers, lamellipodia, and filopodia formation. GTPases act as upstream of mediated ROS production to regulate multiple pathway. Moreover, Ca^{2+} modulates actin dynamics through multiple signaling pathways, mitochondrial calcium dynamics in cytoskeletal remodeling through the modulation of ROS production. Further work will be necessary to characterize the precise contribution of electrical factors to HT-1080 cells regulation at the molecular level.

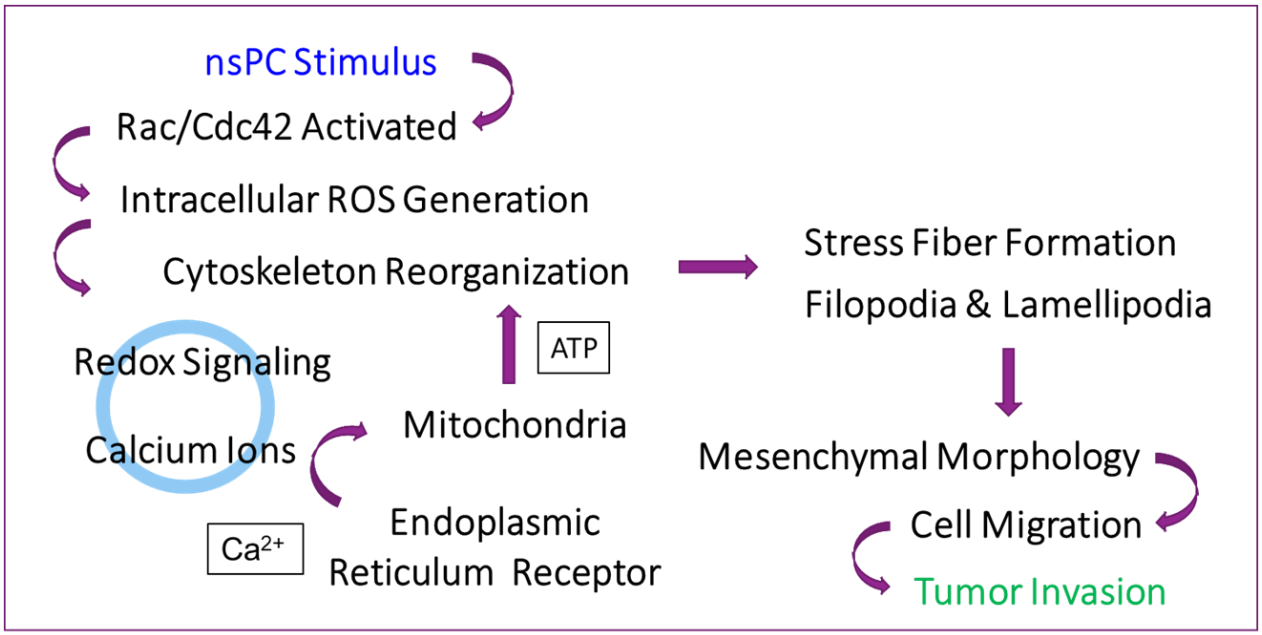

Figure 4.4 Interactions among the components of signaling pathways documented to be involved in the mesenchymal transition of HT-1080 cells stimulated by nsPC.

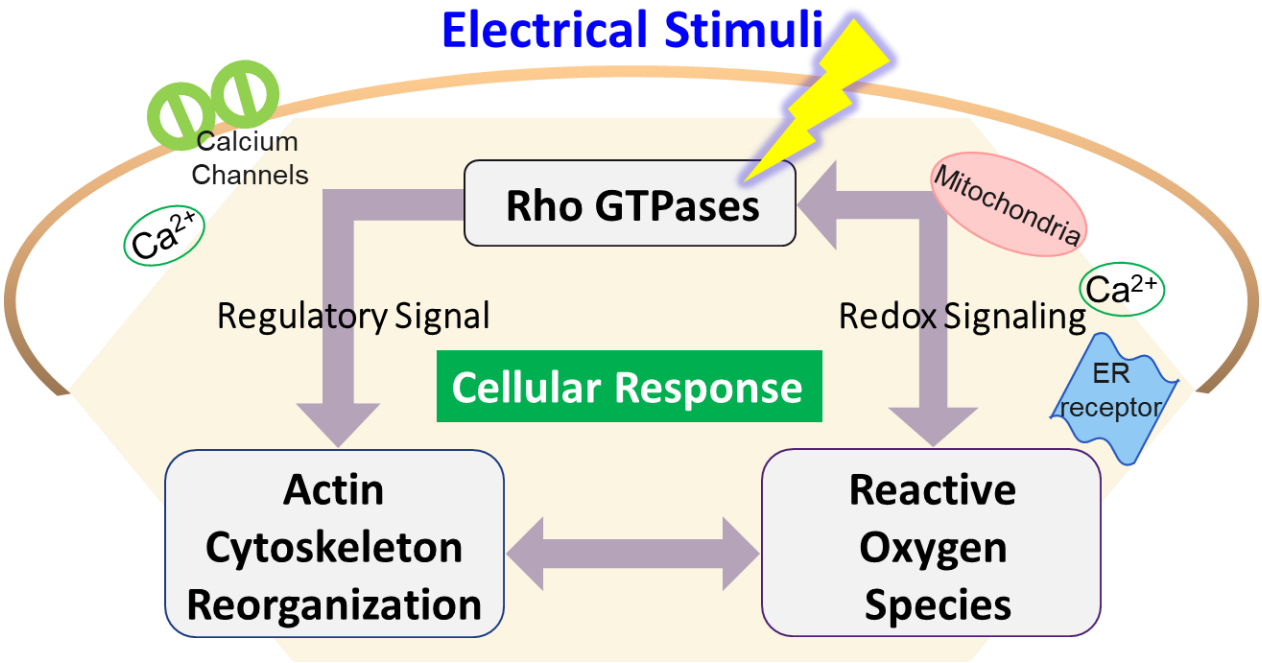

Figure 4.5 Summary of the concept on the mutual interactions by electrical stimulus.

References

[1] C.H. Chang, K. ichi Yano, T. Sato, Nanosecond pulsed current under plasma-producing conditions induces morphological alterations and stress fiber formation in human fibrosarcoma HT-1080 cells, Arch. Biochem. Biophys. 681 (2020) 108252. doi:10.1016/j.abb.2020.108252.

[2] C. Lennicke, J. Rahn, R. Lichtenfels, L.A. Wessjohann, B. Seliger, Hydrogen peroxide - Production, fate and role in redox signaling of tumor cells, Cell Commun. Signal. 13 (2015) 1–19. doi:10.1186/s12964-015-0118-6.

[3] A. Stanley, K. Thompson, A. Hynes, C. Brakebusch, F. Quondamatteo, NADPH oxidase complex-derived reactive oxygen species, the actin cytoskeleton, and rho GTPases in cell migration, Antioxidants Redox Signal. 20 (2014) 2026–2042. doi:10.1089/ars.2013.5713.

[4] P.K. Hepler, The cytoskeleton and its regulation by calcium and protons, Plant Physiol. 170 (2016) 3–22. doi:10.1104/pp.15.01506.

[5] F.C. Tsai, G.H. Kuo, S.W. Chang, P.J. Tsai, Ca2+ signaling in cytoskeletal reorganization, cell migration, and cancer metastasis, Biomed Res. Int. 2015 (2015). doi:10.1155/2015/409245.

[6] F. Li, H. Wang, L. Li, C. Huang, J. Lin, G. Zhu, Z. Chen, N. Wu, H. Feng, Superoxide plays critical roles in electrotaxis of fibrosarcoma cells via activation of ERK and reorganization of the cytoskeleton, Free Radic. Biol. Med. 52 (2012) 1888–1896. doi:10.1016/j.freeradbiomed.2012.02.047.

[7] F. Li, T. Chen, S. Hu, J. Lin, R. Hu, H. Feng, Superoxide Mediates Direct Current Electric Field-Induced Directional Migration of Glioma Cells through the Activation of AKT and ERK, PLoS One. 8 (2013). doi:10.1371/journal.pone.0061195.

[8] E. Hong-Geller, R.A. Cerione, Cdc42 and Rac stimulate exocytosis of secretory granules by activating the IP3/calcium pathway in RBL-2H3 mast cells, J. Cell Biol. 148 (2000) 481–493. doi:10.1083/jcb.148.3.481.

[9] K. Paňková, D. Rösel, M. Novotný, J. Brábek, The molecular mechanisms of transition between mesenchymal and amoeboid invasiveness in tumor cells, Cell. Mol. Life Sci. 67 (2010) 63–71. doi:10.1007/s00018-009-0132-1.

[10] E. Bartolák-Suki, J. Imsirovic, Y. Nishibori, R. Krishnan, B. Suki, Regulation of mitochondrial structure and dynamics by the cytoskeleton and mechanical factors, Int. J.

Mol. Sci. 18 (2017) 7–11. doi:10.3390/ijms18081812.

[11] G.R. Monteith, N. Prevarskaya, S.J. Roberts-Thomson, The calcium-cancer signalling nexus, Nat. Rev. Cancer. 17 (2017) 367–380. doi:10.1038/nrc.2017.18.

[12] M. Nagasawa, I. Kojima, Translocation of TRPV2 channel induced by focal administration of mechanical stress, Physiol. Rep. 3 (2015) 1–12. doi:10.14814/phy2.12296.

[13] S. Yu, S. Huang, Y. Ding, W. Wang, A. Wang, Y. Lu, Transient receptor potential ion-channel subfamily V member 4: a potential target for cancer treatment, Cell Death Dis. 10 (2019). doi:10.1038/s41419-019-1708-9.

[14] N. Ohnishi, Y. Fujiwara, T. Kamezaki, S. Katsuki, Variations of Intracellular Ca2+ Mobilization Initiated by Nanosecond and Microsecond Electrical Pulses in HeLa Cells, IEEE Trans. Biomed. Eng. 66 (2019) 2259–2268. doi:10.1109/TBME.2018.2886602.

[15] A.G. Pakhomov, S. Xiao, O.N. Pakhomova, I. Semenov, M.A. Kuipers, B.L. Ibey, Disassembly of actin structures by nanosecond pulsed electric field is a downstream effect of cell swelling, Bioelectrochemistry. 100 (2014) 88–95. doi:10.1016/j.bioelechem.2014.01.004.

[16] L.B. Sullivan, N.S. Chandel, Mitochondrial reactive oxygen species and cancer, Cancer Metab. 2 (2014) 1–12. doi:10.1186/2049-3002-2-17.

[17] M. López-Lázaro, Dual role of hydrogen peroxide in cancer: Possible relevance to cancer chemoprevention and therapy, Cancer Lett. 252 (2007) 1–8. doi:10.1016/j.canlet.2006.10.029.

[18] O.G. Lyublinskaya, J.S. Ivanova, N.A. Pugovkina, I. V. Kozhukharova, Z. V. Kovaleva, A.N. Shatrova, N.D. Aksenov, V. V. Zenin, Y.A. Kaulin, I.A. Gamaley, N.N. Nikolsky, Redox environment in stem and differentiated cells: A quantitative approach, Redox Biol. 12 (2017) 758–769. doi:10.1016/j.redox.2017.04.016.

[19] V. Paupe, J. Prudent, New insights into the role of mitochondrial calcium homeostasis in cell migration, Biochem. Biophys. Res. Commun. 500 (2018) 75–86. doi:10.1016/j.bbrc.2017.05.039.

[20] G. Thrivikraman, S.K. Boda, B. Basu, Unraveling the mechanistic effects of electric field stimulation towards directing stem cell fate and function: A tissue engineering perspective, Biomaterials. 150 (2018) 60–86. doi:10.1016/j.biomaterials.2017.10.003.

Chapter 5

Distinct biological actions of plasma-induced electrical and chemical factors and their synergistical effects as augmented cytotoxicity

5.1. Introduction

It has been postulated that both electrical and chemical properties of CAP may contribute to the biological action of CAP [1]. As for the chemical properties of CAP, many preceding studies have clearly demonstrated the cytotoxic action of CAP-derived reactive species [2–7]. CAP could provide a wide array of reactive species such as superoxide anions ($O_2\cdot^-$), hydroxyl radicals (·OH), hydrogen peroxide (H_2O_2), and nitrite (NO_2^-). These reactive species are considered to primarily account for the cytotoxic action of CAP [8]. When CAP is applied to aqueous solution (e.g., cell culture medium), such CAP-exposed solution is called "plasma-activated medium" or PAM [9,10]. PAM contains a distinct set of reactive oxygen and nitrogen species (hereafter, referred to as RONS). Typically, PAM contains elevated levels of H_2O_2 and NO_2^- that are maintained over several hours [11]. PAM is well known to exhibit significant cytotoxicity for long periods after

CAP exposure, which is attributed to the persistent presence of elevated H_2O_2 and NO_2^- [12,13]. Based on its cytotoxicity, PAM is considered to be a new indirect way of CAP usage for cancer therapy. In contrast to the well-documented cytotoxic effects of CAP-derived RONS, the biological influence of electrical properties of CAP has remained largely elusive. A major reason for the limited information on the electrical aspect of CAP action is attributed to the strong cytotoxicity of RONS, which easily overwhelms the effects of electrical stimulation under CAP-generating conditions.

Due to charged particles accumulation or electrons transmission processes from CAP have not been completely understood, it is crucial to investigate cancer cells stimulated by the electrical properties without any RONS generation. In this chapter, a needle to medium device was used for plasma production (CAP-generating conditions), created a streamer discharge between the tip of the needle and the liquid surface, also we present the configuration combined the agarose bridges in the incubator not only isolated cancer cells from chemical compositions (RONS) but stimulated with electrical properties supplied by CAP. Long-lived species of RONS generated from plasma irradiation inside medium could maintain several hours to kill cancer cells, but still showed weaker cytotoxicity and take more time to inactivate than CAP-direct treatment. Therefore, there is still some unknown mechanisms to affect the cytotoxicity of the RONS on cancer cells between the direct and indirect treatment of CAP. We attempted to understand the contribution of electrical and chemical factors to the cytotoxicity of CAP. To this end, we treated cells with the electrical properties of CAP in combination with PAM. Intriguingly, the electrical stimulation under CAP-producing conditions did not show apparent cytotoxicity, but cells became more susceptible to PAM. This observation suggests that the electrical properties of CAP can alter the nature of cells, which is not manifested as cytotoxicity.

5.2. Materials and methods

5.2.1. Experimental setup

Figure 5. 1 (a) shows the experimental setup that was composed of three units, a power reservoir, a culture chamber, and a ground reservoir. The power reservoir and the ground reservoir contained Hanks' Balanced Salt Solution (HBSS). A glass-bottomed slide with four small compartments (W10.4 × L20.6 × H11.5 mm each, Eppendorf, cat. no. 0030742028) was used as a culture chamber. The culture chamber was placed in a CO_2 incubator that maintained 37°C and 5% CO_2 conditions. The culture chamber was connected to the power reservoir and the ground reservoir through agarose bridges that were made of 2% agarose gel and PBS (see Appendix B).

A needle to medium device was used for plasma production, created a streamer discharge between the tip of the needle and the liquid surface. The high voltage power amplifier (High Voltage Amplifier model P05034, Trek) was connected to a needle-type electrode that was made of platinum and sharpened to a tip radius of 15 μm. Output from the high voltage power amplifier was controlled by a function generator (Multifunction Generator WF1968, NF). Streamer discharge was generated in ambient air on the surface of HBSS in the power reservoir (Figure 5.1 (a)). The distance between the needle tip and the HBSS surface was kept at 1 mm, so that the streamer discharge directly hit the HBSS surface. Electric waveforms of the discharge were measured using an oscilloscope (Wave Surfer 104MXs-B) through an high voltage probe (HV–P30A, Iwatsu electric co., ltd.) and a pearson coil (Pearson current monitor model 6585, Pearson electronics. Inc.). Applied voltage with a repetitive frequency of 100 Hz was kept at 7.8 kV (Figure 5.1 (b)), and the maximum streamer pulsed current was measured to be typically 1.8 A with a rise time of less than 15 ns (Figure 5.1 (c)).

5.2.2. Cell culture

The human fibrosarcoma cell line HT-1080 was also used in this chapter (see Appendix A). For cell stimulation experiments, 2.5×10^5 cells in 1 ml culture medium were placed in each culture chamber and incubated for 24 hr to allow cell attachment. After replacement of culture medium with 1500 μL of HBSS, cell stimulation was carried out. All experiments were conducted in a humidified incubator at 5% CO_2 and 37°C.

5.2.3 Fluorescence microscopy and viability analysis

For fluorescence microscopy, cells were co-stained with three fluorescent dyes, ethidium homodimer III, Hoechst 33342, and FITC-Annexin V, using an apoptotic/necrotic/healthy cells detection kit (PromoKine, PK-CA707-30018). To assess cell viability, cells stained with ethidium homodimer III (red) were regarded as dead cells. Total cell numbers were obtained from Hoechst 33342 staining (blue). A ratio of red cells to blue cells was obtained from at least 1000 cells.

5.2.4. Measurement of H_2O_2, NO_2^-, and other factors of HBSS

Concentrations of H_2O_2 and NO_2^- in HBSS were analyzed by colorimetric methods using Pack test kits (WAK-H2O2 and WAK-NO2, Kyoritsu Chemical-Check Lab. Corp.) with a digital colorimeter (DPT-MT, Kyoritsu Chemical-Check Lab. Corp.). Electrical conductivity, pH, and temperature of HBSS were measured using a conductivity tester (ECTestr11+, Oakton), a pH meter (B-71X, HORIBA), and a thermometer (E5CN-H, Omron), respectively.

5.2.5. Measurement of lactate dehydrogenase activities

Enzymatic activity of lactate dehydrogenase (LDH) in HBSS was quantified by a colorimetric assay using an LDH cytotoxicity detection kit (Takara, cat. no. MK401) and a Multiskan FC microplate photometer (Thermo Scientific, model: 51119100) (see Appendix G).

5.2.6. Statistical analysis

Each experiment was repeated at least three times, and all data were expressed as mean ± standard deviation (SD). Student's t-test analysis was performed, and statistic significance was presented as follows; *: $p < 0.05$; **: $p < 0.01$.

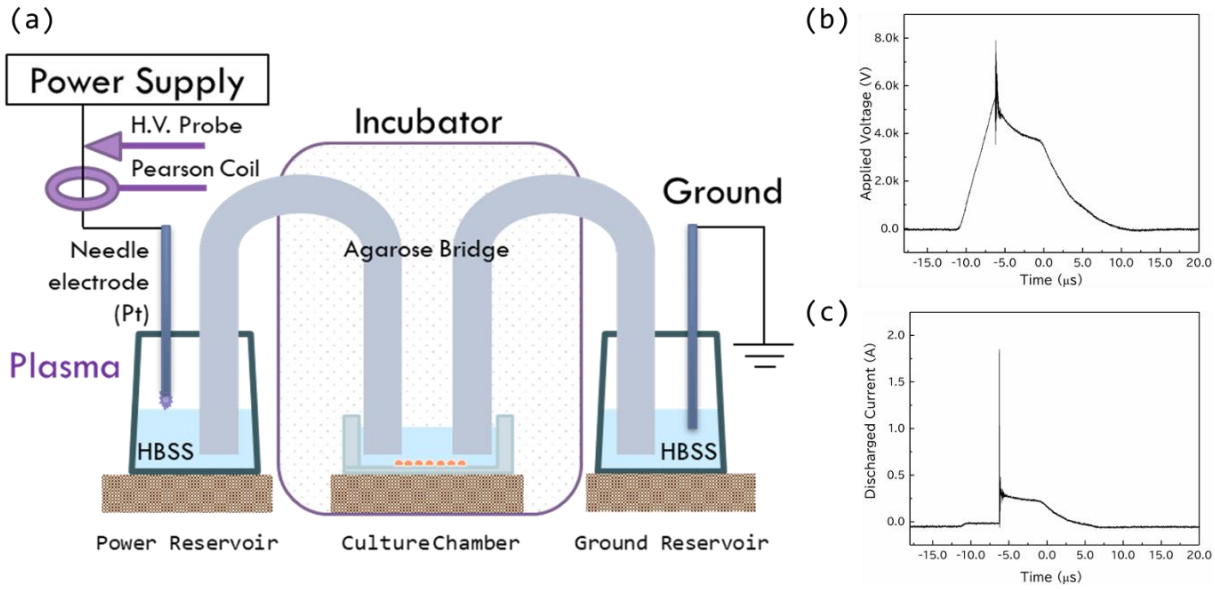

Figure 5.1 Experimental setup and typical electric waveforms.

(a) Schematic representation of experimental setup used in this study. Streamer discharge was generated on the surface of HBSS in the power reservoir. Cells were cultured in the culture chamber that was maintained at 37C and 5% CO_2. Agarose bridges connected the culture chamber to the power reservoir and ground reservoir. (b, c) Typical electric waveforms of streamer discharge. Applied voltage with a repetitive frequency of 100 Hz was kept at 7.8 kV (b), and the maximum streamer pulsed current was measured to be typically 1.8 A with a rise time of less than 15 ns (c).

5.3. Results

5.3.1. Measurement of long-lived RONS and other factors

In this study, we used an experimental setup that was composed of three units, a power reservoir, a culture chamber, and a ground reservoir (Figure 5.1 (a)). Streamer discharge was generated on the surface of HBSS in the power reservoir. Cells were cultured in the culture chamber that was electrically connected to the power reservoir through a salt bridge but sequestered from RONS generated by streamer discharge in the power reservoir. To confirm this, we measured concentrations of H_2O_2 and NO_2^- along with pH fluctuations in three units during 60-min streamer discharge (Figure 5.2). In the power reservoir (Figure 5.2 (a)), we detected significant increases in H_2O_2 and NO_2^-concentrations that were assessed to be 13 ± 2 ppm and 8 ± 1 ppm, respectively, at 60 min. Slight decreases of pH were also observable, presumably due to the increasing NO_2^- concentrations. In the culture chamber, on the other hand, H_2O_2 and NO_2^-were conspicuously absent (below the detection limits), and pH was relatively constant during 60-min streamer discharge (Figure 5.2 (b)). Similar to the culture chamber, very low H2O2 (0.18 ppm) and the absence of NO_2^- were measured in the ground reservoir (Figure 5.2 (c)). Temperature and conductivity of all three units remained constant during 60-min streamer discharge (33.4−34.7°C and 13.3−14.8 mS/cm, respectively. Data not shown), indicating ignorable joule heating under our experimental conditions. Taken together, these observations demonstrated that our experimental setup allowed us to dissect the combined effects of electrical factors and long-lived RONS on cell physiology.

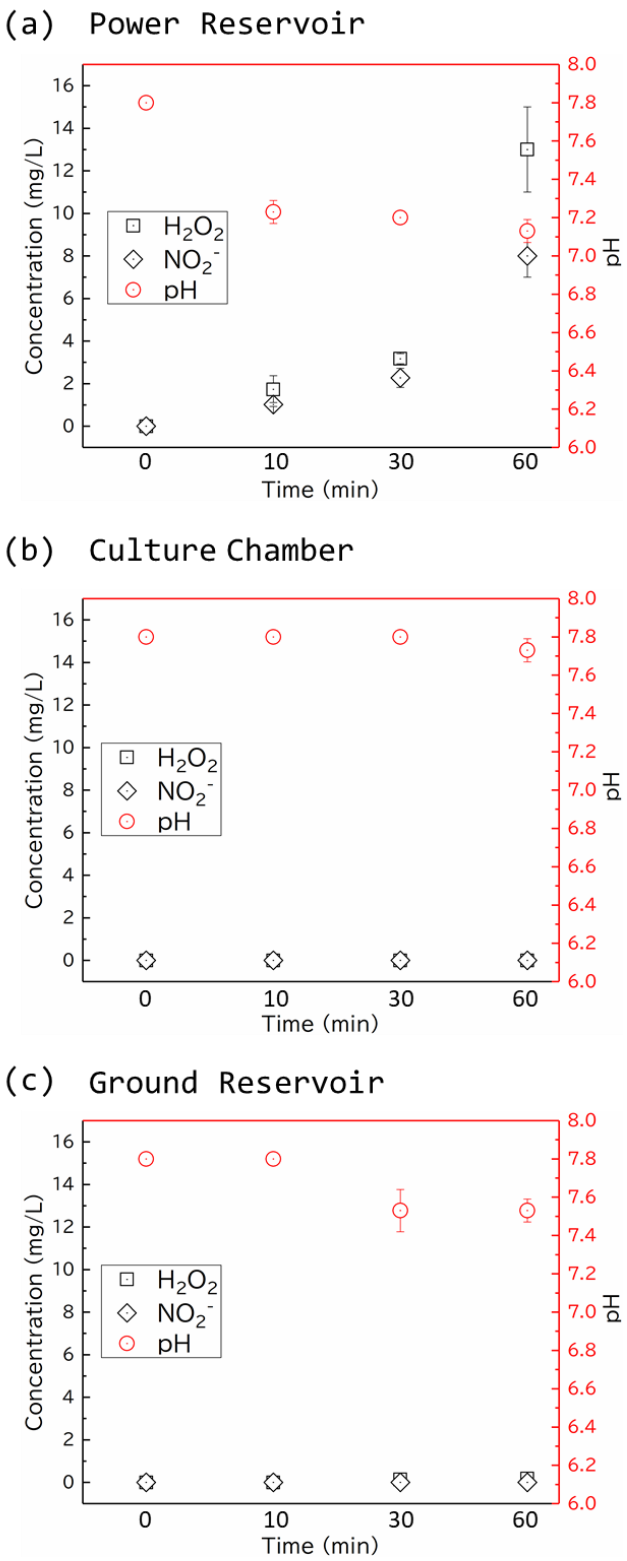

Figure 5.2 Measurement of H_2O_2, NO_2^-, and pH.

Concentrations of H_2O_2 and NO_2^-, and pH in the power reservoir (a), culture chamber (b), and ground reservoir (c) were measured during 60-min streamer discharge. Mean values and SD were calculated from three independent experiments.

5.3.2. Microscopic observation of cytotoxicity of PIE, PAM, and their combinations

We next performed fluorescence microscopy to analyze the effects of electrical factors and long-lived RONS on cells. To investigate cell states, cells were costained with three fluorescent dyes. Ethidum homodimer III is a membrane impermeant dye and stains the nucleus red when the cell membrane is severely damaged. FITC-Annexin V is a green fluorescent dye for the cell membrane of severely damaged cells. Hoechst 33342 stains nuclear DNA blue irrespectively of healthy or damaged state, and thus we used this dye for measuring total cell numbers.

Cell treatment was summarized in Figure 5.3. First, streamer discharge was generated in the power reservoir for 60 min. Because the culture chamber was connected with the power reservoir through a salt bridge, the cells in the culture chamber were electrically stimulated without the influence of RONS (hereafter, called "plasma-induced electrical properties" or PIE). After PIE stimulation for 1 hr, the cells were cultured for 24 hr and subsequently subjected to staining with three fluorescent dyes. As seen in Figure 5.4 (a) majority of the PIE-stimulated cells were stained blue, but not red or green, which was indistinguishable with staining of untreated negative control cells (Figure 5.4 (a), (b)). This observation indicated that PIE stimulation did not cause apparent cytotoxicity, which was in accordance with our previous studies. Next, we examined the effect of plasma-activated HBSS. HBSS was exposed to streamer discharge for 60 min and utilized as plasma-activated medium (PAM). PAM was directly added to cells that were cultured in an isolated chamber (without PIE treatment). When cells were cultured in PAM for 1 hr, we observed red and green fluorescence in several cells (Figure 5.4 (c), upper panel). Cell culture in PAM was continued for 24 hr, and many cells exhibited red and green fluorescence (Figure 5.4 (c), lower panel), indicating the cytotoxicity of PAM. Next, cells were stimulated with PIE in HBSS for 1 hr, and

HBSS in the culture chamber was replaced with that in the power reservoir (PAM). Cells were subsequently incubated in PAM for 24 hr (referred to as "PIE→PAM"). As shown in Figure 5.4 (d), we observed that many cells had red and green fluorescence. When compared to PAM only, more cells appeared to be stained with red and green fluorescence (see blow). Finally, we combined PIE and PAM for cell treatment. Cells were placed in PAM, stimulated with PIE for 1 hr, and further incubated for 24 hr in the presence of PAM (hereafter "PAM+PIE"). As seen in Figure 5.5 (e), PIE stimulation in PAM for 1 hr resulted in strong staining of red and green fluorescence, indicating that cells were severely damaged at this point. After 24 hr incubation in the presence of PAM for 24 hr, many cells appeared to be dead, as judged by compromised cell structures, such as round cell shape, and many detached cells. In summary, PIE showed no apparent effects on cell viability, and the combined use of PIE and PAM exhibited more cytotoxicity than PAM-only treatment.

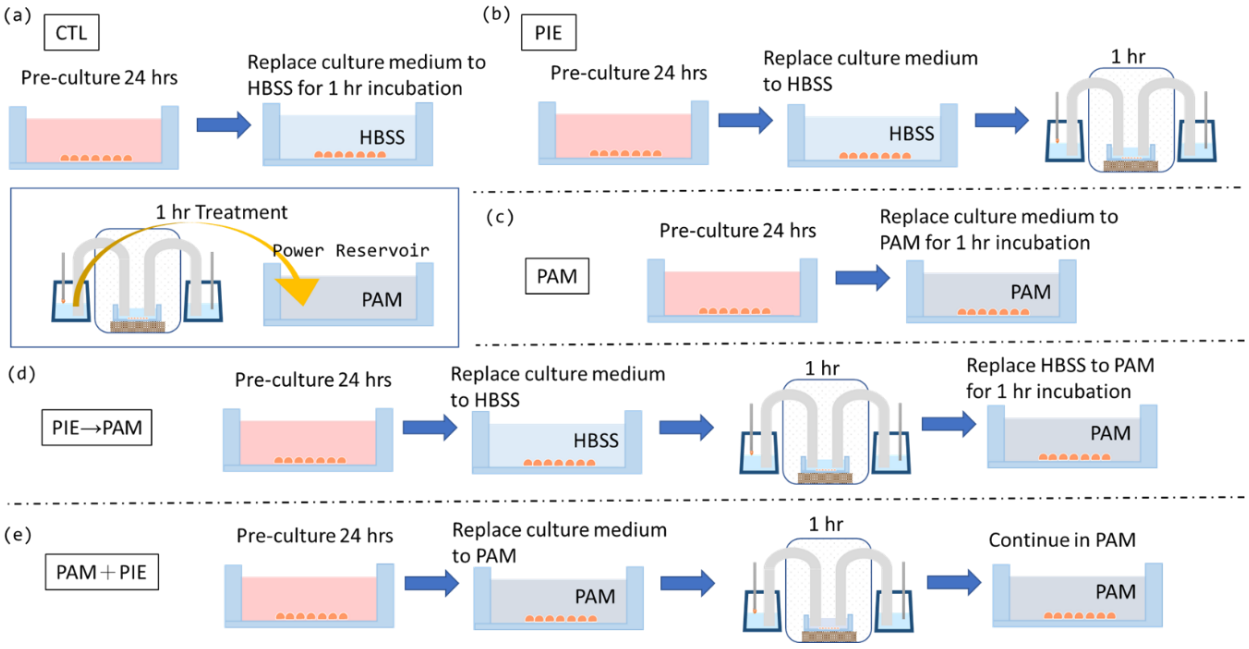

Figure 5.3 Schematic representation of cell treatment.

(a) CTL: Untreated control cells were cultured in HBSS.
(b) PIE: Cells in the culture chamber were electrically stimulated without the influence of RONS. This treatment was referred to as "plasma-induced electrical properties" or PIE in this study. Cells in HBSS were treated with PIE for 1 hr. After PIE treatment, cell culture was continued in HBSS for 24 hr.
(c) PAM: HBSS in the power reservoir was exposed to streamer discharge for 1 hr and utilized as plasma-activated medium (PAM). Cells were cultured in PAM.
(d) PIE→PAM: Cells in HBSS were treated with PIE for 1 hr. After PIE treatment, HBSS in the culture chamber was replaced with PAM. PIE-treated cells were cultured in PAM for 24 hr.
(d) PAM＋PIE: Cells in PAM were treated with PIE for 1hr. Cell culture was continued in the presence of PAM for 24 hr.

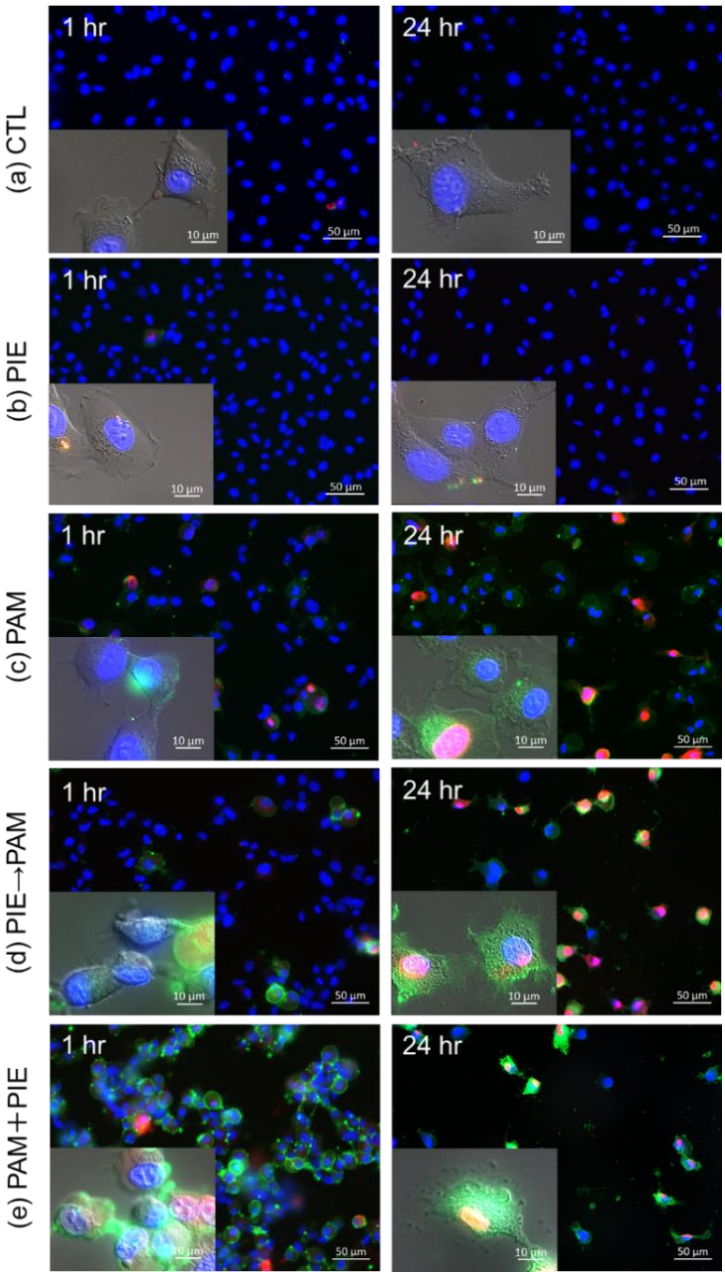

Figure 5.4 Fluorescence microscopy of cells treated with PIE, PAM, and their combination.

Cells were co-stained with Hoechst33342 (blue), FITC-Annexin V (green), and ethidium homodimer III (red).

(a) CTL: Untreated control cells were incubated for either 1 hr (left) or 24 hr (right).

(b) PIE: Cells were treated with PIE for 1 hr and immediately stained (left). Another set of cells were treated with PIE for 1 hr and cultured for 24 hr (right).

(c) PAM: Cells were incubated in PAM for either 1 hr or 24 hr.

(d) PIE→PAM: Cells were treated with PIE for 1 hr and immediately stained (left). Another set of cells were treated with PIE for 1 hr and subsequently cultured in PAM for 24 hr (right).

(e) PAM+PIE: Cells in PAM were stimulated with PIE for 1 hr. Cells were immediately stained (left), or cell culture was continued in the presence of PAM for 24 hr (right).

5.3.3. Quantitative analysis of cytotoxicity of PIE, PAM, and their combinations

To gain further insight into the combined effects of PIE and PAM, we calculated cell viabilities from fluorescence images of cells. Cells with red fluorescence were counted to be dead, and total cell numbers were obtained from blue staining. As shown in Figure 5.5, PIE stimulation did not show an apparent negative effect on cell viability at 24 hr, whereas PAM treatment markedly decreased cell viability. Intriguingly, although PIE stimulation itself did not cause apparent cytotoxicity, PAM incubation of the PIE-stimulated cells resulted in lower cell viability than PAM-only treatment (Compare between "PAM" and "PIE→PAM" at 24 hr in Fig 5.5 $p < 0.05$). This observation suggests that pretreatment of cells with PIE augmented the cytotoxic effect of PAM. As expected, the maximum cytotoxicity was achieved by the simultaneous treatment with PAM+PIE (Figure 5.5).

To verify the effects of PIE and PAM, we employed another measurement. LDH plays a catalytic role in living cells and normally exists in cells. Because damaged cells leak LDH extracellularly, LDH activity in medium is widely utilized as a biochemical index for cell damage. As shown in Figure 5.6, we observed that the LDH value of the PIE-stimulated sample after 24 hr incubation ("PIE" in Figure 5.6) was quite low and indistinguishable with that of the untreated control (CTL). PAM treatment caused high LDH activity at 24 hr, as expected from the result in Figure 5.5. When cells were stimulated with "PIE→PAM" (namely, PIE for 1 hr and then incubated in PAM for 24 hr), the LDH value was significantly higher than that of the PAM-only sample ($p < 0.01$). The highest value was obtained from the "PAM+PIE" sample. These results on LDH in Fig 5 were in good agreement with those in Figure 5.5, further supporting the notion that PIE stimulation augmented the cytotoxic effect of PAM, even though PIE stimulation itself did not

cause apparent cytotoxicity.

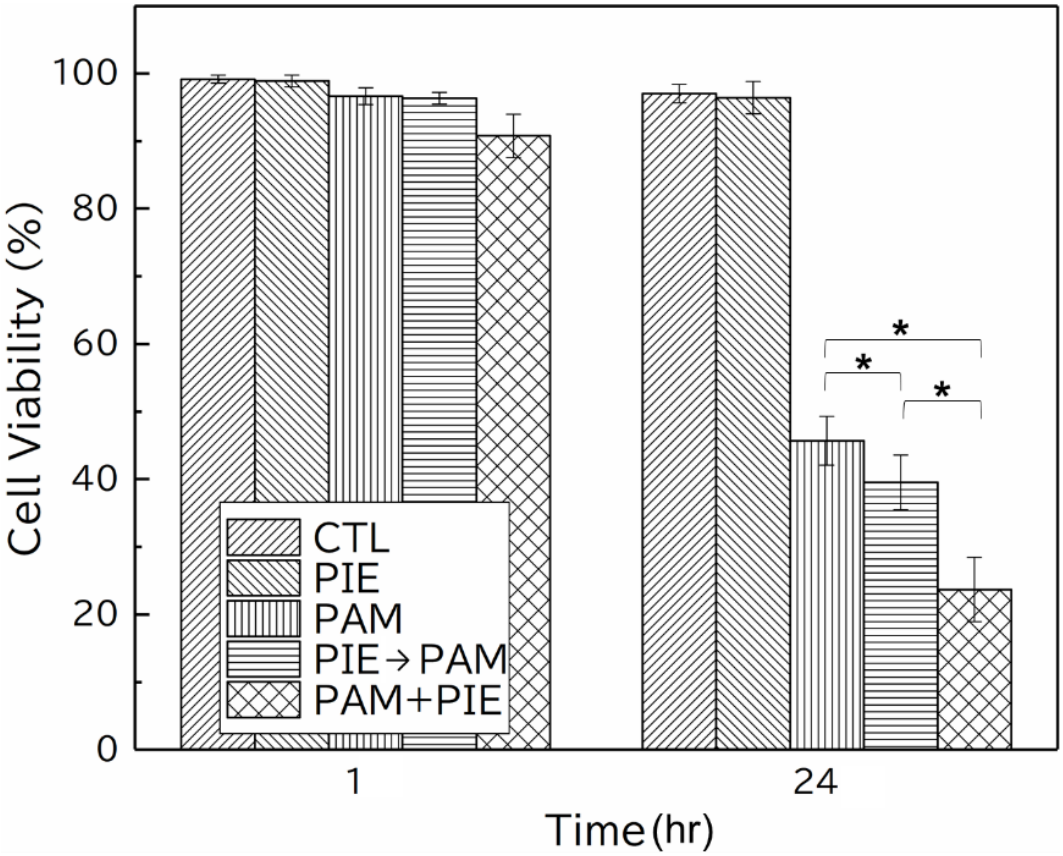

Figure 5.5 Cell viability after treatment with PIE, PAM, and their combination.

Cells were treated as described in Figure 5. 3. Cell viability was calculated from red and blue fluorescence images. Cells with red fluorescence were regarded as being dead. A total cell number was obtained from blue staining. At least 1000 cells were scored in each treatment, and experiments were repeated three times. (*: $p < 0.05$).

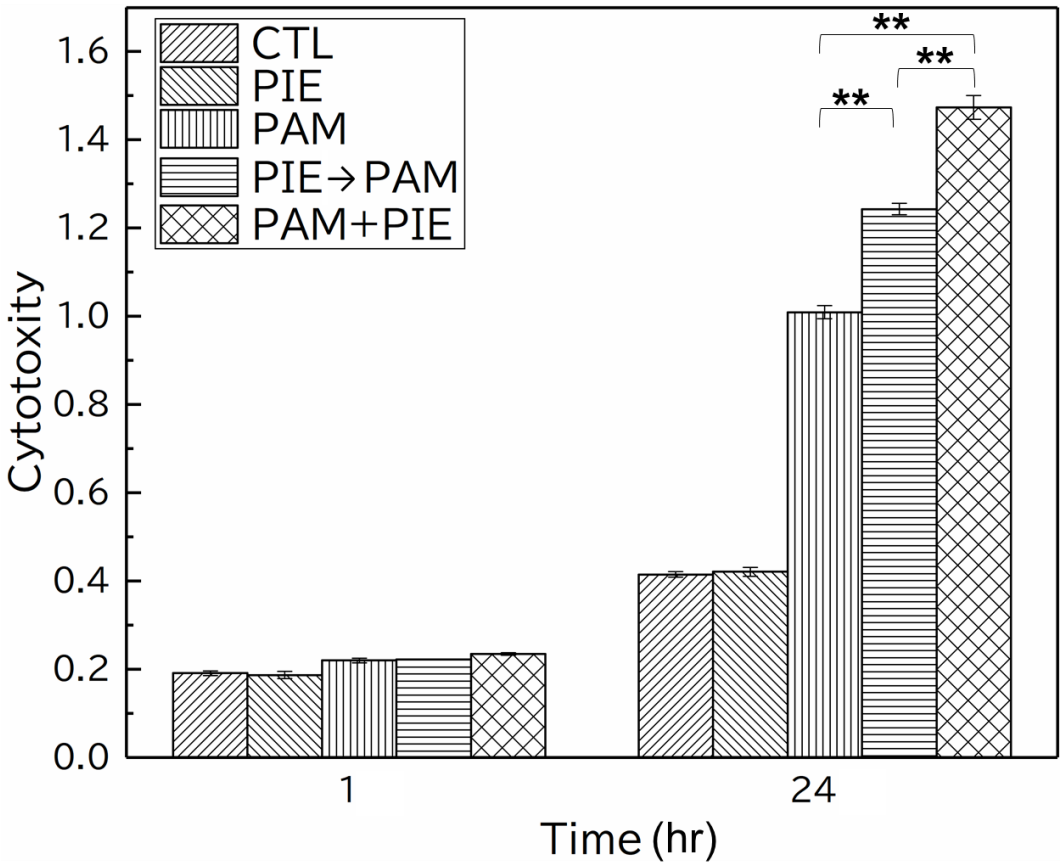

Figure 5.6 Cytotoxicity after treatment with PIE, PAM, and their combination.

Cells were treated as described in Figure 5. 3. Cytotoxicity was measured as an extracellular LDH activity. (**: $p < 0.01$).

5.4. Discussions

CAP provides multiple particles and complex reactions to achieve the medical proposes. For the precise use on the human body, it is necessary to clarify the relationships caused by various factors. Whereas cytotoxic actions of CAP-derived RONS have been well documented so far, a biological contribution of electrical factors of CAP remains largely elusive. In this study, we utilized the experimental setup that enabled to treat cells with a combination of RONS and electrical factors (called PIE in this study) of CAP. Although PIE itself did not generate detectable levels of RONS nor did it have apparent cytotoxic effects, PIE-exposed cells exhibited increased susceptibility to PAM that contained H_2O_2 and NO_2^-. This finding reveals that PIE contributes to biological action of CAP in a way that has not been previously appreciated.

In this chapter, the streamer discharge made PAM and supplied PIE through agarose bridges, and this configuration not only inhibited the chemical compositions out from the cancer cells but maintained the stable electrical properties in the chamber. The chemical compositions in PAM, more specifically the concentrations of H_2O_2 and NO_2^-, regarded as most important species due to their cytotoxicity on cancer cells. Instead of direct treatments, indirect treatments show weaker cytotoxicity in many reports. Hence, we proposed that there was an activated state of cancer cells during the CAP treatment, which is the one of primary reasons for reinforcing cytotoxicity in direct treatment even after several hours. First, it is clear from our results that directly using PIE on cancer cells would not cause the cell damage or growth inhibition, yet it is possible that intracellular organelles or functions might be switched on. Therefore, we compared the various conditions with PAM to investigate cellular sense: changing medium with PAM for 1 hr and then 24 hr incubation in CTL, after PIE, and before PIE. The results are consistent with our assumption that co-treated with PAM and PIE simultaneously would have the best anti-cancer capacity, also found that

numerous early apoptosis would be produced in a short period. In addition, even separating electrical and chemical stimulation, before and after, it still performed better inactivation than the control group after 24 hr. This indicates that cancer cells were activated for a sensitive state which could reinforce effect from PAM. Indeed, the direct treatment with 1 hr CAP afterward 24 hr cultivation had the lowest viability (less than 13%, data no shown) than other conditions in previous results, since there still have other unknown factors (e.g. short-lived species) that also influence the cytotoxicity from CAP treatments.

We speculate that there are at least two possible mechanisms by which PIE treatment causes the augmented cytotoxicity of PAM. First, PIE may elicit structural and/or chemical alterations in the cell membrane, leading to increased PAM cytotoxicity, presumably through increased RONS permeability. The cell membrane is known to be the primary site of action of electrical impacts, such as pulsed electric fields. Milli- to micro-second pulsed electric fields generally act on the cell membrane and produce membrane pores. This phenomenon is called electroporation and widely utilized for DNA transfection [14]. Ultrashort pulsed electric fields in duration of nanoseconds also act on the cell membrane and produce very small membrane pores that elicit Ca^{2+} influx [15] and intricate cellular responses in a Ca^{2+}-dependent manner [16,17]. Assuming that the cell membrane is the primary sites of electrical impact, PIE may cause subtle structural and/or chemical alterations in the cell membrane, which are not manifested as a reduction in cell viability but enhance RONS permeation.

Another plausible mechanism underlying the synergistic action of PIE and PAM involves intracellular signaling pathways that participate in the modulation of cell death induction. Human cells can undergo multiple modes of cell death, including apoptosis, necrosis, and many atypical cell death modalities [18], all of which are influenced by various intracellular signaling pathways [19]. Electrical impacts, such as nanosecond pulsed electric fields, have been reported to

induce several intracellular signaling pathways, including the MAP kinase pathways and the stress response pathway [20,21]. Activation of these signaling pathways frequently exerts facilitatory effects on the execution of cell death. We have previously demonstrated that weak PIE treatment for long periods induces increased cell motility and its associated morphological changes, presumably through the activation of certain intracellular signaling [22,23]. We assume that PIE treatment may activate certain signaling pathway(s), leading to enhanced cell death induction. Further investigation of molecular details of cell death and its associated intracellular responses will provide better understanding of the observed synergy between PIE and PAM. Of note, the aforementioned two plausible mechanisms for the augmented susceptibility of PIE-exposed cells to PAM are not mutually exclusive.

Taken together, we demonstrated that PIE-exposed cells exhibited increased susceptibility to PAM, even though PIE itself did not have apparent adverse effects on viability, proving that electrical factors play the essential role during the CAP treatments for reinforcing anti-cancer capacity on human fibrosarcoma cells.

References

[1] M. Jinno, Y. Ikeda, H. Motomura, Y. Kido, S. Satoh, Investigation of plasma induced electrical and chemical factors and their contribution processes to plasma gene transfection, Arch. Biochem. Biophys. 605 (2016) 59–66. doi:10.1016/j.abb.2016.04.013.

[2] D.B. Graves, Reactive species from cold atmospheric plasma: Implications for cancer therapy, Plasma Process. Polym. 11 (2014) 1120–1127. doi:10.1002/ppap.201400068.

[3] S. Bekeschus, J. Kolata, C. Winterbourn, A. Kramer, R. Turner, K.D. Weltmann, B. Bröker, K. Masur, Hydrogen peroxide: A central player in physical plasma-induced oxidative stress in human blood cells, Free Radic. Res. 48 (2014) 542–549. doi:10.3109/10715762.2014.892937.

[4] S.J. Kim, T.H. Chung, Cold atmospheric plasma jet-generated RONS and their selective effects on normal and carcinoma cells, Sci. Rep. 6 (2016) 1–14. doi:10.1038/srep20332.

[5] H. Jablonowski, T. von Woedtke, Research on plasma medicine-relevant plasma-liquid interaction: What happened in the past five years?, Clin. Plasma Med. 3 (2015) 42–52. doi:10.1016/j.cpme.2015.11.003.

[6] T. Sato, M. Yokoyama, K. Johkura, A key inactivation factor of HeLa cell viability by a plasma flow, J. Phys. D. Appl. Phys. 44 (2011). doi:10.1088/0022-3727/44/37/372001.

[7] M. Yokoyama, K. Johkura, T. Sato, Gene expression responses of HeLa cells to chemical species generated by an atmospheric plasma flow, Biochem. Biophys. Res. Commun. 450 (2014) 1266–1271. doi:10.1016/j.bbrc.2014.06.116.

[8] X. Lu, G. V. Naidis, M. Laroussi, S. Reuter, D.B. Graves, K. Ostrikov, Reactive species in non-equilibrium atmospheric-pressure plasmas: Generation, transport, and biological effects, Phys. Rep. 630 (2016) 1–84. doi:10.1016/j.physrep.2016.03.003.

[9] W. Van Boxem, J. Van Der Paal, Y. Gorbanev, S. Vanuytsel, E. Smits, S. Dewilde, A. Bogaerts, Anti-cancer capacity of plasma-treated PBS: Effect of chemical composition on cancer cell cytotoxicity, Sci. Rep. 7 (2017) 1–15. doi:10.1038/s41598-017-16758-8.

[10] R. Furuta, N. Kurake, K. Ishikawa, K. Takeda, H. Hashizume, H. Tanaka, H. Kondo, M. Sekine, M. Hori, Intracellular responses to reactive oxygen and nitrogen species, and lipid

peroxidation in apoptotic cells cultivated in plasma-activated medium, Plasma Process. Polym. 14 (2017) 1–6. doi:10.1002/ppap.201700123.

[11] D. Yan, W. Xu, X. Yao, L. Lin, J.H. Sherman, M. Keidar, The Cell Activation Phenomena in the Cold Atmospheric Plasma Cancer Treatment, Sci. Rep. 8 (2018) 1–10. doi:10.1038/s41598-018-33914-w.

[12] Z. Machala, B. Tarabová, D. Sersenová, M. Janda, K. Hensel, Chemical and antibacterial effects of plasma activated water: Correlation with gaseous and aqueous reactive oxygen and nitrogen species, plasma sources and air flow conditions, J. Phys. D. Appl. Phys. 52 (2019). doi:10.1088/1361-6463/aae807.

[13] A. Khlyustova, C. Labay, Z. Machala, M.P. Ginebra, C. Canal, Important parameters in plasma jets for the production of RONS in liquids for plasma medicine: A brief review, Front. Chem. Sci. Eng. 13 (2019) 238–252. doi:10.1007/s11705-019-1801-8.

[14] T. Kotnik, L. Rems, M. Tarek, D. Miklavčič, Membrane Electroporation and Electropermeabilization: Mechanisms and Models, Annu. Rev. Biophys. 48 (2019) 63–91. doi:10.1146/annurev-biophys-052118-115451.

[15] P.T. Vernier, Y. Sun, M.A. Gundersen, Nanoelectropulse-driven membrane perturbation and small molecule permeabilization, BMC Cell Biol. 7 (2006) 1–16. doi:10.1186/1471-2121-7-37.

[16] K. Morotomi-Yano, K.I. Yano, Calcium-dependent activation of transglutaminase 2 by nanosecond pulsed electric fields, FEBS Open Bio. 7 (2017) 934–943. doi:10.1002/2211-5463.12227.

[17] T. Koga, K. Morotomi-Yano, T. Sakugawa, H. Saitoh, K. ichi Yano, Nanosecond pulsed electric fields induce extracellular release of chromosomal DNA and histone citrullination in neutrophil-differentiated HL-60 cells, Sci. Rep. 9 (2019) 1–13. doi:10.1038/s41598-019-44817-9.

[18] L. Galluzzi, I. Vitale, S.A. Aaronson, J.M. Abrams, D. Adam, P. Agostinis, E.S. Alnemri, L. Altucci, I. Amelio, D.W. Andrews, M. Annicchiarico-Petruzzelli, A. V. Antonov, E. Arama, E.H. Baehrecke, N.A. Barlev, N.G. Bazan, F. Bernassola, M.J.M. Bertrand, K. Bianchi, M. V. Blagosklonny, K. Blomgren, C. Borner, P. Boya, C. Brenner, M.

Campanella, E. Candi, D. Carmona-Gutierrez, F. Cecconi, F.K.M. Chan, N.S. Chandel, E.H. Cheng, J.E. Chipuk, J.A. Cidlowski, A. Ciechanover, G.M. Cohen, M. Conrad, J.R. Cubillos-Ruiz, P.E. Czabotar, V. D'Angiolella, T.M. Dawson, V.L. Dawson, V. De Laurenzi, R. De Maria, K.M. Debatin, R.J. Deberardinis, M. Deshmukh, N. Di Daniele, F. Di Virgilio, V.M. Dixit, S.J. Dixon, C.S. Duckett, B.D. Dynlacht, W.S. El-Deiry, J.W. Elrod, G.M. Fimia, S. Fulda, A.J. García-Sáez, A.D. Garg, C. Garrido, E. Gavathiotis, P. Golstein, E. Gottlieb, D.R. Green, L.A. Greene, H. Gronemeyer, A. Gross, G. Hajnoczky, J.M. Hardwick, I.S. Harris, M.O. Hengartner, C. Hetz, H. Ichijo, M. Jäättelä, B. Joseph, P.J. Jost, P.P. Juin, W.J. Kaiser, M. Karin, T. Kaufmann, O. Kepp, A. Kimchi, R.N. Kitsis, D.J. Klionsky, R.A. Knight, S. Kumar, S.W. Lee, J.J. Lemasters, B. Levine, A. Linkermann, S.A. Lipton, R.A. Lockshin, C. López-Otín, S.W. Lowe, T. Luedde, E. Lugli, M. MacFarlane, F. Madeo, M. Malewicz, W. Malorni, G. Manic, J.C. Marine, S.J. Martin, J.C. Martinou, J.P. Medema, P. Mehlen, P. Meier, S. Melino, E.A. Miao, J.D. Molkentin, U.M. Moll, C. Muñoz-Pinedo, S. Nagata, G. Nuñez, A. Oberst, M. Oren, M. Overholtzer, M. Pagano, T. Panaretakis, M. Pasparakis, J.M. Penninger, D.M. Pereira, S. Pervaiz, M.E. Peter, M. Piacentini, P. Pinton, J.H.M. Prehn, H. Puthalakath, G.A. Rabinovich, M. Rehm, R. Rizzuto, C.M.P. Rodrigues, D.C. Rubinsztein, T. Rudel, K.M. Ryan, E. Sayan, L. Scorrano, F. Shao, Y. Shi, J. Silke, H.U. Simon, A. Sistigu, B.R. Stockwell, A. Strasser, G. Szabadkai, S.W.G. Tait, D. Tang, N. Tavernarakis, A. Thorburn, Y. Tsujimoto, B. Turk, T. Vanden Berghe, P. Vandenabeele, M.G. Vander Heiden, A. Villunger, H.W. Virgin, K.H. Vousden, D. Vucic, E.F. Wagner, H. Walczak, D. Wallach, Y. Wang, J.A. Wells, W. Wood, J. Yuan, Z. Zakeri, B. Zhivotovsky, L. Zitvogel, G. Melino, G. Kroemer, Molecular mechanisms of cell death: Recommendations of the Nomenclature Committee on Cell Death 2018, Cell Death Differ. 25 (2018) 486–541. doi:10.1038/s41418-017-0012-4.

[19] A. Ashkenazi, G. Salvesen, Regulated Cell Death: Signaling and Mechanisms, Annu. Rev. Cell Dev. Biol. 30 (2014) 337–356. doi:10.1146/annurev-cellbio-100913-013226.

[20] K. Morotomi-Yano, H. Akiyama, K. ichi Yano, Nanosecond pulsed electric fields induce poly(ADP-ribose) formation and non-apoptotic cell death in HeLa S3 cells, Biochem. Biophys. Res. Commun. 438 (2013) 557–562. doi:10.1016/j.bbrc.2013.07.083.

[21] K. Morotomi-Yano, H. Akiyama, K.I. Yano, Different involvement of extracellular calcium in two modes of cell death induced by nanosecond pulsed electric fields, Arch. Biochem.

Biophys. 555–556 (2014) 47–54. doi:10.1016/j.abb.2014.05.020.

[22] C.H. Chang, K.I. Yano, T. Okumura, T. Sato, Effect of plasma-generator-supplied nanosecond pulsed current on cell response, J. Phys. D. Appl. Phys. 51 (2019). doi:10.1088/1361-6463/ab0733.

[23] C.H. Chang, K. I. Yano, T. Sato, Nanosecond pulsed current under plasma-producing conditions induces morphological alterations and stress fiber formation in human fibrosarcoma HT-1080 cells, Arch. Biochem. Biophys. 681 (2020) 108252. doi:10.1016/j.abb.2020.108252.

Chapter 6

Conclusions

6.1. Summary

CAP shows the promising application in medical field, yet the compositions supplied by CAP are extremely complex. To distinguish the influence from chemical components and electrical properties is necessary to elucidate mechanisms on target treatment. Currently, biological actions of CAP are considered to be brought about by the synergistic effects of chemical and electrical factors of CAP. As for chemical components, CAP contains multiple species, such as RONS. Cytotoxicity of CAP is mainly attributed to the action of RONS. Whereas the biological significance of RONS in CAP has been well documented so far, limited information is currently available on the contribution of electrical properties to CAP-induced biological responses. Two major obstacles hampered the effort to understand the biological influence of electrical properties and their transmission process. First, RONS in CAP exert strong cytotoxic effects that easily overwhelm the biological effects of electrical factors. Second, electrical stimulation itself frequently induces cell death, and careful examination of stimulation conditions is required to avoid gross induction of cell death. To summary our study as follows:

Chapter 2. Effect of nanosecond pulsed current supplied by plasma generator on cell morphology and activity

In this chapter, we constructed a novel system for cell stimulation that could physically isolate cells from chemical species generated around electrodes and thus allowed us to evaluate the direct effects of electrical transmission processes on cellular activities. Using this system, we treated human HT-1080 cells with the nsPC by the plasma generator and analyzed various cellular activities. Although the electric stimulation did not affect cell viability or proliferation, also fluorescent microscopy showed that electroporation of stimulated cells did not occur. We observed a significant increase in cell migration along with altered cell morphology. In brief, we speculate that the electrical factors of nsPC may be critical determinants of cellular responses.

Chapter 3. Nanosecond pulsed current under plasma-producing conditions induces morphological alterations and cytoskeleton reorganizations in human fibrosarcoma HT-1080 cells

Previously results demonstrate that the nsPC under CAP-producing conditions significantly promoted the motility of human HT-1080 cells. In this chapter, we explored the effects of nsPC on cell morphology associated with cell motility. We observed that nsPC stimulation caused extended cell shape, increased cell surface area, and membrane protrusion formation, but not cell death induction. nsPC stimulation also caused elevated intracellular ROS and Ca^{2+}. HT-1080 cells can undergo two modes of cell motility, namely mesenchymal and amoeboid motility, and we found that morphological features of mesenchymal motility were partly shared with nsPC-stimulated cells. Moreover, nsPC-stimulated cells had extended stress fibers composed of filamentous actin. In short, this chapter provides a novel insight into the electrical aspect of CAP action, and we speculate that the nsPC activates a certain mechanism involving intracellular signaling for stress fiber formation, leading to altered cell morphology and increased cell motility.

Chapter 4. Cdc42/Rac1 and other possible pathways activated by nsPC to regulate actin dynamics in human fibrosarcoma HT-1080 cells

Former results show the identical phenomena from actin reorganization that nsPC successfully activated cancer cell to mesenchymal motility. As increasing the strength and operation time of nsPCs, HT-1080 cells were induced gradually to mesenchymal mode, which likely linked with Rho family. Our results are consistent with those of a model with Rho/ROCK inhibitor, revealed potential cross talk between nsPCs and intracellular pathways controlling cell motility.

Chapter 5. Distinct biological actions of plasma-induced electrical and chemical factors and their synergistical effects as augmented cytotoxicity

Finally, we reconstructed the new stimulated system with the needle electrode to discharge streamer over medium to compare the effects of plasma-induced chemical and electrical stimuli over HT-1080 cells. The results show that cells co-treated in PAM with PIE whether before or after performed the numbers of early apoptosis and high cytotoxicity than those treated in PAM without electrical stimulation. This demonstrates that cancer cells had be activated by PIE in highly sensitive state to increase susceptibility to extracellular environment. Taken together, we assumed that the electrical stimulation plays the essential role during the CAP treatments for strengthening anti-cancer capacity.

Last but not least, the optimized power source (nsPC) with RONS would be reinforced the efficacy for inactivation without electroporation and thermal influence, and our results have the great agreement with this concept. By changing the species inside solution (with or without anti-cancer species), we might control various CAP treatments for utilizing medical purposes. Further

investigation of molecular details of cell death and its associated intracellular responses will provide better understanding of the observed synergy between PIE and PAM. The summary of our study is given in figure 6.1.

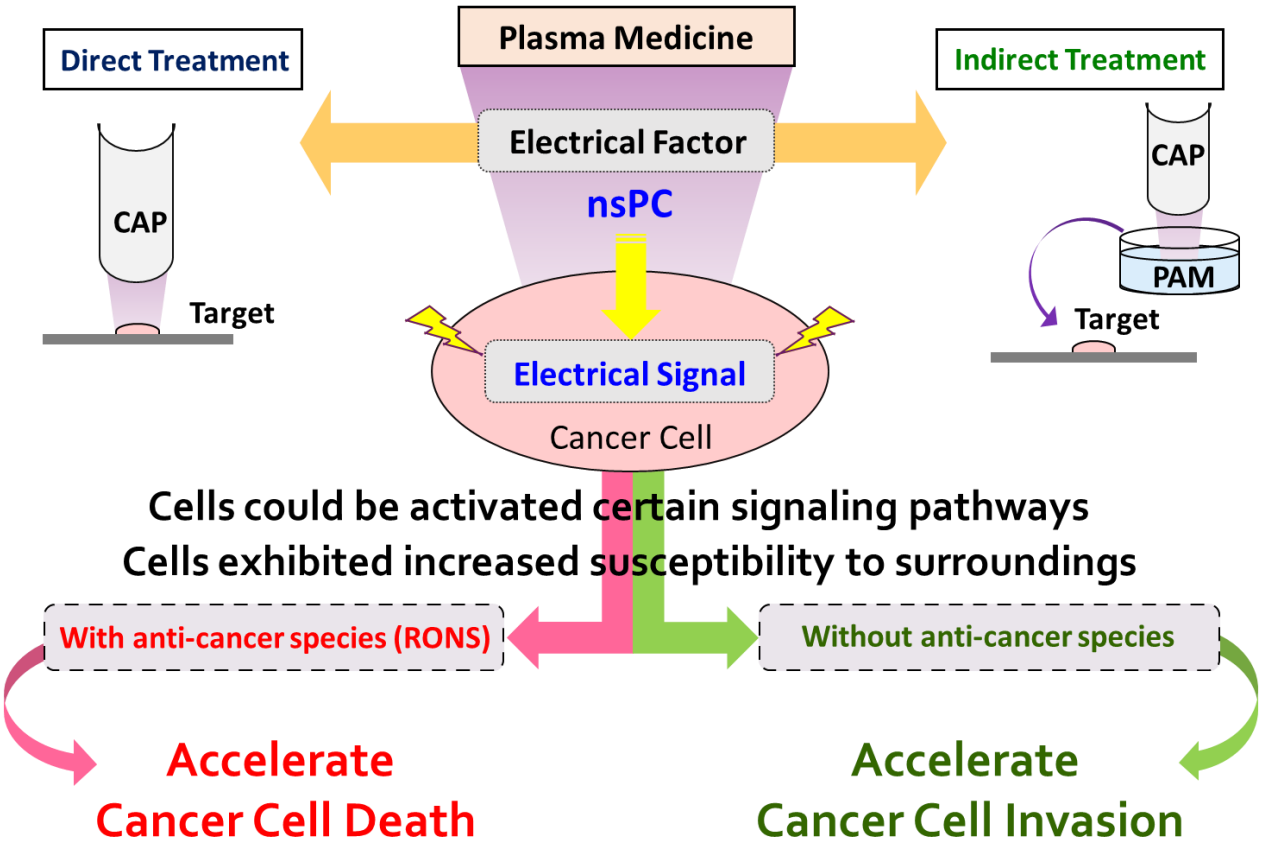

Figure 6.1 The influences of electrical factors from the nsPC on cell responses.

6.2. Perspectives

We describe herein an electrical aspect of human fibrosarcoma cells activated by nsPCs and CAP-generating conditions. Further understanding of the molecular mechanisms of electrical signaling and electric properties on cells and tissues are needed for effective application of "Plasma Medicine".

1. To investigate on intramolecular dynamics in response to organelles in cancer cells
2. To understand the expression of proteins of possible pathways, in which can be activated by electric signals
3. To measure the sources of intracellular molecules (in vivo or in vitro), can be useful for the explanation of possible mechanisms
4. To clarify which components or species in the solution/medium to penetrate or permeabilize into cells
5. To understand the relation between metastastic behaviors and sensitive state in cancer cells activated by electrical stimulus
6. To perform the efficacy of applying electrical signals on more stimulation models, also on normal cells for selectivity
7. To carry out promising new developments in the control of CAP

Appendix

A. Manual for cell culture

Previous Preparation

- Culture Medium

  [500 ml] MEM (Minimum essential medium eagle): Sigma, M4655-500
  [50 ml] FBS (Fetal bovine serum): Invitrogen, 10437077
  [10 ml] Penicillin streptomycin mixed solution: Nacalai Tesque, 26253-84

- Trypsin EDTA

  0.25w/v% Trypsin-1mmol/L EDTA·4Na Solution with Phenol Red: Fujifilm Wako Pure Chemicals, 201-16945

- Phosphate-buffered saline (PBS)

  PBS, pH 7.2: Gibco™, 20012050

Procedure for adherent cells

Detachment

1. Start to heat up the culture medium and trypsin to 37°C (PBS need to be warmed in winter).
2. Inside the water bath, please make sure the positions of opens are higher than the water (use parafilm to seal opens and prevent splashing).
3. Turn on the UV light on the safety cabinet for 15 minutes.
4. Prepare the waste can with some tap water inside to throw the pipettes.
5. Before put into the safety cabinet, use 70% ETOH sterilize outside hands and the bottles, wipe to dry.

6. Take out the cultured disk from the incubator to the cabinet.
7. Remove the waste inside the disk, use 5 ml PBS to wash cells twice and remove (pipette do not directly touch the bottom, through the wall while adding PBS)
8. For detach cells from the disk, mix the 1 ml PBS and 1 ml trypsin, add this solution inside the disk for few seconds (shake around 4 times) and remove soon (avoid cells sticking together), left 1-2 drops after removing. Tap the disk to help cells to detach (force from down to up at 45° for whole the disk)
9. Quickly add 10 ml culture medium (stop the reaction from trypsin), and pipette to disperse cells (make circle around the disk twice).

Counting numbers

1. Dilute cell suspension (10 µl suspension + 40 µl medium)
2. Add 10 µl Trypan blue solution (0.4 %) into one well of 96 well plate
3. Add 10 µl diluted suspension in the well
4. Pipet 10 µl of mixed solution into hemocytometer (Burker Turk)
5. Count living and dead cell by the automated cell counter (Thermo Scientific, AMQAX1000)

For new passage of HT-1080 cells

- Initial cultured number is around 1.5×10^6 cells/disk
- The total cell number inside the flask is suggested to be not more than 5 million.
- The concentration of trypsin should be adjusted by each kinds of cell.
- Proliferation rate is around 2.4-2.5 times over 24 hours. (1.5×10^6 cells/disk → 4.5×10^6 cells/disk)
- For next passage, prepare 12 ml culture medium with 1.5×10^6 cells for one T-75 flask

B. Stimulation system

The cell culture stimulation system including Ag/AgCl electrodes and agarose bridges to help prevent the intermixing of fluids (with chemical species) which might otherwise occur.

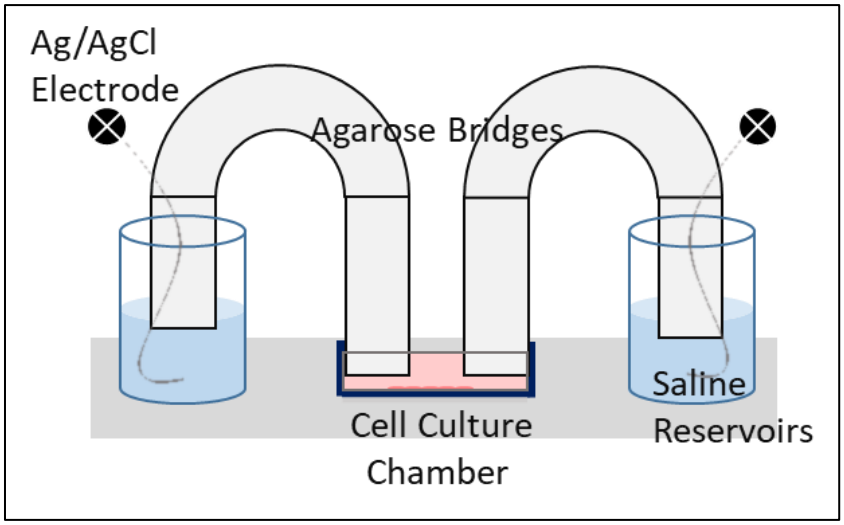

Silver/silver chloride electrodes

Sliver is the most common electrode because are biocompatible, used in laboratory electrophysiology studies, and employed in clinical devices to connect the power supply and the agar bridges. Partially soak silver wire (φ 0.30 mm, L 10 cm, 99.99%) in bleach (Clorox) for 4-6 hr to make Ag/AgCl electrodes.

Agarose Bridges

The agarose bridges design for the purpose of preventing nonreversible faradaic, cytotoxic reactions, such as hydrolysis, from occurring in the medium next to the cells. Agarose bridges are electrochemical cells that work like batteries, transferring electric current to ionic current through agar bridges through a set of oxidation-reduction redox reactions. Glass tubes filled with 2 wt%

agar gel (agar powder + PBS, heating by microwave to make gel) served as bridges between the cell culture chamber and the saline reservoirs.

C. Protocol for cell count reagent SF

Principle of Measurement

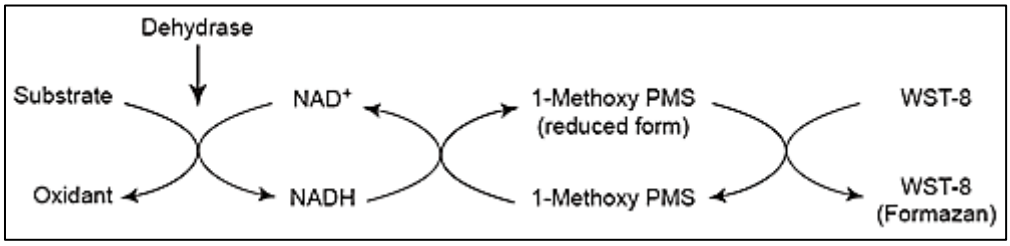

Cell count reagent SF allows sensitive colorimetric assays by utilizing highly water-soluble tetrazolium salt. WST-8 produces a water-soluble formazan dye upon reduction in the presence of an electron carrier. Since the absorbance at 450 nm is proportional to the number of viable cells in the medium, the viable cell number can be determined using the absorbance value of a previously prepared calibration curve. (*reference: Nacalai Tesque, Inc.*)

Previous Preparation

- Cell count reagent SF (Nacalai Tesque, cat. no. 07553-15)
- Microplate reader (Thermo Fisher, Multiskan FC)

Procedure for adherent cells

1. Prepare a cell suspension using an appropriate culture medium, count cells to the desired number and dispense 100 µl of suspension of cells in logarithmic growth phase into each well of a 96-well plate.
2. Pre-incubate the medium in CO_2 incubator.
3. Add 10 µl of Cell Count Reagent SF to each well of the plate.

4. Incubate the medium for 1-4 hours in the incubator.
5. Measure the absorbance at 450 nm by microplate reader

D. Immunostaining protocol

Principle of Measurement

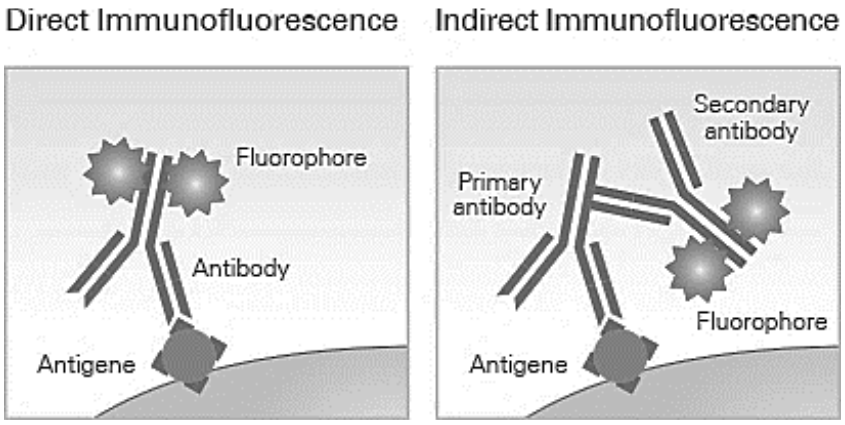

Immunofluorescence (IF) is a powerful approach for getting insight into cellular structures and processes using microscopy, based on the following principal steps: First, specific antibodies bind to the protein of interest, then fluorescent dyes are coupled to these immune complexes in order to visualize the protein of interest using microscopy. (*reference: Cell signaling technology*)

Previous Preparation

- 4%-Paraformaldehyde Phosphate Buffer Solution (4% PFA)
  (Nacalai tesque 09154-14, 5x, 10 ml)
  store at 4°C

- TritonX-100 in distilled-water
  (Sigma-Aldrich T8787-50ML, 50 ml)
  dilute to 0.2% Triton X-100 in D-PBS just before immunostaining, store at room temperature

- Bovine serum albumin (BSA)
  (Globulin Free: Wako Pure Chemical 013-15101, 10 g)
  mix 800 mg/powder with 40 ml D-PBS (-), make aliquots (1.3 ml / microtube), store at -20°C, 2% (20 mg/ml) for immunostaining.

- Anti-alpha-Tubulin
  (mouse monoclonal clone 10G10, Wako 017-25031, 200 ug)
  dilute at 1/25 in 20 mg/ml BSA, store at 4°C for a short period (-20°C for a long period), avoid repeated freeze/thaw, 1/250 dilution for immunostaining.

- Anti-mouse Alexa 488
  (Goat anti-Mouse IgG (H+L) Highly Cross-Adsorbed Secondary Antibody, Alexa Fluor 488, 0.5 mL: Thermo Fisher A11029)
  dilute at 1/10 in 20 mg/ml BSA, avoid light, store at 4°C for a short period (-20°C for a long period), avoid repeated freeze/thaw, 1/200 dilution for immunostaining.

- Rhodamine Phalloidin
  (Amanita phalloides, cat. PHDR1)
  dilute 3.5 µl of 14 µM labeled stock rhodamine phalloidin with 500 µl D-PBS, avoid light, store at 4°C for a short period (-20°C for a long period), 100 nM for immunostaining.

- Mounting medium
  (VECTASHIELD Mounting Medium with DAPI, Funakoshi: H-1200, 10 ml)
  store at 4°C

Procedure for adherent cells

Fixation

Remove medium from a slide chamber and wash chambers with D-PBS 3 times, add 400 ul 4% paraformaldehyde in D-PBS 4°C for 20-30 min

Permeabilization

Remove medium from a slide chamber and wash with D-PBS 2 times, add 400 ul 0.2% Triton X-100 in D-PBS RT for 5-10 min

Blocking

Remove medium from a slide chamber and wash with D-PBS 3 times, add 400 ul 2% BSA in D-PBS 4°C for 20 - 30 min

Immunostaining

1. Remove BSA solution, add 400 ul diluted 1st antibody solution 4°C for at least 2 hr (or overnight)
2. Remove 1st antibody solution and wash 3 with D-PBS three times, add 400 ul diluted 2nd antibody solution 4°C for 1 hr in dark (Avoid light)
3. Add the desired concentration of fluorescent dye–labeled secondary antibody along with a compatible counterstain for the cytoskeleton (e.g., rhodamine phalloidin) and nucleus (DAPI) diluted in 500 µL of 0.1% BSA and incubate for 45 min at room temperature protected from light.

Mounting

1. Wash with D-PBS 4-5 times, remove all D-PBS completely, add VectaStain with DAPI (an antifade agent with a DNA-staining dye)
2. Keep slides in dark for 5-10 min, then microscopy

E. Quantitative analysis of fluorescence intensity by ImageJ

Procedure for Quantify

1. Open captured images from ImageJ software
2. Convert images to 8-bit as gray value (Image-Type-8-bit)
3. Adjust the threshold and select the appropriate area (Image-Adjust-Threshold)
4. Choose the appropriate threshold algorithm (Image-Adjust-Auto Threshold)
5. Set the parameters to be measured (Analyze-Set Measurements)
6. Obtain optical density (OD), calculate mean values as arbitrary units (AU)

Mean = IntDen / Area

Mean: Mean gray value

IntDen: integrated density, namely optical density (OD)

F. Intracellular Ca^{2+} and ROS signals staining

Principle of Measurement

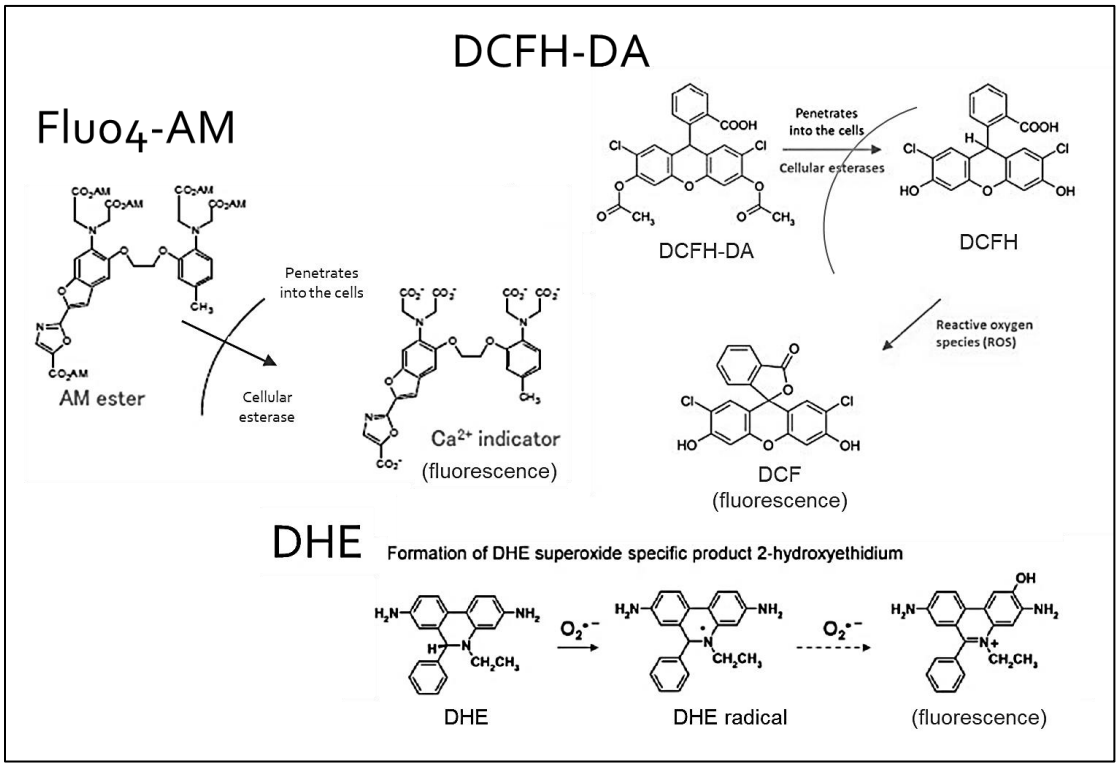

- Fluo4-AM is cell-permeable and converted to the Ca^{2+}-sensitive green fluorescent dye Fluo-4 in a cell to present green fluorescence.
- DCFH-DA is a ROS detector and cell-permeable compound that is metabolically converted to DCFH in a living cell. Oxidation by ROS converts the molecule DCF to present green fluorescent.
- DHE is a $O_2^{\bullet -}$ detector, staining cell nucleus for red fluorescence.

  (*reference: BioTek Instruments, Inc.*)

Previous Preparation

- Fluo4-AM: 10 μM, Thermo Fisher Scientific

- DCFH-DA (2',7'-Dichlorofluorescin diacetate): 10 µM, Sigma-Aldrich
- DHE (Dihydroethidium): 10 µM, Sigma-Aldrich
- HBSS (Hanks' Balanced Salt Solution): calcium, magnesium, no phenol red, Thermo Fisher Scientific

Procedure for adherent cells

Loading

1. Wash cells three times with HBSS+.
2. Incubate 30-45 min with 1 mL of staining solution at room temperature.

De-esterification

1. Remove the staining solution.
2. Wash three times with HBSS+.
3. Incubate 30 min with HBSS+ or serum-free medium at room temperature.

Measurement

Check de-esterification process by monitoring fluorescence signal for a while (1-2 min).

G. Protocol for LDH cytotoxicity

Principle of Measurement

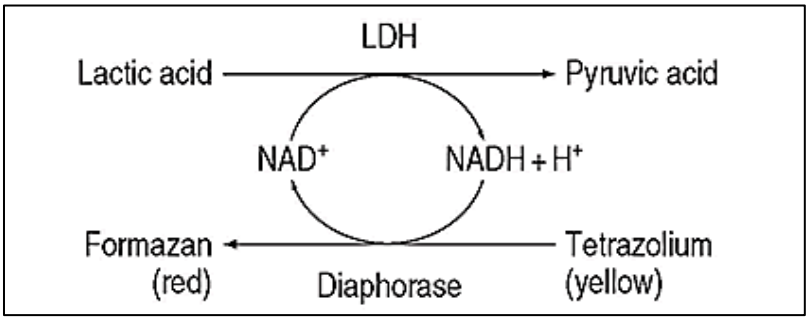

Lactate dehydrogenase (LDH) is a stable cytoplasmic enzyme which is present in all cells. When the plasma membrane is damaged, LDH is rapidly released into the culture supernatant. LDH activity is determined by a colorimetric assay: First, NAD+ is reduced to NADH/H+ by the LDH-catalyzed conversion of lactate to pyruvate. Then, a catalyst included in the reaction mixture (diaphorase) transfers H/H+ from NADH/H+ to the tetrazolium salt INT, which is reduced to a formazan dye. (*reference: TakaraBio, LDH Cytotoxicity Detection Kit*)

Previous Preparation

- LDH Cytotoxicity Detection Kit (Cat. No. 630117)

  [blue cap] solution A: catalyst
  Reconstitute in 1 ml of distilled water and mix thoroughly for 10 min. The reconstituted solution can be stored for several weeks at 4℃.
  [red cap] solution B: dye Solution
  Thawed INT dye solution is ready to use in the assay. Once thawed, the dye solution can be stored for several weeks at 4℃.
  Final reaction mixture (A+B), must be prepared immediately

- Microplate reader (Thermo Fisher, Multiskan FC)

Procedure for adherent cells

1. Incubate the supernatant with freshly prepared reaction mixture
2. Transfer cell-free culture supernatant to optically clear, flat-bottom 96-well plate
3. Measure absorbance at 492 nm

For most cell lines, the optimal cell concentration is between 0.5-2 x 10^4 cells/well in 200 µl (0.25 - 1 x 10^5 cells/ml).

Acknowledgements

It is an honor for me to study in Tohoku University. First, thanks to Prof. Sato Takehiko for giving the opportunity to start my doctoral career and learn to be a good researcher. Second, thanks to Prof. Yano Ken-ichi for teaching me about biological measurements and knowledge, sharing lots of experiences and supporting for my research. Special thanks to Prof. Ishikawa, Prof. Kaneko, and Prof. Nakabayashi for reviewing and providing valuable comments for my dissertation. More, thanks to the former and current staffs, Dr. Okumura, Dr. Uehara, Ms. Akama, and Mr. Nakajima for their supports. During these days, I learn not only research skills but also how to treat people. It will always be the challenge to achieve the research purpose and cooperate with others; fortunately, in here, I could try whatever idea I want to do, and every moment has been comfortable and easy to communicate with people. Also, members in our lab, it is very glade to work with you, helping me when I had problems on Japanese translation or other daily stuffs. Best thanks to my parents and brother, without their supports, I could not make my decision to study abroad and continue my degree. Next, to my friends, when I was frustrated, encouraging and accompanying me all the times. Last, to myself, good job for insisting to accomplishing your research and dissertation; it is not easy to always be positive when you are alone, so thanks for my optimism that I could face every failure and then stand up again to finish my work. Farewell, hope to see you soon, Sendai city!

謝謝東北大學給我機會來這裡研讀博士課程以及提供了許多研究資源。最感謝佐藤教授的指導和秘書赤間小姐在生活上的協助，讓我很快就適應在日本的研究環境。在這四年裡，接觸了形形色色的人們，也學習到了很多待人處事的方法和技巧，以及正視自己的缺點和自己的需求。博士生涯跟我想像得十分不同，一開始真的有點手足無措，但慶幸的

是這裡的實驗風氣讓我有極大的自由度和想法，讓我專心嘗試自己的研究和學習，這點真的十分難得可貴。在此也要特別感謝在熊本大學的矢野教授對我在研究上的教導，不僅在生物實驗上耐心帶領，更細心修改我的論文，如果沒有他我無法完成我的博士學位。也要謝謝奥村教授、上原教授以及技師中島先生，隨時給予我實驗上的協助和規劃。而在實驗室的成員，也十分感謝有各位相伴。特別感謝日本東北台灣留學生的一切，讓在外地求學的留學生有個美好的依靠。最後謝謝我的父母、弟弟和朋友們，在我最失落和低潮期給予我鼓勵和陪伴。希望可以再次相見，仙台市!